Towards the investigation of hot and compressed nuclear matter in heavy-ion collisions

V. D. Toneev

Joint Institute for Nuclear Research, Dubna

H. Schulz

Central Institute of Nuclear Research, Rossendorf, German Democratic Republic

K. K. Gudima

Institute of Applied Physics, Moldavian Academy of Sciences, Kishinev

G. Röpke

Wilhelm Pieck University, Rostock, German Democratic Republic

Fiz. Elem. Chastits At. Yadra **17**, 1093–1172 (November–December 1986)

The subject of the review is the behavior of nuclear matter formed in heavy-ion collisions in a wide range of energies—from moderate energies corresponding to the formation of a two-phase liquid–gas state, to high energies leading to the formation of the hadron-gas phase, and ultrahigh energies associated with the possible transition of the hadrons into a quark–gluon plasma. Ways of obtaining information about the equation of state of heated and compressed nuclear matter and also the results of experimental and theoretical studies in this direction are discussed.

INTRODUCTION

One of the most attractive aspects of heavy-ion physics is the possibility of investigating the properties of nuclear matter under unusual conditions very far removed from those that characterize the behavior of nuclei in the ground state. Beams of high-energy heavy ions make it possible to investigate the response of a nuclear system to a significant change in the energy density in a spatial region encompassing many (in the limit, all) nucleons, whereas beams of elementary particles "dump" their energy in a small part of the nucleus and thus can give information about the response of the nucleus to a strong but localized perturbation. The theoretical analysis of the process of redistribution of the primary energy and momentum of the colliding nuclei between the various degrees of freedom and its final distribution over the accessible phase space is very complicated. The traditional approach, which makes it possible to treat the entire interaction process in the framework of comparatively simple phenomenological models, consists of using two limiting cases: perturbation theory and the thermodynamic approximation. A small-parameter expansion is widely used in the kinetic description of nuclear collisions (for example, versions of the cascade model), and the assumption of the establishment of global or local equilibrium is explicitly contained in a number of other popular models (nuclear fireball, firestreak, hydrodynamical model, etc.). The complementary nature of the equilibrium and perturbative regimes must be borne in mind. The different approximations evidently correspond to different space–time regions occupied during the development of the reaction, and their relative importance can change, depending on the process considered or even the reaction characteristics. Conceptually, both of these approximations must find their place as limiting cases in a more general fundamental theory. Although such a theory, suitable for practical applications, does not at present exist, many interesting experimental consequences can still be understood at a phenomenological level.

The analysis of the experimental data begins with the attempt to understand the main features of the reaction, the mechanisms of the processes of compression and heating of the nuclear matter, the establishment of statistical equilibrium in the system, the mechanisms of the various types of interaction in the final state, and so forth, and one then tries to establish the state of the matter from the distributions of the observed particles and their characteristics. The final aim is to discover the conditions under which the basic equation of state of nuclear matter is valid in the framework of the dynamics of relativistic heavy-ion collisions and to determine the extent to which the predictions made by the nuclear-matter equation of state can be experimentally verified.

One cannot say that the properties of hot and (or) compressed nuclear matter are well known, since they have been obtained by model extrapolation of the properties of nuclear matter at zero temperature, which has a saturation density $\rho_0 = 0.17\,\mathrm{F}^{-3}$ and a binding energy per nucleon $E_B = -16$ MeV. The compression modulus, the value of which is known experimentally with considerable uncertainty, $K \sim 220 \pm 20$ MeV, usually restricts the accuracy of the theoretical predictions. Thus, any experimental information about the nuclear equation of state outside the region of the saturation density is of fundamental interest for the development of general many-body theory and makes it possible to test existing theories.

The discussion of the possibility or impossibility of various phase transitions in nuclear matter, for example, transitions to the isomer state of anomalous nuclear density, pion

 0090-4759/86/060485-36$04.40

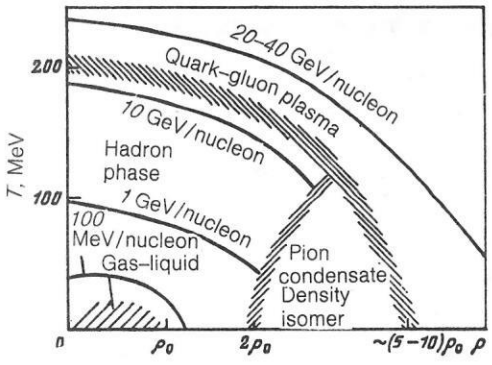

FIG. 1. Phase diagram of possible states of nuclear matter. The curves indicate the regions of densities and temperatures attained in nuclear collisions at different bombarding energies.

condensate, or a quark–gluon plasma, depends to a large degree on the form of the effective nucleon–nucleon interaction and the employed approximate computational schemes. From the general point of view, nuclear matter at low densities and temperatures can be described as consisting of structureless hadrons, and the baryon and meson degrees are the corresponding degrees of freedom. When the energy density is increased, by an increase in the temperature and (or) density, a state of nuclear matter may be reached in which the quarks and gluons are deconfined. Recent estimates made in the framework of the lattice theory of quantum chromodynamics (QCD)[1–3] show that the deconfinement temperature is $T \simeq 200 \pm 50$ MeV at zero mean density of the baryons in the system. At zero temperature the phase transition appears at densities that are 5–10 times greater than the normal density of nuclear matter.[4] In Sec. 3, we briefly describe the present state of this extremely interesting field, which, however, is not the main subject of the present review.

Our main attention will be devoted to discussing the physics of heavy-ion interactions in the region of primary-beam energies from approximately 100 MeV/nucleon to 3.5 GeV/nucleon. To be more specific, Fig. 1 shows the well-known phase diagram of nuclear matter in density–temperature variables; this gives a picture of the new interesting phases of nuclear matter. In discussing the various phases, it is important to emphasize that at the present time we have reliable information from experiments only near the region $\rho \simeq \rho_0$ and $T \simeq 0$.

It is expected that at densities below the nuclear saturation density ρ_0 and at temperatures $T \lesssim 20$ MeV nuclear matter behaves as a liquid–gas mixture like the classical van der Waals gas. In Sec. 1, we consider this interesting region in the density–temperature plane and discuss possible signals of the occurrence of a phase transition.

Figure 1 also shows the region of pion condensation, which was intensively discussed some years ago. It is expected that this phase will be manifested at densities $\rho \gtrsim 2\rho_0$ and at low temperatures through the appearance in the system of long-range correlations.[5,6] If the compression is increased still further, then the attractive potential due to two-pion exchange can give rise to another phase transition, in which an anomalous state of nuclear matter with high density is formed (see Ref. 7). In the present paper, we shall not discuss these two types of phase transition but refer the reader to the literature quoted above. Also omitted from the review are some other forms of nuclear matter not shown in the phase diagram, for example, neutron and supernova stars, though these can in principle give valuable information about the equation of state.

We shall call the wide region in Fig. 1 bounded at high temperatures by the critical curve for the transition of the hadrons into the quark–gluon phase, at high densities and low temperatures by the region of the pion condensate, and by the two-phase liquid–gas region the hadron-gas phase. This phase has been the subject of intensive experimental and theoretical investigation during the last decade. As can be seen from Fig. 1, the hadron-gas phase corresponds to the transitional region from ordinary nuclear matter to the quark–gluon phase. We call it the "hadron-gas phase" because, when the system is heated to a temperature $T \simeq m_\pi c^2$, the main components of the system are various types of (excited) mesons and baryons (here, m_π is the pion rest mass). At $T > m_\pi c^2$, so many hadrons are formed that their quark wave functions overlap appreciably, and the transition to the quark–gluon plasma can take place.

The investigation of the transitional region has given us much valuable information about the behavior of nuclear matter under extremal conditions. It is a necessary intermediate step for the development of new methods and experimental facilities, for the testing of existing theoretical predictions, and ultimately will permit relativistic heavy-ion physics to enter the unexplored region corresponding to a new form of nuclear matter—the quark–gluon plasma. Therefore, the greater part of the present review is devoted to the theoretical and experimental analysis of the hadron-gas phase.

In this review, we consider heavy-ion physics in the three energy regions shown in Fig. 1, in which we have also estimated the densities and temperatures that can be achieved at different energies of the colliding nuclei. The complete ρ-T plane can be divided into three principal energy regions:

(i) the two-phase (liquid–gas) region of nuclear matter, reached at a primary beam energy $E_0 \lesssim 200$ MeV/nucleon;

(ii) the hadron-gas region, the attainment of which requires an energy in the range $0.2 \lesssim E_0 \lesssim 3$–4 GeV/nucleon;

(iii) the region of the quark–gluon phase transition, which, it is assumed, can be realized at $E_0 \gtrsim 10$ GeV/nucleon.

The two-phase region is considered in Sec. 1. We derive a simple equation of state of nuclear matter and discuss the occurrence of two-phase instability. The following part of the section is devoted to the description of the fragmentation of nuclear matter in the framework of a statistical model. Possible experimental indications of the occurrence of a phase transition and the multifragmentation regime are discussed at the end of Sec. 1.

In Sec. 2, we consider the hadron-gas region. We discuss the details of the equation of state in this phase and theoretical models that describe the dynamics of heavy-ion

collisions. The main attention in this section will be devoted to the description of possible ways of obtaining information about canonical parameters of the equation of state such as the temperature, the volume (density), the entropy, and the pressure in the system. We also devote much attention to the results of the analysis of this information. The available experimental data on the production of strange particles from the hadron-gas phase are discussed in the final part of the section; this is of interest in connection with the search for signals indicating the formation of a quark–gluon plasma.

In Sec. 3, we briefly consider the present situation in heavy-ion physics at ultrarelativistic energies. Here, the experimental data are obtained from the interaction of cosmic rays with nuclear photoemulsions.

In Sec. 4 we make some concluding comments.

1. FRAGMENTATION OF NUCLEAR MATTER AT MODERATE EXCITATION ENERGIES

As can be seen from Fig. 1, temperatures $T \lesssim 30$ MeV and a density $\rho \lesssim 2\rho_0$ are attained in heavy-ion reactions at beam energies up to 200 MeV/nucleon. One of the fundamental questions that arise in the investigation of this region is that of the manner in which this intermediate highly excited nuclear system will decay. This process is extremely complicated, and its complete theoretical description is very difficult and involved. It is therefore necessary to look for approximate schemes that reflect the main physical facts.

Wide use is made of models in which the decaying nuclear system is regarded as infinite and experimentally observed quantities such as the yield of light particles (nucleons, deuterons, tritium nuclei, helium-3, α particles) are calculated using the concepts of thermodynamic and chemical equilibrium.

For a temperature below the critical value ($T_c \simeq 15$–20 MeV), the equation of state predicts the typical van der Waals behavior that is currently widely discussed in the literature.[8–19] The existence of a liquid–gas phase transition is characteristic of systems with short-range repulsion and long-range attractive forces. The presence of the long-range Coulomb repulsion does not affect this property of the system. If the temperature exceeds the critical value, the surface energy of a "hot" fragment disappears,[20] and transition to the gas phase becomes unavoidable. This transition is revealed by the fact that in nucleus–nucleus collisions at high energies only the lightest nuclear fragments are observed experimentally.

In Sec. 1, we discuss the expansion and fragmentation of a nuclear system that is not too highly excited. Using a nucleon–nucleon interaction of Skyrme type, we consider a nuclear-matter equation of state that preserves all the interesting features of the coexistence of two phases. We then investigate the process of expansion of the initially heated region of the nucleon participants and its transition into the region of phase instability, and we establish the characteristic time scales; we then discuss the experimental conditions needed for separation of the phases. We present models of statistical multifragmentation, which combine elements of thermodynamics and the important effects of a finite nuclear system. Signals of a phase transition and a brief description of the experimental data on multifragmentation are given in the final part of the section. The dynamical conceptions underlying the multifragmentation process are not considered in the present review. The dynamical theory has not yet been developed to the level of predictive strength, although the first successful attempts in this direction have already been made (see Refs. 21 and 22).

Nuclear-matter equation of state at moderate excitations

The properties of nuclear matter are usually characterized by two canonical variables—the density ρ of the system and its temperature T. It must be borne in mind that nuclear matter is a simplified picture of real excited systems. A heavy-ion collision does not realize a situation corresponding to infinite nuclear matter, and global equilibrium cannot be reached at high bombarding energies. The assumption that statistical equilibrium is established in nuclear collisions must be tested by the application of microscopic theories and investigation of the evolution of the system from the nonequilibrium stage to the stage of at least local equilibrium.

The investigation of the thermodynamic properties of nuclear matter is usually based on an equation of state derived from microscopic models for the nucleon–nucleon interaction,[23] or from phenomenological models of nuclear matter like the Skyrme model,[24] or from the relativistic mean-field theory of Walecka.[25] In Refs. 26 and 27, the first attempts were made to go beyond the mean-field approximation and investigate the properties of composite particles (clusters) embedded in a hot nuclear medium.

For the following discussion it is desirable to have a reliable equation of state that reflects all the interesting features of the coexistence of two phases but is at the same time sufficiently simple and transparent. We consider a nuclear-matter equation of state obtained on the basis of a nucleon–nucleon interaction of Skyrme type.[28] If this interaction, which ignores the velocity dependence of the forces, is used, the nuclear-matter equation of state takes a very simple form.

We consider symmetric nuclear matter. At temperature $T = 0$, the energy density of the system is written as

$$E(\rho) = \tau(\rho) + v(\rho), \tag{1}$$

where

$$\tau(\rho) = \frac{\hbar^2}{2m}\frac{3}{5}\left(\frac{3\pi^2}{2}\right)^{2/3}\rho^{5/3} \tag{2}$$

is the kinetic-energy density and $v(\rho)$ is the density of the effective interaction. Various parametrizations of $v(\rho)$ exist.[15] As restrictions on the parametrization of $v(\rho)$ we use, in addition to the binding energy

$$E_B = E(\rho_0)/\rho_0 = -16 \text{ MeV} \tag{3}$$

per nucleon and the saturation density $\rho_0 = 0.17\text{F}^{-3}$, the compressibility

$$K = 9\rho_0^2 \left.\frac{\partial^2 (E(\rho)/\rho)}{\partial \rho^2}\right|_{\rho=\rho_0} \tag{4}$$

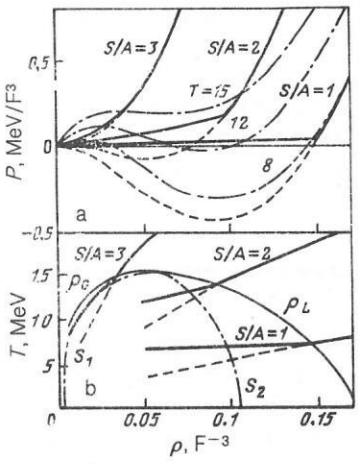

FIG. 2. Density dependence of the pressure (a) and temperature (b): a) the chain curve is the T isotherm, the continuous curve is the isentrope calculated by means of the Maxwellian construction for the equilibrium of two phases, and the broken curve is the same for a superheated liquid; b) the thin continuous curve is the T–ρ phase diagram, the thick continuous curve and the broken curve are the same as in (a), and the chain curve bounds the metastable region determined by the condition $\partial P/\partial\rho = 0$.

In the following calculations, we shall use the analytic expression

$$v(\rho) = a_1\rho^2 + a_2\rho^{7/3} + a_3\rho^{8/3} \tag{5}$$

of Ref. 29 with the parameter values $a_1 = 8818.25$ MeV/F^{-3}, $a_2 = 1371.06$ MeV·F^4, and $a_3 = -556.55$ MeV·F^5, for which we obtain $K = 180$ MeV.

To obtain the equation of state at finite temperature, we assume that the effective interaction will be the same as in the case $T = 0$, and we take into account the entire effect of the temperature in the kinetic-energy density

$$\tau(\rho, T) = \left(\frac{1}{\pi^2\hbar^3 m}\right)\int \frac{p^4\,dp}{\exp\left[(p^2/2m - \tilde{\mu})/T\right]+1} \tag{6}$$

of a Fermi gas with nucleon-number density

$$\rho(\tilde{\mu}, T) = \frac{2}{\pi^2\hbar^3}\int \frac{p^2\,dp}{\exp\left[p^2/2m - \tilde{\mu})/T\right]+1}. \tag{7}$$

Since the effective interaction does not depend on the temperature, the specific entropy of the Fermi gas takes the form

$$S/A = \left(\frac{5}{3}\tau - \tilde{\mu}\rho\right)\Big/\rho T. \tag{8}$$

The chemical potential μ can be calculated in terms of the free energy, this giving

$$\mu = \tilde{\mu} + \partial v/\partial\rho. \tag{9}$$

The pressure (equation of state) is determined as

$$P = \rho^2\,\frac{\partial E(\rho, S)}{\partial\rho}\Big|_S = \frac{2}{3}\tau - v(\rho) + \frac{\partial v}{\partial\rho}. \tag{10}$$

To discuss the effect of compression, it is convenient to separate the total energy into the thermal energy $E_T(\rho,T)$ and the compression energy $E_c(\rho,T)$:

$$E(\rho, T) = E_T(\rho, T) + E_c(\rho)\rho + E_B\rho_0, \tag{11}$$

where

$$E_c(\rho) = E(\rho, T = 0)/\rho - E_B. \tag{12}$$

Extensive numerical investigations in the framework of the liquid-drop model[30] have provided the two most widely used functional forms for $E_c(\rho)$:

$$E_c(\rho) = K_l(\rho - \rho_0)^2/(18\rho\rho_0); \tag{13}$$

$$E_c(\rho) = K_q(\rho - \rho_0)^2/(18\rho_0^2), \tag{14}$$

and these can be employed for the parametrization of the equation of state.

Before we begin to discuss the main properties of the equation of state, we give some approximate thermodynamic relations needed for qualitative discussions in the following sections. In the low-density limit ($\rho\Lambda^3 \ll 1$) we have

$$\rho(\mu, T) = \frac{4}{\Lambda^3}\exp(\mu T); \tag{15}$$

$$\tau(\rho, T) = \frac{3}{2}\rho T; \tag{16}$$

$$S(\rho, T)/A = \frac{5}{2} - \ln(\rho\Lambda^3/4); \tag{17}$$

$$P_T(\rho, T) = \rho T, \tag{18}$$

where $\Lambda = (2\pi\hbar^2/m_N T)^{1/2}$ is the nucleon thermal wavelength. On the other hand, for temperatures below the Fermi energy $\varepsilon_F = (\hbar^2/2m_N)(3\pi^2/2)\rho^{2/3} \simeq 38$ MeV the following expansion can be used:

$$S/A = \frac{m_N}{\hbar^2}\left(\frac{2\pi}{3}\right)^{2/3} T/\rho^{2/3}; \tag{19}$$

$$\tau(\rho, T) = \frac{m_N}{2\hbar^2}\left(\frac{2\pi}{3}\right)^{2/3} T^2\rho^{1/3}. \tag{20}$$

We now turn to a discussion of the equation of state. The upper part of Fig. 2, which is taken from Ref. 31, shows the pressure P as a function of the density ρ at fixed temperature (isotherm) and at fixed entropy (isentrope). It is readily seen that the nuclear matter behaves as a van der Waals gas. The critical temperature is about 16 MeV. Walecka's theory[25] gives $T_c \simeq 20$ MeV and a harder equation of state if the parametrization (5) is used. In Ref. 27, the influence of clustering effects on the critical temperature was investigat-

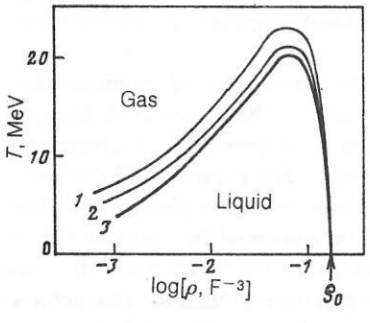

FIG. 3. Phase diagram of hot nuclear matter. The boundary curves for the coexistence of the two phases are calculated in the Hartree–Fock approximation without explicit allowance for clusters (curve 1), with allowance for only deuterons (curve 2), and with allowance for all light clusters up to $A = 4$ (curve 3). The clusters are taken into account in the "ladder" approximation.[31]

ed. As follows from the results presented in Fig. 3, the critical temperature is lowered when correlation effects are taken into account, but this takes us outside the framework of mean-field theory.

The lower part of Fig. 2 shows the phase diagram of nuclear matter. The boundaries of the phases (the thin continuous curves in Fig. 2) are identified by the symbols ρ_G and ρ_L for the gas and liquid phases, respectively. The spinodals s_1 and s_2 bound the region in which the nuclear matter becomes dynamically unstable, i.e., the region in which the compressibility K [see (4)] becomes negative. The region between the boundary curves ρ_G and ρ_L and the spinodals s_1 and s_2 corresponds to the metastable region. The significance of the region of metastability and the region of dynamical instability will be discussed below when we consider the evolution in time of an initially compressed droplet of nuclear matter in the direction of the region of coexistence of two phases.

The stage of expansion of the nuclear system and liquid–gas phase transition

In order to discuss the phase-transition processes, we assume that the heated and compressed intermediate nuclear system expands, say isentropically, until it reaches the region of phase instability. During this expansion stage, the density of the system decreases to the value of the decay density, which is fixed at the moment when the mean free path of the various clusters that have formed becomes comparable with the diameter of the system.[1)]

We consider the various situations that can be realized in heavy-ion collisions.

Static treatment

We first discuss the static case and consider the isentrope for a superheated liquid with $S/A = 3$ (broken curve in Fig. 2). In this case, the experimental conditions are such that the pressure remains positive in the complete range of densities. If we assume that the density of the system is approximately $\rho_0/3$, then the intermediate nuclear system decays before the region of coexistence of the two phases is reached. As can be seen from Fig. 2, the curve $S/A = 3$ is the critical isentrope, above which the nuclear matter is always in a homogeneous phase. In Ref. 18, the value $S/A \simeq 3.3$ of the critical entropy was found on the basis of an equation of state that differs only little from the one given above. The connection between the critical entropy and observable effects will be discussed below.

If we follow along the isentropes with S/A values equal to 1 and 2 to the region of coexistence of the two phases, the two different limiting situations shown in Fig. 2 are possible. The broken curve shows the path in the ρ-T plane if the existence of the two-phase separation is ignored, i.e., if the liquid becomes superheated without decaying into liquid and gas phases. The path must be continued into the instability region, where the matter becomes hydrodynamically unstable. The process of decay of the system takes place as a spinodal breakup into constituent parts,[33] i.e., this is a process that takes place from a homogeneous system which has arrived at a situation in which the smallest fluctuations of the density will spontaneously grow until the nonlinear effects restrict the growth. In contrast to the nucleation mechanism, i.e., to the formation of nucleating centers of a new phase, which takes place in the metastable region, the spinodal breakup into constituent parts does not require an activation energy (see the review of Ref. 34 on this subject). It appears to us that the formation of fragments from an initially homogeneous medium by chaotic growth of instability is an attractive scenario for multifragmentation of nuclei.

The other situation depicted in Fig. 2 is realized under the condition that thermodynamic equilibrium between the phases is established at any instant of time. The entropy of the two-phase mixture can be calculated by means of the Maxwell construction,

$$S/A = x(\rho, T) S_G + (1 - x(\rho, T)) S_L,$$

where

$$x = \frac{\rho_G}{\rho} \frac{\rho_L - \rho}{(\rho_L - \rho_G)} = \frac{A_G}{A}$$

is the mixing coefficient, equal to the ratio of the particles in the gas phase to the total number A of particles. The probabilities given by ρ_L and ρ_G are shown in Fig. 2.

We now turn to the metastability region. Here, the transition to the gaseous phase becomes the only one possible if the thermal quantum fluctuations make it possible to overcome the corresponding potential barriers, this leading to the formation of critical bubbles (nucleating centers), which ultimately grow into the new phase.[32,35] Nucleation due to thermal and quantum fluctuations was investigated in Ref. 32 on the basis of a field-theoretical approach. It was shown that a phase transition of nuclear matter can develop only in a very restricted region of the phase diagram for temperatures that remain only a few mega-electron-volts below the critical temperature. This is due to the fact that for lower temperatures there always exists a potential barrier that strongly hinders the formation of bubbles or droplets that could then grow into the new phase. The phase transition is restricted to the region near the spinodal. For small values of the entropy, $S/A < 1$, there exist only compound nuclei that shed their excitation basically by the evaporation of particles, the emission of γ rays, and by fission. This estimate is in close agreement with the results of the statistical model of multifragmentation, in the framework of which it was shown that compound nuclei do not exist at a temperature above the "cracking" temperature of 4–6 MeV and the corresponding specific entropy $S/A \simeq 1$ (see the discussion below of the statistical theory of fragmentation for more information).

Dynamical treatment

The possible development of a phase transition depends to a large degree on the time needed for the system to pass through the region of metastability. Using the Maxwellian construction, we assume that the region of coexistence of the two phases is formed instantaneously, and we consider the stage of expansion of the heated droplet of nuclear liquid—the fireball. The equations that must be solved are[31]

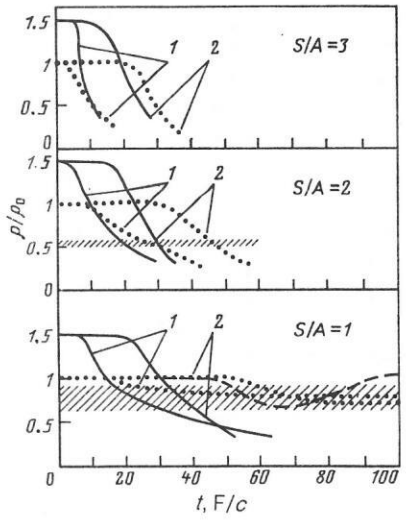

FIG. 4. Time evolution of the density in two volume elements for adiabatic expansion and different initial compressions $\varkappa = \rho/\rho_0$: 1) peripheral cell situated at distance 0.8 of the fireball radius at the initial time of expansion; 2) central cell. The metastable region is hatched. For $S/A = 1$ and $\varkappa = 1$ one observes a monotonic expansion (dotted curves) when the Maxwellian construction is introduced or oscillations appear (broken curve) which could be associated with monopole vibrations.

$$\partial R\,(m,\ t)/\partial t = v\,(m,\ t);$$
$$\partial v\,(m,\ t)/\partial t = -4\pi R^2 \partial P/\partial m;$$
$$\frac{1}{\rho} = \frac{4\pi}{3}\left(\frac{R^2}{m_N}\right)\frac{\partial R}{\partial m};\quad \frac{\partial E}{\partial t} = \frac{P}{\rho^2}\frac{\partial \rho}{\partial t},$$

where $R(m,t)$ is the radius of a mass shell containing mass m and moving with velocity $v(m,t)$. The initial condition is specified by the compression $\varkappa = \rho(t=0)/\rho_0$ at the time $t = 0$.

Figure 4 illustrates the expansion of a nuclear droplet containing 200 nucleons. It shows the time development of cells situated at the center and at the periphery of the fireball.

For isentropes with $S/A > 2$ there is no pronounced difference between the cases when one does and does not consider the Maxwellian construction, since the pressure $P(\rho,T)$ is basically positive and the rapid expansion is not retarded. The situation is significantly changed for $S/A = 1$ and $\varkappa = 1$. In this case, the droplet of nuclear liquid is stable but expands very slowly, since the controlling force is almost zero. If the Maxwellian construction is ignored, the mass shell begins to oscillate when the system enters the metastable region (see also Ref. 36). The obtained oscillation period is approximately 40 F/c and agrees well with the time of monopole vibrations given by the relation $\tau_{MP} = \hbar/15$ MeV = 41 F/c. Since the isentrope $S/A = 1$ is very close to the isotherm $T = 8$ MeV (see Fig. 2), we expect that for a temperature below 8 MeV the heated liquid drop will strongly resemble an ordinary compound nucleus in its properties. Compared with the conclusion drawn above for the static picture of the phase transition, the treatment of the final time of the expansion restricts the development of the coexistence of two phases to a region close to the critical temperature. For temperatures below 8 MeV, the expansion of the fireball is strongly retarded, so that the instability region can be reached only when the initial compression of the fireball is comparatively great, $\varkappa > 1.5$, but such conditions cannot be realized experimentally.

The situation can be characterized as follows. For temperatures below 8 MeV ($S/A \lesssim 1$) compound nuclei are mainly formed. For temperatures between 8 and 12 MeV ($1 \lesssim S/A \lesssim 2$) the formation of two coexisting phases is very difficult, but the introduced energy and the initial compression are sufficient to carry the intermediate system to the instability region, where the system decays. For temperatures near the critical value a phase transition can occur, but clear signals of the actual transition are absent, since the majority of the produced particles are light.

Statistical theory of nuclear fragmentation

Using a simple equation of state, we have considered above how an initially compressed and heated nuclear system can evolve into the region of instability or into the two-phase region. In this section, we shall consider the final stage of the interaction, namely, the decay of the excited nuclear system. For the theoretical description, we use the statistical approach. We assume that the degree of excitation of the intermediate nuclear system can be characterized by a temperature that does not exceed the critical value $T_c \simeq 20$ MeV. Figure 5 illustrates the variety of fragmentation processes in the different temperature regimes. At low temperatures, we have only compound nuclei, but with increasing temperatures we obtain a fairly characteristic set of distributions, which range from a U shape to a rapidly decreasing distribution function at high temperatures. The appearance of the U-shaped mass spectrum serves as a signal that we are observing a multifragmentation process in which fragments are produced in a wide range of masses with almost equal probabilities. The rapidly decreasing mass spectrum indicates that the system decays mainly into light particles such as nucleons, deuterons, tritium nuclei, helium-3 and α particles, which are components of the gaseous phase of nuclear matter. Figure 5 also shows a fission-type process, which, appearing already at an excitation energy of order 10 MeV,

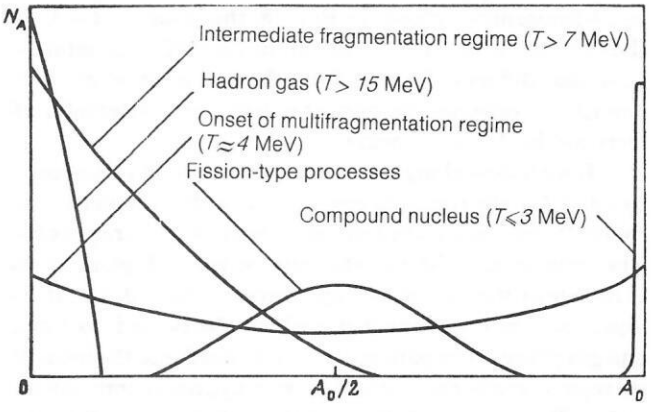

FIG. 5. Schematic representation of the mass distribution for different types of fragmentation process as a function of the temperature T of the complete system. The scale is logarithmic.

differs from the fragmentation processes and will not be considered in the present paper.

Fragments with $Z > 2$ have been observed at high and intermediate energies in proton–nucleus interactions (see, for example, Refs. 37–44), and also in nucleus–nucleus collisions in a wide range of energies of the primary nucleus.[45–51] With regard to proton–nucleus reactions, in which complex fragments have been measured for proton energies of several giga-electron-volts, the multifragmentation process is preceded by the knocking out of several nucleons from the target nucleus by the high-energy proton. In accordance with the scenario described above, the excited residual nucleus begins to expand and breaks up when a certain critical density is reached. The theoretical description of a nucleus–nucleus collision and the subsequent transition to the fragmentation regime is even more complicated, since it is necessary to take into account the dependence of the interaction process on the impact parameter, and also simultaneously consider the decay of not only the excited spectators but also the nucleon participants.

Various models are used for the theoretical description of the multifragmentation of comparatively weakly excited nuclear matter. They include the modified evaporation approach to decay of compound nuclei,[52] direct "cleaving" of a fragment (cold fragmentation),[53,54] statistical emission of fragments from an excited intermediate nuclear system (Refs. 15, 26, and 55–64), breakup of the target nucleus into "small pieces" by means of the projectile nucleus,[65–67] dynamical treatment of the fragmentation in the framework of mean-field theory,[21] and the use of percolation theory to describe the fragmentation process.[68,69]

In this section we shall consider the statistical model of multifragmentation, following Refs. 61, 63, and 64. The model is fairly general and contains interesting features characteristic of a finite system. Further, we shall present some interesting predictions of the model about the temperature at which the compound nucleus "expires," the connection between multifragmentation and possible experimental manifestations of a liquid–gas phase transition, and also the percolation approach to fragmentation. At the end, we discuss some characteristic experimental data on multifragmentation.

Statistical fragmentation model

Following Refs. 61, 63, and 64, we assume that at the time of decay the intermediate nuclear system consists of M fragments, each of which is characterized by a mass and charge (A,Z), energy $E_{A,Z}$, and other quantum numbers needed to determine the internal state. The number of fragments with given values of A and Z, $N_{A,Z}$, is related to the total multiplicity M by

$$M = \sum_{A,\,Z} N_{A,\,Z}. \tag{21}$$

The set of numbers $\{N_{A,Z}\}$ characterizes the various ways of breaking up the system into fragments. The conservation laws for the mass A_0, the charge Z_0, and the total energy E_0 require fulfillment of the relations

$$\sum_{A,\,Z} N_{A,\,Z}A = A_0, \quad \sum_{A,\,Z} N_{A,\,Z}Z = Z_0, \quad \sum_{A,\,Z} N_{A,\,Z}E_{A,\,Z} = E_0. \tag{22}$$

The last equation of (22) shows that for a simplification we have assumed for all nuclei with the same (A,Z) the same total energy. We shall see below that the energy $E_{A,Z}$ is a known function of the temperature, so that the temperature of the system can be found in terms of the energy conservation law.

The probability of the given configuration $\{N_{A,Z}\}$ is

$$W(\{N_{A,\,Z}\}) = \frac{1}{\xi} \frac{V_f^{M-1}}{\left(\frac{1}{A_0}\sum\limits_{A,\,Z} N_{A,\,Z}A^2\right)^{3/2}\left(\frac{m_N A_0 T}{2\pi\hbar^2}\right)^{3/2}} \times \prod_{A,\,Z}\left[\frac{1}{N_{A,\,Z}!}\left(g_{A,\,Z}e^{S_{A,\,Z}(T)}\right)^{N_{A,\,Z}}\right], \tag{23}$$

where ξ is the normalization constant, and $g_{A,Z}$ is the degeneracy factor of the internal quantum state of the fragment. In the derivation of (23), we have taken into account the conservation of the total momentum and the position of the system's center of mass. This is particularly important in the case of a low total multiplicity M, this case corresponding to the low-temperature regime, which is precisely where the fragmentation process occurs. In (23), the quantity V_f is the volume accessible for free motion of the fragments. For a given observable quantity Q, which may be, for example, the temperature, total entropy, multiplicity M, mass distribution, etc., the mean value is found in accordance with

$$\bar{Q} = \Sigma Q(\{N_{A,Z}\})\, W(\{N_{A,Z}\}). \tag{24}$$

The direct calculation of (24) is in practice very difficult because of the large possible number of ways in which the nucleus can be broken up. Even if one does not consider the isospin degrees of freedom, one obtains about $2\cdot 10^8$ different possibilities for a nucleus with mass number $A_0 = 100$. Therefore, wide use is made of approaches (Refs. 15, 26, 55–57, and 59) in which one considers infinite systems, and the most probable division of the system is calculated. The total mass, charge, and energy are conserved only on the average. In this case, one does not take into account at all one of the most important effects of the finite size of the system—the effect of the Coulomb interaction between the clusters, which is something that is particularly important in the case of low-temperature decay. In this energy region comparatively large fragments can be formed. At higher temperatures, when the system decays into small pieces, the neglect of the Coulomb interaction becomes more justified.

In Refs. 61, 63, and 64, the Monte Carlo method was used to calculate the mean values in accordance with Eq. (24). This method permits a complete treatment of the effects of the finite size of the system without recourse to artificial restrictions on the possible ways in which the nucleus can fragment. In other words, the use of the Monte Carlo method makes it possible to simulate to a certain degree the complicated process of decay of originally homogeneous nuclear matter into arbitrary fragments. This in fact is the final stage in the evolution of an excited and compressed "piece" of nuclear matter when the instability region is reached. The

main process of matter redistribution is due to spinodal decay and (or) a randomly growing instability, as discussed above in connection with the consideration of the behavior of an excited droplet of nuclear liquid.

The crucial quantity that determines the probability of a definite breakup $\{N_{A,Z}\}$ of the nucleus is the associative entropy. It can be calculated by means of the liquid-drop model, generalized to finite temperatures. For the energy and entropy we have, respectively,

$$E_A = \begin{cases} \frac{3}{2}T - B_{A,Z}^{\exp}, & A \leqslant 4, \\ \frac{3}{2}T + \left(W_0 + \frac{T^2}{\varepsilon_0}\right)A + \left(\beta - T\frac{d\beta}{dT}\right)A^{2/3} + \gamma\frac{(A-2Z)^2}{A} \\ + \frac{3}{5}\frac{Z^2 e}{R_{A,Z}}\left(1 - \frac{R_{A,Z}}{R_{A,Z}^c}\right), & A > 4; \end{cases} \tag{25}$$

$$S_{A,Z} = \begin{cases} \frac{5}{2} + \ln\left(\frac{m_N AT}{2\pi\hbar^2}\right)^{3/2}, & A \leqslant 4, \\ \frac{5}{2} + \ln\left(\frac{m_N AT}{2\pi\hbar^2}\right)^{3/2} + \frac{2T}{\varepsilon_0}A - \frac{d\beta}{dt}A^{2/3}, & A > 4, \end{cases} \tag{26}$$

where $B_{A,Z}^{\exp}$ are the experimental binding energies of the fragments (A, Z), $W_0 = -16$ MeV, $\gamma = 25$ MeV, and the constant $\varepsilon_0 = 16$ MeV characterizes the internal energy T^2A/ε_0 of a fragment. Equations (25) and (26) contain two new elements. First, the surface energy $A^{2/3}\beta(T)$ depends on the temperature and tends to zero for $T \geqslant T_c$, since in this case, as we have seen above, a liquid phase of nuclear matter does not exist. This is a direct consequence of the van der Waals behavior of the nuclear matter, which disappears above the critical point. Details of the calculation of the surface energy can be found in Ref. 20. Second, the Coulomb interaction between the clusters has been calculated in the decay stage in the Wigner–Seitz approximation, which was found to be very effective. The parameters $R_{A,Z}$ and $R_{A,Z}^c$ are, respectively, the radius of the cluster (A, Z) and the radius of the Wigner–Seitz cell in which the fragment is embedded.

The free volume accessible for the motion of the fragments is not an adjustable constant, as in Refs. 55 and 62, but depends on the widths $2d$ of the "gap" between the fragments and the total multiplicity of the decaying system,

$$V_f = \{[1 + d\,(M^{1/3} - 1)/R_0]^3 - 1\}\,V_0, \tag{27}$$

where $R_0 = 1.17A^{1/3}$ and $V_0 = (4\pi/3)R_0^3$ is the volume of the system at zero excitation energy. Thus, the free volume V_f given by (27) possesses the necessary properties at low and high values of the multiplicity.

Model predictions and comparison with experimental data

Mean temperature and mean multiplicity. Figure 6 shows the mean temperature as a function of the excitation energy for three different regions of mass numbers. The results were obtained by the Monte Carlo method described above.[64,70] It can be seen from Fig. 6 that the behavior changes rapidly in a narrow region near the cracking temperature T^*; at the same time, the compound-nucleus state expires and the multifragmentation process comes into play. The onset of the multifragmentation regime is signaled by a rapid growth in the specific heat of the system (see Refs. 62 and 70). The rapid transition is due to the fact that at the cracking temperature the gain in the surface energy of the system by the formed fragments is compensated by transformation of excitation energy into translational motion of these fragments. The mutual influence of these two competing processes is a typical manifestation of the effects of the finite size of the system. At temperatures somewhat exceeding T^*, the mass spectrum has a U shape, indicating that all fragments have an approximately equal probability of formation.

There appear to be strong experimental indications of the existence of a cracking temperature. Compound nuclei in the mass region $A_0 \simeq 200$ with degree of excitation characterized by a temperature 5–6 MeV have recently been observed.[71]

It can be seen from Fig. 6 that at excitation energies above 7 MeV/nucleon the system behaves like a free gas if the initial nucleus is sufficiently heavy. For lighter compound nuclei the free-gas limit is reached only in the case when a sufficient number of fragments is produced. Figure 7 shows the multiplicity M as a function of the excitation energy for three different nuclei. It can be seen that near the cracking temperature the total multiplicity is low and that it then gradually increases with increasing excitation energy. At $T \simeq 11$ MeV, the total multiplicity increases more sharply, indicating that the fragments must be only light. This is illustrated for the case $A_0 = 100$ by showing additionally the multiplicity $M_<$ with fragments $A < 4$. This transition is also a physical consequence of the model. Since light clusters, which, it is assumed, are constituents of the gaseous phase, do not have excited states, they occupy a comparatively small part of the accessible phase space. But at temperatures above $T \simeq 11$ MeV the total multiplicity can be increased only by the formation of a large number of light fragments. Therefore, $M_<$ increases, whereas the multiplicity of heavy fragments decreases. The temperature corresponding to this transition point is below the critical value $T_c = 16$ MeV but

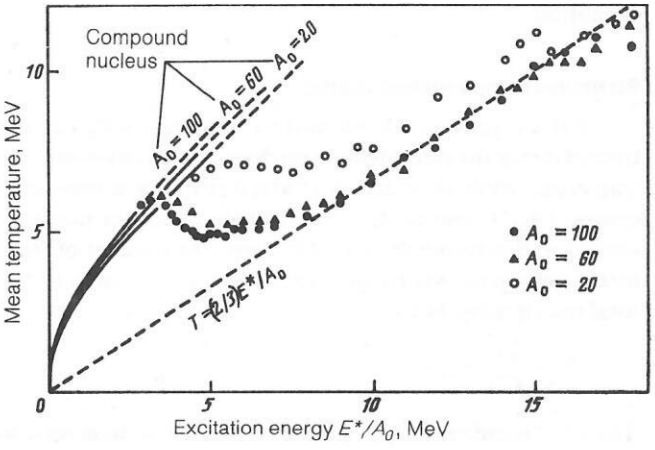

FIG. 6. Dependence of the temperature on the excitation energy for three different initial masses A_0. The broken line shows the limiting relationship for a gas of classical particles.

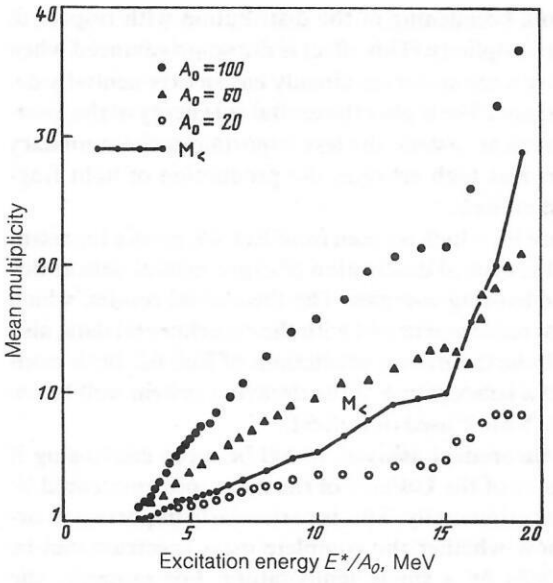

FIG. 7. Multiplicity of primary fragments as a function of the excitation energy. The continuous line shows the results for the case $A_0 = 100$ when only clusters with $A < 4$ are considered.

varies monotonically with it. The transition temperature would be equal to T_c if the gas phase consisted solely of nucleons.

Our discussion (see also Ref. 70) shows the close connection between the transition at $T \simeq 11$ MeV and the liquid–gas phase transition discussed mainly for an infinite system.[8–19] Therefore, $T \simeq 11$ MeV could be called the equivalent temperature of the liquid–gas transition in finite systems.

Liquid–gas phase transition. It is now of interest to compare the results obtained for fragmentation of a finite system with the result that follows from considering infinite nuclear matter, as was done at the beginning of this section. In Fig. 8, we show once more the phase diagram for infinite nuclear matter [cf. Fig. 2(b)] together with the density–temperature dependence obtained in the multifragmentation model. For $S/A \lesssim 1$, the system can be regarded as a heated compound nucleus. This agrees well with the predictions of Refs. 31, 32, and 35. The system then becomes superheated, and large fluctuations appear in the decay density. The calculated decay density is near $\rho_0/3$ and is in the region in which infinite nuclear matter becomes dynamically unstable. At the critical point ($T_c \simeq 16$ MeV, $\rho = \rho_0/3$) the total specific entropy is $S/A_0 \simeq 3.2$, in reasonable agreement with the results of the calculation for infinite nuclear matter.[18]

In Refs. 17 and 42, the experimental cross sections for the fragment yield were described by a power-law dependence $A^{-\tau}$ in agreement with Fisher's condensation theory.[72] From the obtained behavior of the exponent τ it was concluded that the liquid–gas phase transition occurs at the critical temperature $T_c \simeq 12$ MeV. In contrast, in Ref. 70 it was shown that the power-law dependence gives in the best case information about the cracking temperature T^*, at which there exists a relatively wide fragment mass spectrum, but not about the critical temperature T_c, when light clusters are dominant. Moreover, it must be borne in mind that the power law $A^{-\tau}$ was used to describe the experimental mass spectrum, which is not primary and, therefore, includes the effects of evaporation and secondary decay processes.

Percolation theory of fragmentation. Recently, percolation models[68,69] have been used to describe the manifold of mass spectra shown schematically in Fig. 5. The percolation treatment is based on a simple criterion for the binding of nucleons into a complex fragment. The nucleus is regarded as a lattice whose faces are occupied by nucleons. The probability of occupation of a particular face is determined by the percolation parameter $\mathcal{P}$. If $\mathcal{P} \simeq 1$, then all faces are occupied and one large nucleus if formed. For $\mathcal{P} \simeq 0.6$, formation of a compound nucleus is impossible, and the mass spectrum has a U shape. For still lower values of the parameter $\mathcal{P}$ the mass spectrum goes over into an exponentially decreasing function, indicating that only light clusters are formed. In Ref. 73, some predictions of the percolation theory, which describes fairly well the mass spectrum without recourse to any nuclear information, were compared with the predictions obtained in the framework of the multifragmentation model. Comparison of the behavior of the multiplicity of particles with $A \geqslant 4$ calculated in the percolation approach with the corresponding results of the multifragmentation model revealed that the quantity $1 - \mathcal{P}$ is approximately proportional to the excitation energy of the system. Of course, the qualitative agreement between these two theories is not complete. For example, the onset of the fragmentation regime takes place very rapidly in the multifragmentation model but rather smoothly in the percolation approach. This is explained by the fact that in the percolation theory the temperature dependence of the binding energy of the nucleus is not taken into account. These problems are discussed in more detail in Ref. 73. One of the reasons for the successful

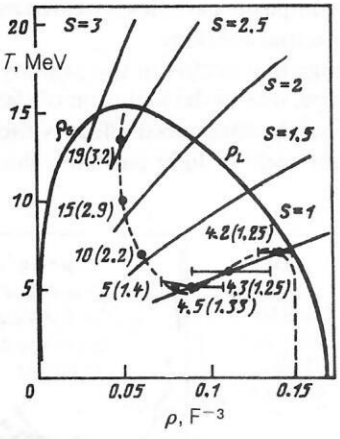

FIG. 8. Phase diagram for infinite nuclear matter. The heavy curve shows the boundary of coexistence of the phases ρ_L and ρ_G. The thin continuous curves illustrate the path of the system in the case of isentropic expansion (the corresponding values of the specific entropy are shown). The broken curve plots the results of calculation of the decay density and mean temperature of our finite system. The numbers next to the curve are the corresponding values of the excitation energy and the entropy (in brackets). The uncertainty in the value of the decay density in the region of temperatures 5–7 MeV is due to the onset of the multifragmentation regime (see Figs. 6 and 7).

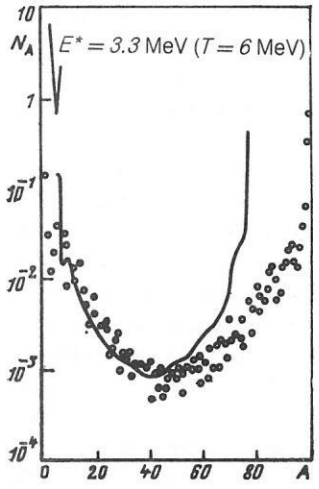

FIG. 9. Primary (open circles) and averaged secondary (curve) fragmentation spectra calculated by the Monte Carlo method. The mean multiplicities of the fragments for these cases are, respectively, $M_1 = 1.5$ and $M_2 = 12.6$.

application of the percolation model is that the inclusive mass spectrum does not contain sufficient physical information to permit separation of the purely statistical elements of the experimental data from the essential physical content.

Statistical multifragmentation and secondary decays of fragments. So far we have discussed only the primary mass spectrum without considering the subsequent decay of the produced fragments. In Ref. 64, a two-stage model was developed to calculate a mass spectrum that can be compared with experiment. The first stage describes the formation of a fragment as a result of breakup of an excited intermediate nuclear system in the framework of the fragmentation model presented above. This process takes place in a time of approximately 10^{-22} sec, i.e., almost an order of magnitude faster than the ordinary evaporation process. The evaporation of nucleons and heavier composite particles is treated as a second stage, following the initial breakup.

Figure 9 shows the change that occurs in the primary spectrum, which has a U shape, due to the inclusion of the evaporation processes. The most pronounced effect is the significant enhancement of the yield of light particles, this leading to a broadening of the distribution with respect to the total multiplicity. This effect is not so pronounced when the primary mass spectrum already has an exponentially decreasing shape. The higher the excitation energy of the intermediate nuclear system, the less important is the secondary decay, since at high energies the production of light fragments is dominant.

Figure 10, which is taken from Ref. 64, gives a representation of the typical description of experimental data at different bombarding energies. The theoretical results, which are in reasonable agreement with the experimental data, also agree with the theoretical predictions of Ref. 62. Both models predict a temperature of the decaying system well below the value 15 MeV used in Ref. 52.

The theoretical analysis would be more convincing if the existence of the U shape of the mass spectrum could be verified experimentally. This is particularly important in order to know whether the complete mass spectrum can be characterized by a single temperature. For example, the presence in the spectrum of heavy fragments with mass up to the mass of the target nucleus (Fig. 10) is a clear indication that not all fragments derive from a single source. Very heavy fragments are probably formed in distant peripheral collisions. In order to obtain a deeper picture of the reaction mechanisms, we require correlation measurements between the heavy fragments and light particles.

2. HADRON-GAS PHASE

We now turn to the consideration of the part of the phase diagram in Fig. 1 designated as "hadron gas." This phase is formed in collisions of nuclei with an energy above about 200 MeV/nucleon and is accompanied by strong heating ($T \gtrsim 30$ MeV) and compression ($\rho \gtrsim 2\rho_0$) of the nuclear matter. Under these conditions, as was shown in Sec. 1, a liquid–gas phase transition does not occur, and one could therefore expect the equation of state to have a simpler form and to be able to extract this information more readily from observable quantities. However, with increasing energy the mechanism of the nucleus–nucleus interaction becomes even more complicated, since possibilities appear for the production of new particles, meson—and under certain conditions quark—degrees of freedom are "unfrozen," relativistic ef-

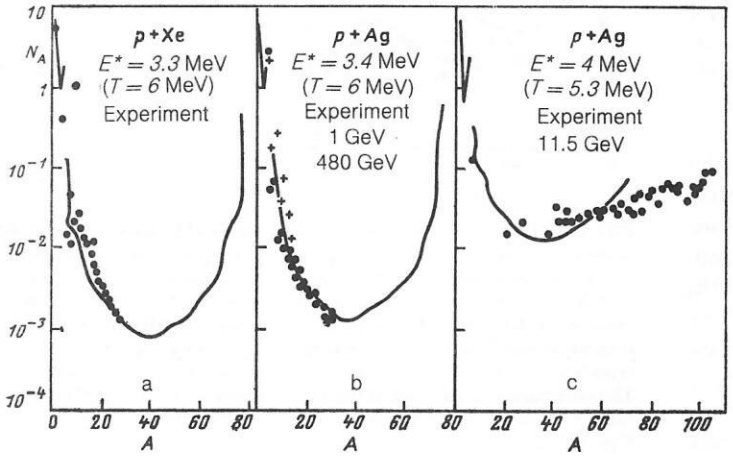

FIG. 10. Comparison with experiment of the calculated mass distribution for the reactions p + Xe at energies 80–350 GeV (Ref. 42) (a), p + Ag at 480 MeV (Ref. 41) (b), and 11.5 GeV (Ref. 74) (c). In the figure we show the adopted initial excitations of the nuclei (per nucleon) and the corresponding temperatures.

fects occur, and the interaction process becomes strongly nonequilibrium. Therefore the acquisition of information about the hadron-gas state requires as a necessity a theoretical and experimental study of the conditions of establishment of complete or local thermodynamic equilibrium in the system.

Canonical parameters of the equation of state such as the temperature, density, entropy, pressure, etc., can be experimentally estimated only using the decay products of the system. It is therefore extremely important to understand to what point of the interaction a measured quantity corresponds. The solution to this problem depends on the experimental method employed to obtain the data. This being the case, it is particularly important to investigate quantities that are conserved during the interaction process or some stage of it, for example, the entropy, and also to study "tagged" particles, for example, particles with nonzero strangeness.

We begin with a brief discussion of the nature of the equation of state in this region of the phase diagram and the main theoretical models used in this range of energies, and we then turn to an analysis of the variables that characterize the equation of state. We discuss the conditions of thermalization of the excited intermediate system and the behavior of the temperature as deduced from the slope of the inclusive particle spectra, and also a method of estimating the volume of the decaying system and the baryon density associated with it. Knowledge of the temperature and density gives us an indication of the part of the phase diagram occupied. We also consider a possible estimate of the entropy using the measured ratio of the numbers of deuterons and protons. We give the results of an analysis of the momentum flux of the particles produced in a heavy-ion collision; this can give information about the pressure due to the compression of the nuclear matter. We also attempt to estimate the compression coefficient of the excited nuclear matter using the pion excitation function. In the final part of the section, we present the results of investigation of the production of strange particles, which carry information about the local properties of the hadron phase formed in the early stage of heavy-ion interactions.

Equation of state of the hadron gas

At the beginning of Sec. 1, we presented a simple equation of state of weakly excited nuclear matter, the potential energy depending only on the density, while the kinetic energy contained the contribution of the ordinary thermal energy. At high excitation energies (high temperatures), the equation of state must be improved in several aspects. First, the equation must be relativistically covariant and, second, it must reflect the new features of this energy region, which arise largely through the production of particles such as pions and kaons and through the excitation of resonances, among which the $\Delta(1232)$ is particularly important. Kaon production introduces a further new element, namely, conservation of strangeness.

From what has been said it is clear that a complete field-theoretical treatment is hard to realize; in fact, it may not be necessary for the dynamical approach to heavy-ion collisions, in which a number of simplifying assumptions (see below) and phenomenological approximations can be made in order to achieve a description of the essentially new characteristic features.

With regard to the nucleon degrees of freedom, there exists the relativistic mean-field model developed by Walecka.[25,75,76] This theory is relativistically covariant, self-consistent from the thermodynamic point of view, and renormalizable. In Walecka's field-theory model,[25] the nucleon field interacts with the scalar meson field σ and the massive vector field $\mathscr{A}^{\mu}$. The corresponding Lagrangian is

$$\mathscr{L} = \bar{\psi}\left[\gamma^{\mu} - (i\partial_{\mu} - g_v \mathscr{A}_{\mu}) - (m_N - g_s\sigma)\right]\psi + \frac{1}{2}\partial_{\mu}\sigma\,(\partial^{\mu}\sigma) - \frac{1}{2}m_s^2\sigma^2 - \frac{1}{4}F_{\mu\nu}F^{\mu\nu} + \frac{1}{2}m_v^2\mathscr{A}_{\mu}\mathscr{A}^{\mu}, \quad (28)$$

where m_N, m_s, and m_v are, respectively, the masses of the nucleon, scalar meson, and vector meson. Further, g_s and g_v are the scalar and vector coupling constants, and

$$F^{\mu\nu} = \partial^{\mu}\mathscr{A}^{\nu} - \partial^{\nu}\mathscr{A}^{\mu} \quad (29)$$

is the field tensor of the vector field. In Refs. 75 and 76, the sigma potential is taken in the form of a potential of fourth degree in σ, this permitting a more realistic fitting to the experimental data of the compressibility and the effective mass.

The partition function for the system is

$$\mathfrak{Z}^{\mathrm{T}} = \mathrm{Tr}\, e^{-(H-\mu N)/T}, \quad (30)$$

where the chemical potential μ can be expressed in terms of a path integral in Euclidean space and calculated in the mean-field approximation for infinite nuclear matter. The equations for the baryon-number density, the scalar density, the energy density, and the pressure can be represented in the form

$$\rho_B = \frac{2}{\pi^2}\left(\frac{m_N c^2}{\hbar c}\right)^3 \int k^2\,dk\,(f^+(k) - f^-(k)); \quad (31)$$

$$\rho_S = \frac{2}{\pi^2}\left(\frac{m_N c^2}{\hbar c}\right)^3 m^* \int \frac{k^2\,dk}{(k^2 + m^{*2})^{1/2}}\,(f^+(k) + f^-(k)); \quad (32)$$

$$E = \frac{1}{2}\frac{(\hbar c)^3}{(m_N c^2)^2}C_v^2\rho_v^2 + \frac{(m_N c^2)^4}{2C_s^2(\hbar c)^3}(1 - m^*)^2 + \frac{2}{\pi^2}\frac{(m_N c^2)^4}{(\hbar c)^3}\int k^2\,dk\,(k^2 + m^{*2})^{1/2}(f^+(k) + f^-(k)); \quad (33)$$

$$P = \frac{1}{2}\frac{(\hbar c)^3}{(m_N c^2)^2}C_v^2\rho_B^2 - \frac{(m_N c^2)^4}{2C_s(\hbar c)^3}(1 - m^*)^2 + \frac{2}{3\pi^2}\frac{(m_N c^2)^4}{(\hbar c)^3}\int \frac{k^4\,dk}{(k^2 + m^{*2})^{1/2}}\,(f^+(k) + f^-(k)), \quad (34)$$

where

$$f^{\pm} = [\exp((k^2 + m^{*2})^{1/2} \mp \nu)/\overline{T} + 1]^{-1},\ \overline{T} = T/m_N c^2 \quad (35)$$

are, respectively, the nucleon and antinucleon distribution functions. The values of $C_v^2 = (g_v^2/\hbar c)(m_N/m_v)^2 = 195.7$ and $C_s^2 = (g_s^2/(\hbar c)^3)(m_N/m_s)^2 = 266.9$ were adjusted in order to describe the binding energy and density of the nuclear matter. The chemical potential μ is related to ν by

$$\mu = \nu m_N c^2 + C_v^2\rho_B\frac{(\hbar c)^3}{(m_N c^2)^2},$$

and the effective mass must be determined in a self-consistent manner from the equation

$$m^* + C_s^2 \left(\frac{\hbar c}{m_N c^2}\right)^3 \rho_s = 1. \tag{36}$$

The energy per particle, E_A, is given by

$$E_A = E/\rho - m_N c^2, \tag{37}$$

and the specific entropy can be represented in the form

$$S/A = (E - P - \mu\rho_B)/T\rho_B. \tag{38}$$

We now consider some limiting cases.

For $\rho_B \Lambda^3 \ll 1$, we obtain the equation of state of a rarefied gas (see Sec. 1):

$$E = \frac{3}{2} T\rho_B + \rho_B, \quad P = T\rho_B. \tag{39}$$

For densities $\rho < \rho_B$ and $T \lesssim T_c \simeq 21$ MeV the equation of state given above reflects the van der Waals behavior studied recently in connection with the liquid–gas phase transition in Refs. 32 and 35.

In the limit $\rho_B \to \infty$ and for arbitrary T (infinite-density limit)

$$E = \frac{1}{2} c_v^2 \rho_B^2 \frac{(\hbar c)^3}{(m_N c^2)^2} + \frac{3}{4} k_F \rho_B \hbar c; \tag{40}$$

$$P = \frac{1}{2} C_v^2 \rho_B^2 \frac{(\hbar c)^3}{(m_N c^2)^2} + \frac{1}{4} k_F \rho_B \hbar c, \tag{41}$$

and the high-temperature limit ($T \to \infty$) gives

$$E = \frac{7\pi^2}{90} \frac{T^4}{(\hbar c)^3}, \quad P = \frac{1}{3} E. \tag{42}$$

Thus, Walecka's equation of state covers the entire region of the energy–density variables in which the nucleon degrees of freedom play the decisive part. Despite the fact that relativistic mean-field theory has such attractive and realistic features, its inclusion in the dynamics of heavy-ion collisions is still far from realization.

For example, the compression energy of nuclear matter was calculated in Ref. 76. It was found that the equation of state is extremely sensitive to the choice of the compressibility K and the nucleon effective mass m^* at the saturation density ρ_0. Variation of m^* and K in the range 10–20% leads to a change in the compressibility energy by several times. This demonstrates the impossibility of predicting the properties of nuclear matter on the basis of the currently known properties of the ground state, and is one further indication that for reliable extrapolations it is necessary to study the region of high densities.

At the present time, the equation of state of hot nuclear matter is frequently described in the limit of a noninteracting relativistic gas, as given by Eqs. (33) and (34), in which, in addition, the dependence on m^* is ignored and it is assumed that $C_s^2 = C_v^2 = 0$. The description of the hadron gas is then improved by taking into account the production of other particles and resonances, which are characterized mainly by their masses and degeneracy factors. In the case of pions and other Bose particles, the Bose–Einstein distribution is used instead of the function (35). It is assumed that these Bose particles have zero chemical potential, i.e., that they can be freely produced or absorbed in the hadron gas. Then the equation of state of the hadron gas is determined by the calculation of the chemical potentials, which fix the number of different particles and, ultimately, permit calculation of the pressure $P(\rho, T)$. This simplified equation of state, which treats the noninteracting gas of hadrons as consisting of several particle species in thermal equilibrium, must be improved in the case when the potential and the interaction effects still play a certain part. For example, an additional potential energy, dependent only on the total baryon density, was introduced in Refs. 77 and 78, it being assumed that all the nucleon resonances are subject to the same interaction.

It should be noted that the thermodynamic approach provides no answer to the question of what and how many particles and resonances must be included in the treatment. The question is answered purely practically—one chooses the minimal number of particles that make it possible to obtain agreement with experiment in a particular case. However, from the general theoretical point of view the introduction of new particles into the scheme for describing the hadron phase as a mixture of ideal gases is tantamount to taking into account the strong interactions. As was shown by Hagedorn[79] in the framework of the bootstrap hypothesis, systematic allowance for the strong interactions requires the introduction of a continuous spectrum of masses m with an exponentially increasing density of states:

$$\rho^{\mathrm{H}}(m) = a \left(\frac{T_0}{m}\right)^3 \exp\left(\frac{m}{T_0}\right), \tag{43}$$

where T_0 is the limiting temperature. Of course, the equation of state and thermodynamic properties of such a hadron gas will differ from what is expected for a mixture of noninteracting gases.

It becomes obvious from this discussion that relativistic heavy-ion physics gives us a great stimulus for investigating the behavior of nuclear matter in the region of energy densities in which the equation of state is known very poorly. Comparison of theory with experimental facts will give information about the degree to which investigation of the hadron gas in the framework of the simplified equation of state corresponds to reality.

Models of high-energy nucleus–nucleus collisions

At the present time we are forced to use simplified and phenomenological approaches to describe the inelastic collisions of two nuclei at high energies. The reason for this is that the traditional low-energy schemes of approximation of the many-body Schrödinger equation are here invalid. For example, the time-dependent Hartree–Fock method,[80] which became an effective tool at energies up to 10 MeV/nucleon, cannot be used, since it presupposes a large mean free path and ignores two-particle collisions. Moreover, because particle production processes appear at sufficiently high energies, a rigorous quantum-mechanical description becomes even more complicated.

As a rule, the phenomenological approaches are restricted to the use of classical representations. The main

models and approaches currently employed are as follows:

(i) the method of nuclear–molecular dynamics;

(ii) the intranuclear-cascade model;

(iii) the hydrodynamical description.

We shall give here a very brief description of their main distinguishing features. For a more detailed review, we refer the reader to Refs. 81 and 82.

The method of nuclear–molecular dynamics. The collision of two nuclei can be described at the classical level in exactly the same way as the interaction of two molecular beams. For a given nucleon–nucleon potential, the system of classical equations of motion for interacting nucleons is solved (see Refs. 22 and 83–90), and the total distribution function of the A particles is found. Actually, one solves the classical Liouville equation, and in this respect the procedure is more fundamental than the solution of kinetic equations. The main problem in the method is that the classical potential does not give a good approximation to NN scattering or to the description of the nucleus as a bound system. Fundamental difficulties arise when one attempts to extend this method to relativistic energies and to take into account pion production processes.

Depending on the relationships between the characteristic space–time scales for the actually considered problem, the method of nuclear–molecular dynamics can be simplified. The characteristic spatial scales are the range of the forces $\hbar/m_\pi c$, the mean free path $\lambda = 1/\rho\sigma_{NN}$ of a particle in the nucleus, and the radius $R = r_0 A^{1/3}$ of the nucleus. If $\hbar/m_\pi c \ll \lambda$ $(\rho/\rho_0 \ll 1)$, the cascade model is a good dynamical approximation, whereas the hydrodynamical description must be used when $\lambda \ll R$. In practice, these inequalities are not satisfied all that rigorously, and therefore it is not that simple to estimate the internal accuracy of the hydrodynamical and cascade descriptions.

Intranuclear cascade. In the intranuclear-cascade model, the complicated process of nuclear collisions is represented as a succession of nucleon–nucleon collisions and is described by a kinetic Boltzmann equation for the single-particle distribution function. The main input information consists of the integral and differential cross sections of elastic and inelastic interaction of the particles. The cascade models that have been developed[91–103] take into account many additional effects, for example, Fermi motion of the nucleons, Pauli-principle restrictions, the effects of binding of the nucleons in the nucleus, the relativistic kinematics, the production of pions, Δ isobars, kaons, and other particles and their subsequent interaction in accordance with the experimental cross sections, and final-state interaction of the nucleons, which leads to the formation of clusters.

The cascade model is only the first, fast stage of the interaction. When the cascade has been completed, the spectator nucleons form excited residual nuclei, and their subsequent behavior must be described in the framework of fragmentation theory (see Sec. 2).

Hydrodynamical description. The hydrodynamical equations are equations for the moments of the single-particle distribution function for the conserved quantities. In contrast to the cascade models, the hydrodynamical description (see Refs. 9, 102, and 104–126) does not proceed from consideration of individual elementary events but from the nuclear-matter equation of state.

In contrast to the cascade model, the effects of the potential energy are taken into account in hydrodynamics through the equation of state. The nonequilibrium nature of the interaction process can be taken into account by means of the effects of viscosity and heat conduction. In the hydrodynamical approach, one can describe fairly reliably the process of expansion of strongly compressed nuclear matter, whereas the cascade model applies, in principle, only for the case of low densities. However, it is important to recall that hydrodynamics is valid under the condition $\lambda \ll R$ and when local thermodynamic equilibrium is established. Neither of these conditions is satisfied in peripheral collisions, and even in the more appropriate case of central collisions one cannot expect that the nucleons which interact in the surface layer of the nucleus attain the state of local thermodynamic equilibrium.

Despite the obvious restrictions, both the cascade model and the hydrodynamical model can be successfully applied to the description of data on high-energy nucleus–nucleus collisions and have made it possible to extract from experiments valuable information about the reaction mechanism and the basic equation of state of nuclear matter.

Tendencies in the further development of the models. The apparent contradiction between the hydrodynamical description and the cascade model as representatives of the kinetic approach does not have deep significance, since we are concerned merely with a different level of approximation in the description of one and the same physical process. From the kinetic equations giving a more detailed picture of the process one can deduce the hydrodynamical equations. Therefore, in the comparison of the kinetic and hydrodynamical approaches, the key question is that of the equation of state to which a given dynamical equation corresponds. In this connection, great interest attaches to the tendency, which has developed recently, to combine collective and single-particle effects; it consists of constructing models on the basis of other kinetic equations having an equation of state that differs from the ideal-gas equation of state.

In Refs. 127 and 128 the Vlasov–Uehling–Uhlenbeck equation was used. This theoretical approach includes not only the average field of the nucleons but also two-particle interactions with allowance for the Pauli principle. The equation for the single-particle distribution function has the form

$$\frac{df}{dt} = \frac{\partial f}{\partial t} + \mathbf{v}\frac{\partial f}{\partial \mathbf{r}} - \nabla U \frac{\partial f}{\partial \mathbf{p}} = -\int \frac{d^3p_2\, d^3p_1'\, d\Omega_2'}{(2\pi)^3}\sigma(\theta)\, v_{12} \times [ff_2(1-f_1')(1-f_2') - f_1'f_2'(1-f)(1-f_2)]\,\delta(\mathbf{p}+\mathbf{p}_2-\mathbf{p}_1'-\mathbf{p}_2'). \quad (44)$$

The main input information for this equation is the potential U of the average field and the nucleon–nucleon differential cross sections $\sigma(\theta)$. The potential of the average field is calculated in the framework of the Skyrme model, $U(\mathbf{r})$ being a function of the local density. When the collision term in (44) is omitted, we obtain the Vlasov equation. The intranuclear-cascade model follows from Eq. (44) when $U = 0$.

In Ref. 129 the use of the Boltzmann–Enskog equation

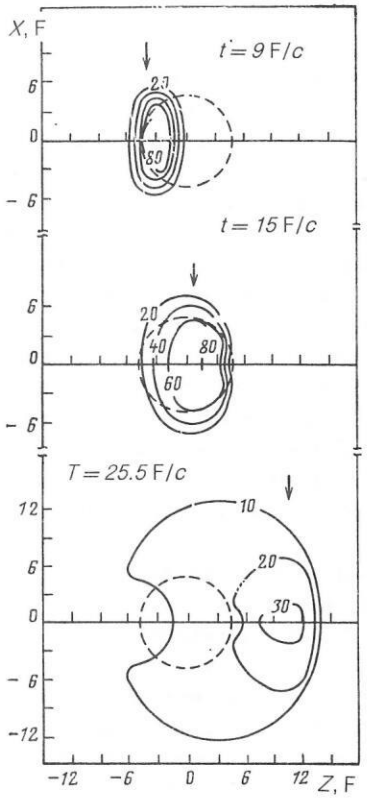

FIG. 11. Temperature field of cascade nucleons produced in central Ar + Ar collisions (800 MeV/nucleon) at different instants of time t (the values on the contours of constant temperature are given in mega-electron-volts). The broken circle of radius $R_{1/2} = 1.07A^{1/3}$ F indicates the position of the undisturbed target nucleus; the arrow corresponds to the position of the center of the projectile nucleus if it were to pass through the target nucleus without interaction.

was proposed. Compared with (44), it does not contain the potential $U(\mathbf{r})$ of the average field, but in the collision term allowance is made for the two-particle correlations, which prohibit the approach of two nucleons to each other, to distances less than ~ 1 F. This leads to an equation of state of van der Waals type.

This developing tendency is very attractive for the theoretical investigation of the basic properties of hot and compressed nuclear matter formed in the course of a high-energy heavy-ion collision. It must, however, be borne in mind that the measured characteristics are sensitive to different degrees to the equation of state. Therefore, the search for quantities that are most sensitive to the equation of state and make it possible to discriminate between the different models is of exceptional interest (see also the discussion of the compression effects below).

Temperature of the hadron gas

The temperature of the excited system of hadrons is one of the most important canonical parameters that determine the state of the system. It characterizes the mean energy of the random motion per particle. However, the concept of a temperature is a simplification of the real situation, since it presupposes the establishment in the system of thermodynamic equilibrium. The time of relaxation of the excited system to the state of thermodynamic equilibrium can be estimated in the framework of kinetic theory. The solution of the Boltzmann equation for an infinite medium[130] and the estimates made in the framework of the cascade model[99,131] for the collision of nuclei in the range of energies 0.8–2 GeV/nucleon show that each nucleon must undergo three or four collisions before the equilibrium state is established. Allowance for the meson degrees of freedom accelerates the attainment of the equilibrium regime.

Figure 11 shows the evolution of the temperature field for a central Ar + Ar collision at energy 800 MeV/nucleon.[103] At the initial time, the heating has a local nature with large temperature gradients, which is an indication that the state of the hadron-gas system is formed far from equilibrium. In the stage of expansion of the excited system, the temperature field becomes more uniform. This indicates that the concept of a temperature is better suited to the description of this final stage of the interaction.

In what follows, we shall consider how far the excited system of nucleons formed in a heavy-ion collision is from the state of thermodynamic equilibrium, and we shall discuss the experimentally deduced values of the temperature.

Thermalization and complete stopping of the nuclei

If the excited system of hadrons, the fireball, decays from the state of thermodynamic equilibrium, its decay products must have an isotropic angular distribution in the coordinate system in which the fireball is at rest. Therefore, the proximity of the state of the decaying system to the equilibrium state can be characterized by the ratio of the mean transverse momentum of the particles to their longitudinal momentum:

$$\mathscr{R} = \frac{2}{\pi} \frac{\Sigma_i p_{\perp, i}}{\Sigma_i p_{\parallel, i}},$$

where the numerical factor $2/\pi$ takes into account the difference between the numbers of degrees of freedom for motion in the longitudinal and transverse directions. In the case of complete thermalization, $\mathscr{R} = 1$.

In recent experiments,[132] the value of $\mathscr{R}$ for the proton participants was measured in collisions of the symmetric systems Ca + Ca and Nb + Nb. Figure 12 shows the distribution with respect to $\mathscr{R}$ in the $\langle p_\perp \rangle$, $\langle p_\parallel \rangle$ plane for individual events. It can be seen that in the case of Ca + Ca collisions at 400 MeV/nucleon the main bulk of the events is rather far from the region $\mathscr{R} = 1$, which is represented in the figure by the diagonal line. The clearly observed peak at small $\langle p_\perp \rangle$ but large $\langle p_\parallel \rangle$ corresponds to the peripheral interaction of the heavy ions, where fragments of the projectile nucleus make the dominant contribution to $\mathscr{R}$. Naturally, there is no contribution to this region if one goes over to central collisions by selecting events with high multiplicity M_c of the secondary charged particles. Then the maximum of the distribution is displaced significantly to the side of the diagonal, but only very few events take place in the region $\mathscr{R} = 1$.

It should be noted that for symmetric systems the indicator of hadron thermalization, $\mathscr{R} = 1$, is identical to the indicator of complete stopping of the colliding ions, when

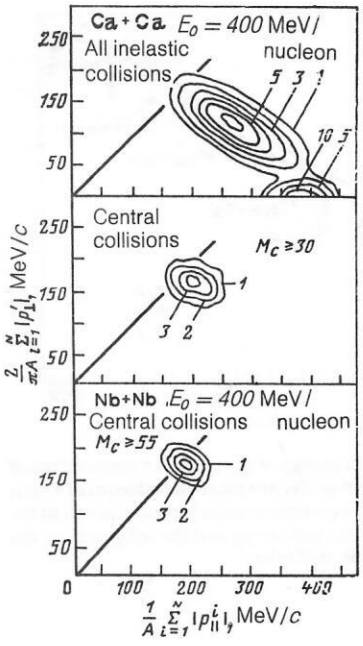

FIG. 12. Contours of constant yield for the distribution with respect to the mean transverse and longitudinal momentum of charged particles produced in all inelastic and central (with high particle multiplicity M_c) Ca + Ca and Nb + Nb collisions at energy 400 MeV/nucleon.[132]

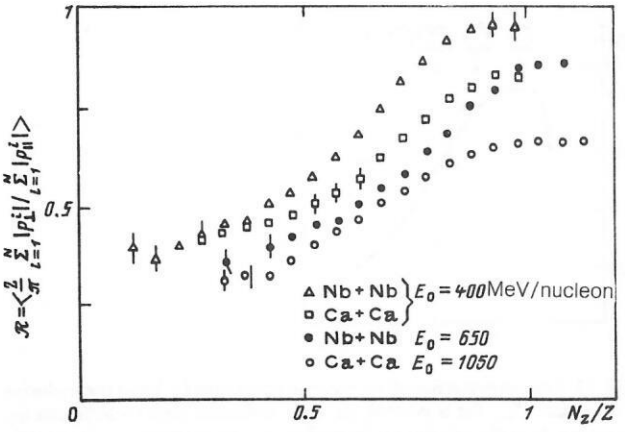

FIG. 13. Dependence of the ratio $\mathscr{R}$, which characterizes the proximity to the state of thermodynamic equilibrium, on the relative number of produced charged particles.[132] The type of reaction is indicated in the figure.

the entire energy of their relative motion is transformed into the random motion of the nucleons and the energy of the produced particles. In this connection one may say of the central Nb + Nb collisions shown in the same Fig. 12 that in a large number of cases they lead to complete stopping of the nuclei, since the maximum of the distribution is situated precisely in the region $\mathscr{R} = 1$.

A comparison of the degree of thermalization attained in different combinations and at different energies of the colliding ions is shown in Fig. 13 as a function of the fraction N_z/Z of the total charge of the particles that can be detected. The increase in the value of $\mathscr{R}$ with increasing multiplicity of the charged particles is due to the decrease in the relative yield of spectator nucleons in a central collision. The spectator nucleons from the projectile nucleus carry a large longitudinal momentum, and this leads to small values of $\mathscr{R}$ in the case of peripheral interactions.

Thus, analysis of the ratio of the mean values of the transverse and longitudinal momentum components indicates that for central Nb + Nb collisions at 400 MeV/nucleon almost complete stopping of the nuclei occurs and the system is in a state very close to thermodynamic equilibrium. On the transition to peripheral collisions, or to lighter nuclear systems, or to higher collision energies, the angular distribution of the particles ceases to be isotropic, this being due to the admixture of leading particles and fragments of the projectile.

The possibility of complete stopping of colliding heavy ions is intimately related to the problem of attaining the maximal energy density needed for the phase transition of the hadrons into a quark–gluon plasma (see Sec. 3). In accordance with the hydrodynamical estimates,[15] two uranium nuclei can still completely dissipate the energy of their relative motion if the energy of the bombarding ion does not exceed 4–5 GeV/nucleon. The energy density then attained is close to the critical value for the phase transition of the hadrons into quarks. With a further increase in the energy and entry into the ultrarelativistic region, complete stopping of the colliding nuclei becomes impossible because of the change in the interaction mechanism, which leads to an increase in the "transparency" of nuclear matter.

Determination of the inclusive temperature

If a source that emits particles is in thermodynamic equilibrium, it is possible to estimate from the slope of the observed inclusive spectrum the "apparent" or "inclusive" temperature by using the relation[2)]

$$E\frac{d^3\sigma}{dp^3} = C_0 E_{\text{cms}} \exp(-E_{\text{cms}}/T_{\text{inc}}). \qquad (45)$$

Although the inclusive temperature T_{inc} extracted in this manner reflects the temperature of the decaying hot fireball, it must be borne in mind that the description of the excited system by the introduction of a single temperature is a rather crude idealization. We have seen above that the temperature field corresponding to the effective source is nonuniformly distributed in space and varies with time. Figure 14 shows the time dependence of the mean temperature $\langle T \rangle$ calculated from the temperature field (see Fig. 11) and T_{inc} determined by (45). The uniform decrease of the temperature $\langle T \rangle$ in the fireball expansion stage is due to the fact that as the particles separate their thermal energy is transformed into the energy of the collective motion of the particles as a common flow. Near the point of decay of the system, the collisions between the particles cease and, therefore, from this moment on, the shape of the momentum distribution of the particles hardly changes. This means that the inclusive temperature T_{inc}, determined from the slope of the spectrum, will no longer depend on the time, this being true up to the time at which the particles are detected. It can be seen from Fig. 14 that the time dependence of T_{inc} does indeed tend to a constant.

Secondary processes like final-state interaction, decay

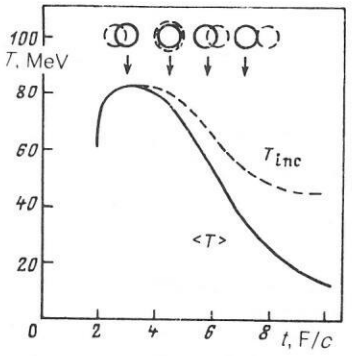

FIG. 14. Time dependence of the mean temperature $\langle T \rangle$ and the inclusive temperature T_{inc} for a central Ar + Ar collision (0.8 GeV/nucleon). Above we show the relative position of the nuclei at the time indicated by the arrow under the assumption that they pass through each other without interaction; the radius of the circles corresponds to $R_{1/2} = 1.07A^{1/3}$.

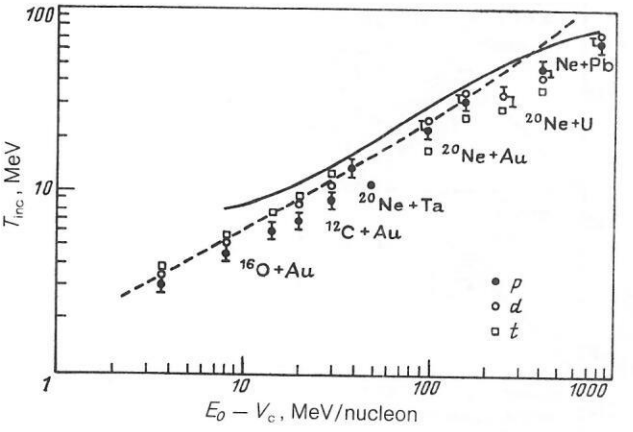

FIG. 15. Dependence on the initial energy of the inclusive temperature of fast protons, deuterons, and tritium nuclei produced in collisions of a light nucleus with a heavy nucleus.[134] The continuous curve corresponds to the Fermi-gas relationship (47) between the energy and the temperature; the broken curve corresponds to the fireball model.

of the Δ isobars, and so forth lead to an additional difference between T_{inc} and $\langle T \rangle$.

The practical application of Eq. (45) to data obtained in nucleus–nucleus collisions requires a certain degree of care. The presence in the inclusive spectrum of particles having a different origin (for example, from the decay of spectator nuclei) or a small admixture of incorrectly identified particles (for example, deuterons in the proton spectrum[133]) can lead to serious distortions of T_{inc}.

It should be noted that instead of (45) one can also use the noninvariant inclusive distribution $d^2\sigma/d\Omega dE$, but it is then necessary to take into account correctly the pre-exponential factor. This method is, in particular, popular at nonrelativistic energies for the determination of the effective temperature and the velocity of the "moving source" from a simultaneous description of the particle spectra at several angles. The experimental data are fitted by the relation

$$\frac{d^2\sigma}{d\Omega\, dE} = \text{const}\, E^{1/2} \exp\left[-(E + E_s - 2E^{1/2}E_s^{1/2}\cos\theta)/T_{inc}\right], \quad (46)$$

where E_s is the kinetic energy of the moving source, corresponding to approximately half the velocity of the bombarding ion.

The results of such an analysis are presented in Fig. 15, where, to separate the participant particles, the spectra have been taken at angles $\theta > 40°$, at which the evaporation component is discarded.[134]

The tendencies in the behavior of the temperature as a function of the bombarding-ion energy E_0 can be qualitatively understood in terms of the Fermi-gas model. From the relation (19),

$$T = \frac{\hbar^2}{m}\left(\frac{2}{3}\pi\right)^{-2/3}\left(\frac{S}{A}\right)\rho^{2/3}. \quad (47)$$

For a qualitative estimate of the density that can be attained and its relationship to the energy E_0, we can use the approximation of a shock adiabat[135]:

$$\rho = \frac{\rho_0}{2}(3 + 5\gamma_{cms}(E_0)). \quad (48)$$

Since the specific entropy S/A varies weakly with E_0, the temperature must increase with the energy of the primary beam approximately as a power, in agreement with the results shown in Fig. 15. The applicability of (48) breaks down in the region $E_0 \gtrsim 1$ GeV/nucleon, where it does not reproduce the appreciable retardation in the growth of the inclusive temperature T_{inc} (E_0). Such behavior of the temperature indicates the need to include in the treatment the production of resonances, in the first place Δ isobars. The Hagedorn model,[79,136] which takes into account a continuous spectrum of resonances with an exponentially increasing density of masses [see Eq. (43)], predicts the existence of a limiting temperature T_0. In Figs. 16 and 17, we have plotted the theoretical curves for two values of T_0 equal to 134 and 200 MeV. The first value of T_0 reproduces well the experimental mass spectrum of the resonances, while the

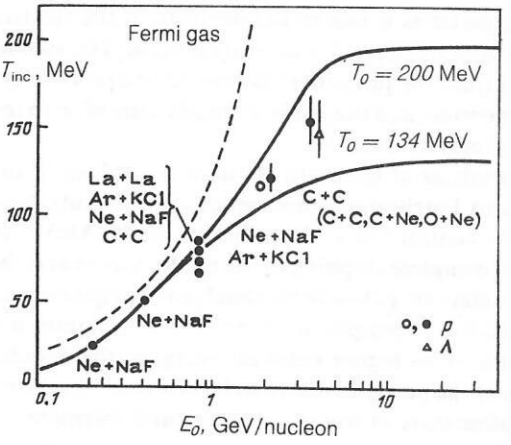

FIG. 16. Inclusive temperature of the baryons as a function of the primary energy for the collision of identical nuclei. The experimental points are taken from Refs. 137–139; the black circles correspond to all inelastic interactions, and the open circles and open triangles to central collisions; the broken curve is the dependence obtained in the Fermi-gas approximation (47); the continuous curves are calculated in accordance with the Hagedorn model with the indicated values of the limiting temperature T_0 [see (13)].

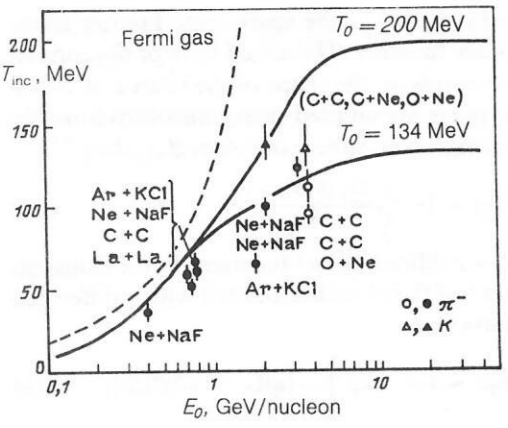

FIG. 17. Inclusive temperature of mesons as a function of the energy of the bombarding ion for a collision of identical nuclei. The notation is the same as in Fig. 16.

second corresponds approximately to the critical temperature of the phase transition of the hadrons into quarks (see Sec. 3). Unfortunately, the existing data do not permit an unambiguous conclusion as to the existence of a limiting temperature. Experiments at higher energies of the primary beams are needed.

With regard to the dependence of the inclusive temperature on the combination of colliding nuclei, for nucleons it is reflected qualitatively correctly by Eq. (47); namely, the transition to heavier systems leads, through the effects of the finite size of the nuclei, to a higher compression and, therefore, to an increase in T_{inc}. In the case of pions, it is necessary to take into account the resonance nature of their production.

In Refs. 137 and 138 it was shown that the inclusive temperature depends on the species of observed particles. As can be seen from Figs. 16 and 17, the temperatures of the pions, protons, and K^+ mesons satisfy the relation

$$T^{\pi}_{inc} < T^{p}_{inc} < T^{K+}_{inc},$$

i.e., in the language of the time dependence of the temperature (see Fig. 14) the kaons are emitted in an earlier stage of the interaction. In agreement with this conclusion is the fact that the mean free paths $\lambda = 1/\sigma\rho$ for these particles are related in the same manner:

$$\lambda^{\pi N} < \lambda^{pN} < \lambda^{K+N},$$

whereas for the thermodynamic treatment of the primary temperatures one would expect $T^{\pi}_{inc} \simeq T^{p}_{inc} \simeq T^{K^+}_{inc}$.

Population temperature

There exists one further way of determining the temperature of a decaying system—using the relative population of the ground and excited states of the nuclear fragments. Such experiments are much more complicated than the inclusive ones. It is necessary to detect γ rays in coincidence with a fragment or the products of its decay, if it is unstable. Moreover, the investigated excited states must cover a sufficiently large part of the excitation spectrum but must not be populated by the decay of other unstable nuclei or more highly excited states of the given nucleus. Recent correlation measurements in the Ar + Au reaction at 60 MeV/nucleon with production of ^{5}Li, ^{6}Li, and ^{9}Be fragments determined a temperature around 4.5 MeV.[140] This value of the temperature describes well the yield of fragments with respect to the masses in the framework of multifragmentation theory (see Sec. 1) but is much lower than the value $T_{inc} \simeq 20$ MeV determined from the slope of the energy spectrum of the fragments.[141] This discrepancy remains an open problem.

Volume and density of the decaying system

In the investigation of the equation of state, the volume V or density ρ of the system, as canonical variables, play the same part as the temperature. Besides the heating of the nuclear matter, it is also made denser in the initial stage of the interaction of the nuclei, this leading to the formation of a region of hot and compressed matter. When the maximal density is attained, the system goes over into the expansion stage with subsequent decay. These features can be traced in the evolution of the density profile shown in Fig. 18 for the case of Ne + U collisions at 400 MeV/nucleon.[101]

Thus, the density and volume of the hadron gas change appreciably during the reaction. However, the experimentally measured characteristics correspond to the moment at which the system decays, when the interaction between the

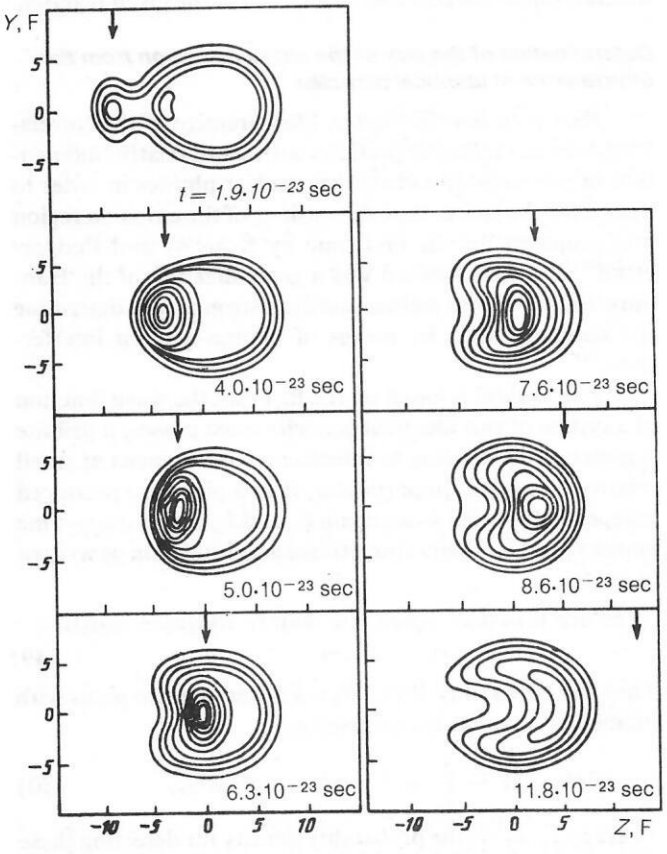

FIG. 18. Diagram of the evolution of the density of nucleons in a central Ne + U collision (400 MeV/nucleon). The outer contour corresponds to the density level 0.02 F^{-3}, and on the transition to each next level the density increases by 0.04 F^{-3}. The arrow indicates the position that the center of the projectile nucleus would have if it were to move without interaction.

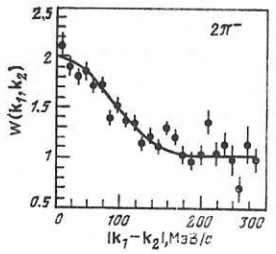

FIG. 19. Correlation function (with allowance for Coulomb correction) of two π^- mesons emitted in an Ar + KCl collision at energy 1.8 GeV/ nucleon.[151] The fitted curve is calculated in accordance with Eq. (53).

particles basically stops. Moreover, the extraction of information about V or ρ is a more complicated problem than that of estimating the temperature, since information about the temperature is already contained in the single-particle distribution function, whereas to determine the interaction region it is necessary to measure correlations between the particles.

We begin by considering the correlations of identical particles and the discussion of the results obtained by this method. We shall then present a different method of estimating the decay density of the system using the coalescence radius of composite particles. We conclude this section by considering the dynamical trajectory of the reaction in the T–ρ plane, which makes it possible to estimate the experimental conditions that can be attained in the given reaction.

Determination of the size of the emission region from the interference of identical particles

Pion–pion interferometry. Measurement of the correlations between identical particles with small relative momentum in problems of hadron and nuclear physics in order to determine the space–time dimensions of the emission region was proposed for the first time by Kopylov and Podgoretskiĭ.[142,143] This method was a generalization of the Hanbury-Brown–Twiss method used in astronomy to determine the radius of stars by means of photon–photon interference.[144]

The method is based on the fact that the wave function of a system of two identical particles must possess a definite symmetry, this leading to interference phenomena at small relative momenta. In particular, if two pions are produced independently with 4-momenta k_1 and k_2 at the space–time points x_1 and x_2, their symmetrized amplitude can be written in the form

$$\psi \approx \exp\left[i-(k_1x+k_2x_2)\right]+\exp\left[-i(k_1x_2+k_2x_1)\right]. \tag{49}$$

Then the probability $W(k_1, k_2)$ of observing two pions with momenta k_1 and k_2 is expressed as

$$W(k_1, k_2) \sim \int |\psi|^2 \rho(x_1, x_2)\, d^4x_1 d^4x_2, \tag{50}$$

where $\rho(x_1, x_2)$ is the probability density for detecting these particles in a source at the points x_1, x_2. For uncorrelated particles $\rho(x_1, x_2) = \rho(x_1)\rho(x_2)$, and the relation (50) reduces to

$$W(k_1, k_2) \sim 1 + |\rho(k_1 - k_2)|^2, \tag{51}$$

where $\rho(k_1 - k_2) \equiv \rho(q)$ is the space–time Fourier transform of the source function. The actual form of the correlation function depends on the shape of the source. If we assume that the pions are emitted instantaneously from the surface of a homogeneous sphere of radius R_H, then[143]

$$W_H(k_1, k_2) \sim 1 + \left[\frac{2J_1(q_\perp R_H)}{q_\perp R_H}\right]^2, \tag{52}$$

where $J_1(y)$ is a modified Bessel function. For a Gaussian distribution $\rho(x)$, if the pions are emitted with a difference in time τ, we have

$$W_G(k_1, k_2) \sim 1 + \exp\{-[\mathbf{q}\mathbf{R}_G + \omega^2\tau^2]/2\}, \tag{53}$$

where

$$\mathbf{q} = \mathbf{k}_1 - \mathbf{k}_2 \quad \text{и} \quad \omega = \sqrt{k_{\perp,1}^2 + m_\pi^2} - \sqrt{k_{\perp,2}^2 + m_\pi^2}.$$

It can be seen from (53) that the correlation function $W(k_1, k_2)$ contains information about not only the spatial distribution of the source but also its lifetime, i.e., the interference method is a means for studying not only geometrical aspects of the reaction but also the dynamics of the process.

In order to estimate correctly the geometrical and time parameters of the source distribution function $\rho(x)$, it is necessary to take into account the possible correlations of the particles in the volume of the source, this leading to the appearance of an additional free parameter Λ in front of the interference term in (52) and (53), and also the effects of Coulomb interaction, the absorption of slow pions by the ambient nuclear medium, and final-state interaction of the particles (see Refs. 145–147).

Proton–proton interferometry. The correlations of two protons with nearly equal momenta are governed by their Fermi nature. The wave function of a pair of protons contains a singlet and a triplet part, $\psi = \psi_1 + \psi_3$ [cf. Eq. (49)], and this leads to an "anticorrelation" effect: The two-proton correlation function $W(k_1, k_2)$ has at $k_1 = k_2$ a minimum, and not a maximum as in the case of the $\pi\pi$ correlations. Moreover, the effects of the interaction of the protons in the final state due to the Coulomb and nuclear forces have a large influence on the shape of the correlation curve.[148–150]

Main results of measurements. Figure 19 shows the correlation function for a pair of negative pions produced in an Ar + KCl collision at 1.8 GeV/nucleon. Fitting of the experimental points by means of the distribution (53) yielded $R_G = 3.0 \pm 0.3$ F.[151] This value corresponds approximately to the region of overlapping of the nuclei for the most probable impact parameter.

Comparing the results of different experiments, one must bear in mind that the deduced parameter R depends on the chosen form of the source function $\rho(x)$. The existing data on the determination of the emission region by pion–pion interferometry are given in Table I together with the radius R_{eq} of the equivalent homogeneous sphere.[152] It can be seen that the size of the source is appreciably greater than the region of strong hadron–hadron interaction and increases on the transition to heavier projectile ions or to smaller impact parameters for a fixed combination of the colliding nuclei. In the study of Ref. 156, made at 3.4 GeV/

TABLE I. Radii of pion emission sources.[152]

Reaction	E_0, GeV/nucleon	Radius, F, from data of original studies (references in square brackets)	R_{eq}, F
Ar+BaI_2	1.8	3.05±1.10 [153]	3.74±1.35
Ar+Pb_3O_4	1.8	3.30±0.93 [153]	4.04±1.14
Ar+Pb_3O_4 (center)	1.8	3.98±0.78 [153]	4.87±0.96
Ar+KCl	2.1	3.12±0.33 [151]	3.82±0.40
Ar+KCl	1.5	4.93±0.44 [154]	6.04±0.54
Ar+KCl (center)	1.2	3.80±0.55 [155]	4.65±0.61
d+Ta	3.4	2.20±0.50 [156]	2.20±0.50
^{4}He+Ta	3.4	2.90±0.40 [156]	2.90±0.40
C+Ta	3.4	3.40±0.30 [156]	3.40±0.30
C+C	3.4	2.75±0.76 [157]	2.75±0.76
C+C (center)	3.4	3.76±0.88 [157]	3.76±0.88

nucleon, it was shown that the emitting region does not depend on the sign of the charge of the detected identical pions.

The correlations of two identical protons were measured in Refs. 156–158. For C + C collisions at 3.4 GeV/nucleon it was shown that for protons from the target fragmentation region ($p < 300$ MeV/c) $R_{eq} \simeq 3$ F is almost twice the radius of the source for fast ($p > 300$ MeV/c) protons and does not change on the transition to central events.[157]

Even in the case of "central" collisions, the data given above are averaged over a fairly wide range of impact parameters. In the recent study of Ref. 159, proton interference measurements were made at fixed multiplicity N_p of the charged particles participating in the interaction, these being mainly protons. Figure 20 shows the dependence of the parameter R_G of the spatial distribution of the source as a function of N_p. For both combinations of the colliding nuclei the radii of the distributions increase monotonically with N_p. If these dependences are approximated by a function of the form

$$R_{eq} = r_0 (N_p A/Z)^{1/3} \sqrt{\frac{5}{2}}, \tag{54}$$

where A/Z takes into account the presence of neutrons in the source, and the factor $\sqrt{5/2}$ transforms the parameter R_G of the Gaussian distribution into the equivalent radius R_{eq} of the homogeneous sphere, we obtain $r_0 = 1.9$ F. Comparing this value with the value $r_0 = 1.2$ F for nuclei in the ground state, we find that the density of the decaying source is about 25% of the saturation density ρ_0.

This result differs strongly from the estimate of the decay density that was also made by the interferometry method in Refs. 138 and 160, in which approximately twofold and fivefold increases in the density were obtained, respectively, in the reactions Ne + NaF → pp + X and Ne + Pb → $K^+K^+ + X$ for data averaged over all impact parameters. The difference is evidently due to the use in Refs. 138 and 160 of R_G instead of R_{eq} in the estimate of the interaction volume, i.e., it is due to the loss of the factor $(5/2)^{3/2}$.

Coalescence of nucleons and the size of the interaction region

Another possibility for estimating the size of the baryon interaction region is the experimentally detected property of scaling of the inclusive spectra for the fragments. It has been found that the cross section for the production of a fragment with mass number A_F can be represented as

$$E_{A_F} \frac{d^3\sigma_{A_F}}{dp^3_{A_F}} = C_{A_F} \left[E_p \frac{d^3\sigma_p}{dp^3_p} \right]^{A_F}, \tag{55}$$

if the difference between the proton and neutron spectra is ignored and the fragment momentum is $p_{A_F} = A_F p_p$. It is found that the constant C_{A_F} does not depend on the fragment emission angle or on the energy of the bombarding nucleus.[161]

In the framework of the coalescence model,[162] nucleons within a sphere of radius p_0 in the momentum space coalesce, forming a fragment. Then the coefficient C_{A_F} can be expressed in terms of the coalescence radius p_0:

$$C^{COAL}_{A_F} = \frac{(N/Z)^{A_F - Z_F}}{Z_F!\,(A_F - Z_F)!} \left[\frac{4\pi p_0}{3 m_N \sigma_R} \right]^{A_F - 1} \tag{56}$$

where N and Z are the numbers of neutrons and protons in the complete interacting system, and σ_R is the reaction cross section.

The thermodynamic theory,[56,163] which presupposes the establishment of chemical equilibrium in the system, also makes it possible to represent the differential cross section for the emission of a composite particle in the form (55). Then for the coefficient C_{A_F} we obtain

$$C^{THERM}_{A_F} = A_F^3 \left(\frac{N}{Z} \right)^{A_F} \exp(E_B/T) \left(\frac{\hbar^3}{V} \right)^{A_F - 1}. \tag{57}$$

Thus, from comparison of the experimental spectra in accor-

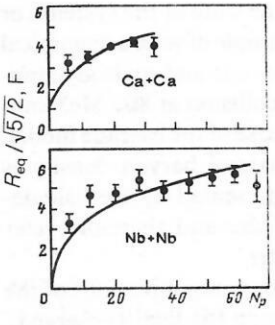

FIG. 20. Radius of a Gaussian source as a function of the proton multiplicity deduced in the experiment of Ref. 159 for the two systems Ca + Ca and Nb + Nb at 400 MeV/nucleon. The approximating curves are calculated in accordance with Eq. (54).

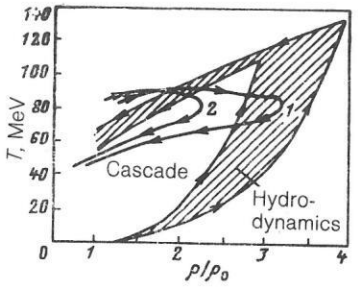

FIG. 21. Dynamical trajectories in the T–ρ phase plane for the state of nuclear matter in a central Ca + Ca collision at energy 800 MeV/nucleon. The hatched region corresponds to the results of hydrodynamical calculations[167] with allowance for the uncertainty in the input parameters; the continuous curves are calculated in accordance with the cascade model[102] with a linear dimension of the cell equal to 1.5 F (curve 1) and 3.0 F (curve 2).

dance with (55) we find the coefficient C_{A_F}, which can be set equal to either the coalescence radius, $C_{A_F} = C_{A_F}^{\text{COAL}}$, or the radius of the equilibrium system, $C_{A_F} = C_{A_F}^{\text{THERM}}$. The studies of Refs. 161, 162, and 164 are still far from a systematic investigation. The baryon decay densities found by this method are $\sim (0.4\text{–}0.6)\rho_0$, a result that does not contradict the size of the region found from the experiments using the identity correlations of two protons. Nevertheless, the physical content of the spatial parameters deduced by these two methods is different. Whereas the interference method carries information about the region from which the particles were emitted, the thermodynamic description uses the volume in which not only thermodynamic but also chemical equilibrium is established. In this connection, it is of interest to note the first results obtained in the determination of the region of emission of complex particles. Interference measurements of *dd* and *tt* correlations have given a value 1.5–2 times greater than the *pp* correlation radius for the ^{16}O + Au reaction at 25 MeV/nucleon,[165] whereas the coalescence radius was found to be practically constant for all fragments up to $A_F = 14$ produced in the Ar + Au reaction at 92 and 135 MeV/nucleon.[166]

Dynamical trajectory in the plane

The information about the evolution of the system shown above in Figs. 11 and 18 can be represented in a compressed form in the T–ρ phase diagram in the form of a dynamical trajectory that indicates the state of the system (or its parts) at a given time t.[97] An example of such a dynamical trajectory, calculated using the cascade and hydrodynamical models for a central Ar + Ar collision at 800 MeV/nucleon, is shown in Fig. 21. For the case of the cascade model, the state in the cell with the maximal baryon density is shown. The hydrodynamics is represented by the calculations of Ref. 167 using the shock adiabat and, therefore, refer to the mean value over all the matter.

Note that the models predict opposite directions of the motion of the states in time, although the final (observed) states of the system agree well. It must be borne in mind that the hydrodynamics presupposes local thermodynamic equilibrium between all particles in the considered volume element. In the cascade model, the hypothesis of local thermodynamic equilibrium is used only to translate the calculated energy distributions into temperature language. The cascade results given in the figure imitate the hydrodynamics, which presupposes the establishment of thermodynamic equilibrium between all baryons in the given volume element. In the final stage of the interaction practically all the nucleons are involved, and therefore the predicted cascade and hydrodynamical trajectories differ very little.

The dynamical trajectories enable us to obtain an idea of the extremal values of the temperature, the baryon density, and the energy density attained for definite combinations of the colliding heavy ions and, on this basis, to choose the optimal reaction.

The experimental determination of ρ and T opens up the basic possibility of testing the behavior of the dynamical trajectories of the state in the phase plane. Unfortunately, the densities determined at the present time by the interference of identical particles correspond to the region $\rho \lesssim \rho_0$. Advance into the region of larger values of ρ involves using interference measurements of particles that interact weakly with nuclear matter (K^+ mesons, leptons, photons), and also separation of the component corresponding to the earlier stages of the interaction (selection of large multiplicities, etc.).

The entropy problem

The investigation of the entropy of a system formed by the collision of relativistic heavy ions can become a method for studying the behavior of nuclear matter in a state far from the ground state. In the process of the collision, the initially highly excited region, characterized by its temperature and volume, expands and cools, i.e., the particles separate, and their velocity vectors become ever more closely oriented along the radial direction. In this process, the stochastic nature of the motion is gradually decreased. In thermodynamic language, this means that the thermal energy is transformed into the collective energy of the flow of particles [we have already investigated this process (see Sec. 1), when we considered the expansion of an excited droplet of nuclear liquid in the direction of the region of coexistence of two phases]. This conversion of the energy is still continued when the collisions between the particles cease. Measured quantities such as the composition and energy spectrum of the particles are "frozen" at this time. From our treatment it is clear that the investigation of a system in terms of the temperature and volume is not simple, since both quantities vary rapidly with the time.

Siemens and Kapusta[168] suggested that instead of the temperature and volume (density) one should study the entropy of the system. The entropy of the system will remain almost constant during the expansion stage and will thus make it possible to "observe" the early stage of the interaction, when the matter was hot and compressed. Cascade[169,170] and hydrodynamical[114,171] calculations confirmed that the entropy hardly changes during the expansion phase.

Following Ref. 168, we can calculate the specific en-

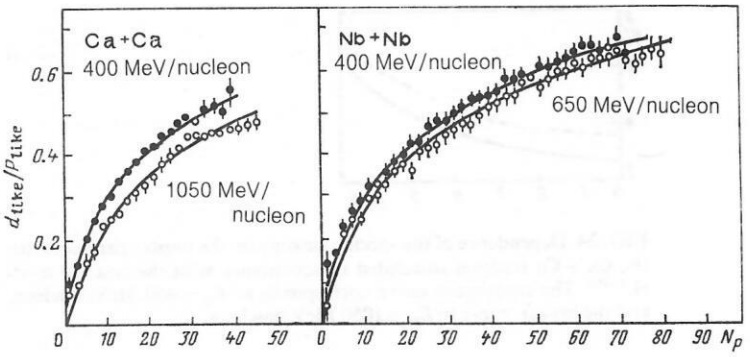

FIG. 22. Ratio of the deuterons to the protons as a function of the number of nonevaporation protons for the two colliding systems Ca + Ca and Nb + Nb at different energies.[175] The curves are the results of fitting of the data with respect to the Sato–Yazaki formula.[176]

tropy in terms of the ratio of the numbers of deuterons and protons, R_{dp}:

$$S/A = \frac{5}{2} - \ln (R_{dp}/3\sqrt{2}). \tag{58}$$

This last relation is obtained by considering an ideal mixture of nucleons, deuterons, tritons, etc., in the limit of a rarefied gas. The use of the inclusive cross sections for the production of the particles[138] made it possible to deduce the "experimental" value of the specific entropy: $S/A \simeq 5.5 \pm 0.5$. This value of S/A is too large if one attempts to explain it in the framework of the ordinary equation of state of nuclear matter. The mysterious increase in the entropy could be explained by invoking the idea of the excitation of new degrees of freedom,[172] but before this is done it is necessary to investigate in detail the applicability of the simple formula (58). For example, the effects of the influence of the medium, which take into account the fact that at the time of freezing the deuterons are still subject to the influence of the ambient medium,[173] and treatment of the subsequent decay of the excited nuclear fragments[167] lead to smaller values of the entropy. Moreover, as we shall show below, the difference between the values of the specific entropy calculated in the framework of the cascade model and the estimates given above reaches two units.

Measurements of the cluster production cross sections by means of a 4π detector[174,175] made it possible to re-examine the entropy problem. Figure 22, which is taken from Ref. 175, gives the ratio of the deuteronlike clusters $d_{\text{like}} = d + (3/2)(t + {}^3\text{He}) + 3{}^4\text{He}$ to the number of protonlike particles $p_{\text{like}} = p + d + t + 2({}^3\text{He} + {}^4\text{He})$ as a function of the proton multiplicity N_p for the two systems. The experimental data show that the cross sections for the production of d, t, ^{3}He, ^{4}He increase monotonically with increasing multiplicity of the charged baryons (or the total charge of the emitted baryons) and then tend to a constant value at high values of the multiplicity. Thus, it follows from these experimental data that there is a strong correlation between the impact parameter and the cluster yield. From the point of view of these new data it became obvious that the thermodynamic models that presuppose chemical equilibrium[177,178] and the initial version of the coalescence model,[162] which predict a cluster yield that does not depend on the size of the source, can be used only for events with high multiplicity (small impact parameters), for which the limit of infinite nuclear matter can be reached asymptotically.

The cascade model makes it possible to calculate separately the ratio R_{dp} and the specific entropy and thus provides us with a fairly good method for investigating the connection between the entropy and the production of clusters as assumed by Eq. (58).

In the recent studies of Refs. 169 and 170, the entropy was calculated in the approximation of independent particles by introducing the probability for population of the single-particle state and a certain volume in the phase space. In the Fermi gas approximation,

$$S = -\int d\gamma \, [f \ln f + (1 - f) \ln (1 - f)], \tag{59}$$

where $d\gamma$ is the volume element of the phase space, containing the usual spin and isospin degeneracy factor, and the distribution function f is normalized to the number of particles A in the system. In the classical limit $\langle f \rangle \ll 1$, and we arrive at the expression

$$S/A = 5/2 - \ln [2^{3/2} \langle f \rangle], \tag{60}$$

and by comparing it with the Siemens–Kapusta[168] formula (58) we obtain

$$R_{dp} = 12 \langle f \rangle. \tag{61}$$

Here R_{dp} is the ratio of the deuteronlike fragments to the protonlike particles. We shall show below that the relation (61) holds only for an infinitely large subsystem. This indicates that the specific entropy must increase on the transition to more peripheral collisions, since, as can be seen from Fig. 22, the ratio R_{dp} tends to zero at small values of N_p. In fact, such a tendency was found in Refs. 170 and 179. In Ref. 170, the evolution of the distribution function f in the phase space was calculated under the assumption that in each volume element into which the system can be divided local thermodynamic equilibrium is established. Such a procedure makes it possible to separate the translational motion from the random motion characterized by the time-dependent temperature field (see Fig. 11). The entropy is calculated by replacing the integration in (59) by a summation over finite elements. It was found that the final value of the entropy is not particularly sensitive to the choice of the size of the partitioning cells. By comparison with the results of Ref. 169, which used a direct partitioning into cells of the six-dimensional phase space, the method of Ref. 170 gives somewhat smaller values of the entropy.

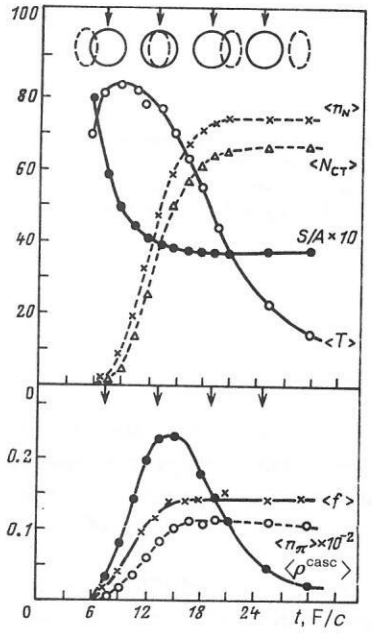

FIG. 23. Evolution of characteristics of central Ar + Ar collisions (800 MeV/nucleon) calculated in accordance with the cascade model.[93,103] The upper part of the figure shows schematically the disposition of the nuclei at the time indicated by the arrow.

In Fig. 23, taken from Ref. 170, we show the time evolution of the entropy, the mean temperature, and the density for the Ar + Ar reaction at 800 MeV/nucleon. As was to be expected, the entropy remains almost constant, whereas the temperature and density decrease rapidly. It should be noted that the entropy hardly changes once the maximum of the overlap density has been reached. Such a tendency has also been observed for heavier systems (Nb + Nb), and also for noncentral collisions.

Figure 24 shows the dependence of the specific entropy on the impact parameter for the Ca + Ca reaction at 0.4 and 1.05 GeV/nucleon. One can clearly see (see also Ref. 179) the increase in S/A with the impact parameter (with decrease in the multiplicity). This means that along the curve R_{dp} shown in Fig. 22 the entropy does not remain constant, in contrast to the assumption of Ref. 175, in which the R_{dp} values were fitted at constant values of the decay density and temperature extracted from the proton spectra. We shall return once more to this problem below.

Figure 25 shows the entropy S/A as a function of the energy of the primary beam for central collisions. The cascade results are compared with the values obtained in Ref. 175 by means of the methods of Stöcker[15] and Kapusta.[18] At low energies, the cascade model does not enable one to give preference to any one of the methods, but at high energies the predictions of the cascade model evidently follow the predictions of the Kapusta model. Although the predictions of the models do not completely agree, it can be seen that they predict values of the entropy less than those obtained by applying the simple Siemens–Kapusta formula (58) to the inclusive measurements of the ratio R_{dp}.

Comparing the R_{dp} values obtained for central

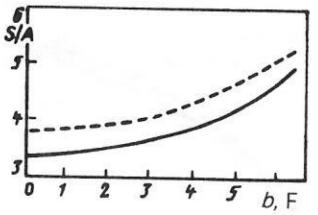

FIG. 24. Dependence of the specific entropy on the impact parameter for the Ca + Ca reaction calculated in accordance with the cascade model.[93,103] The continuous curve corresponds to $E_0 = 400$ MeV/nucleon, and the broken curve to $E_0 = 1050$ MeV/nucleon.

Ca + Ca collisions at 0.4 and 1.05 GeV/nucleon with the mean population numbers $\langle f \rangle$ calculated in terms of the value of the entropy shown in Fig. 24, we see that R_{dp} is smaller by about a factor 2 than follows from the relation (61). The failure of the relation (61) can be ascribed exclusively to the fact that the effects of the finite size were not considered in the derivation of (58). Indeed, the ratio of the quasideuterons to the protonlike particles is given by the general expression

$$R_{dp} = \frac{3}{2} \int \frac{d^3R\, d^3P}{(2\pi\hbar)^6}\, d^3r\, d^3p\, f^{(2)}(\mathbf{r}, \mathbf{p}, \mathbf{R}, \mathbf{P})\, g_D(\sigma, \mathbf{p}), \quad (62)$$

where f^2 is the two-particle distribution function, and g_D is the Wigner transform for the deuteron density. The factor 3/2 derives from the spin–isospin degeneracy, and the integration must be performed with respect to the relative coordinate and the center-of-mass coordinate. In the model of independent particles, we have $f^{(2)} \simeq f(\mathbf{r}_1, \mathbf{p}_1) f(\mathbf{r}_2, \mathbf{p}_2)$. Approximating the deuteron wave function by the Gaussian form

$$g_D(\mathbf{r}, \mathbf{p}) = \frac{1}{\pi^3} \exp\left(-\frac{r^2}{r_d^2} - \frac{p^2}{4} r_d^2 \right), \quad (63)$$

we can integrate in (62) analytically:

$$R_{dp} = \frac{12\langle f \rangle}{\left(1 + \frac{r_d^2}{2R_p^2}\right)^{3/2} \left(1 + \frac{\hbar^2}{m_N T r_d^2}\right)^{3/2}}, \quad (64)$$

where

$$\langle f \rangle = \frac{A_{\text{cas}} \Lambda^3}{4(4R_p^2\pi)^{3/2}} = \frac{\langle \rho \rangle \Lambda^3}{4 \cdot 2^{3/2}}. \quad (65)$$

Here, A_{cas} is the number of particles that undergo at

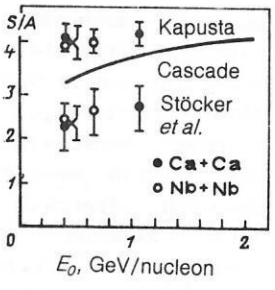

FIG. 25. Dependence of the specific entropy on the kinetic energy of the bombarding ion for central Ar + Ar collisions. The "experimental points," taken from Ref. 175, were obtained using the models of Kapusta[18] and Stöcker *et al.*[15] (see the text).

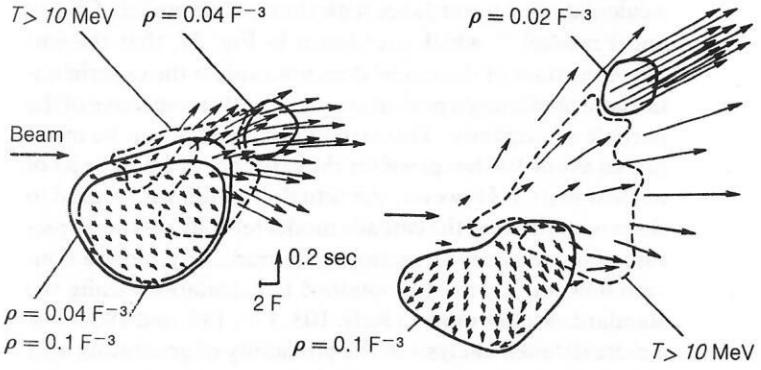

FIG. 26. Velocity field near the time of decay of a system formed by a peripheral ($b = 6$ F) Ne + U collision (400 MeV/nucleon). The figure also shows levels of equal density and temperature. The calculations were made in the framework of the hydrodynamical[15] and cascade[103] models.

least one collision, and R_p is the radius of the emitting source, whose spatial distribution of the nucleons is approximated by a Gaussian curve. Substitution of (65) in (64) reduces the relation for R_{dp} to the form obtained by Sato and Yazaki[176] and used in Refs. 174 and 175 to fit data by means of the two parameters r_d and r_0, it being assumed that $R_p = r_0(2N_p)^{1/3}$. The results of the fitting are shown by the continuous curves in Fig. 22. This fitting procedure is based on the concept of a constant decay density, but this is evidently quite unrealistic for the treatment of noncentral collisions. In the cascade model, R_p (N_p) is a calculable quantity, and, therefore, the data cannot be fitted but one must consider what follows from Eq. (64) for the values of R_{dp}. In addition, the temperature T and the source radius R_p are also not independent, and the effective deuteron radius r_d is also evidently subject to strong influence of the ambient medium.[180] There is no doubt that the finite-size effects, taken into account by (64), reduce the value $12\langle f\rangle$ obtained for infinite matter, bringing it closer to the experimental values. However, it is still necessary to do work on establishing the actual connection between the ratio R_{dp} and the specific entropy for both central and peripheral collisions. Despite the absence of final results of this work, the mystery of the entropy problem has evidently been significantly reduced, at least in the energy range between 0.4 and 2 GeV/nucleon.

Effects of compression

A topic of fundamental interest is that of whether it is possible to verify experimentally the effect of compression predicted by the equation of state and the hydrodynamical calculations.

Figure 26 shows diagrams of the velocity field for the excited hadron gas in the expansion stage, calculated in accordance with the cascade and hydrodynamical models. It can be seen that in the case of noncentral interactions the hydrodynamical description predicts the appearance of a "jet," a stream of particles emitted at a nonzero angle. This effect is due to the pressure P_c produced by compression of the nuclear matter [see Eqs. (10) and (11)].

One cannot say that the first attempts to test these predictions by looking for nuclear shock waves were convincing.[93] It has recently been suggested[181] that the compression energy should be estimated from the energy dependence of the yield of pions from nuclear collisions. Another signal of the compression effect would be the direct detection of a flow of nuclear matter, a subject that is currently attracting much attention of both theoreticians and experimentalists.

Energy fluxes. For each individual event in the center-of-mass system there is defined the energy-flux tensor[3)]

$$F_{ij} = \sum_k p_i^{(k)} p_j^{(k)}/2m,$$

which is then diagonalized. The angle θ_F between the principal axis of the ellipsoid F_{ij} and the direction of the primary beam is called the flow angle. Figure 27 shows the distribution $dN/d\cos\theta_F$ for different values of the multiplicities of the charged particles from the Ca + Ca and Nb + Nb reactions at 400 MeV/nucleon (see Refs. 184 and 185). It is

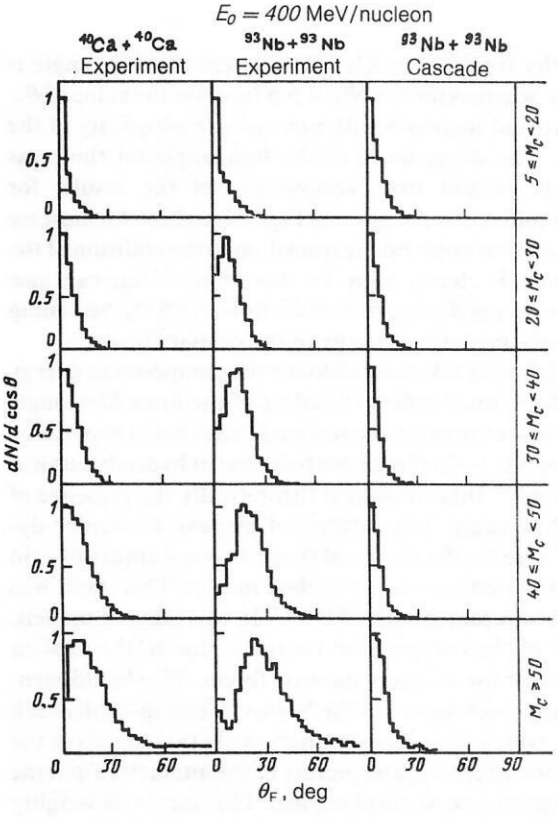

FIG. 27. Distribution with respect to the flow angle for different intervals of the multiplicity M_c of the secondary particles. The experimental values are taken from Ref. 184, and the calculations are in accordance with the Yariv–Fraenkel[96] cascade model. In the case of the Ca + Ca reaction, the multiplicities are equal to half the indicated values of M_c.

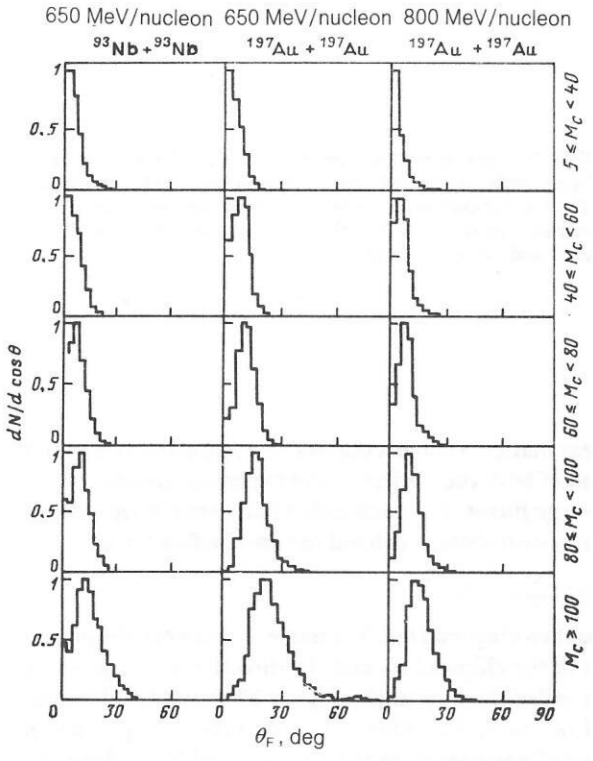

FIG. 28. Distribution with respect to the flow angle for Nb + Nb reactions at $E_0 = 650$ MeV/nucleon and Au + Au reactions at $E_0 = 650$ and 800 MeV/nucleon.[185] For the Nb + Nb case, the multiplicities correspond to half the indicated values of M_c.

noteworthy that for the Ca + Ca system the flow angle is near zero, whereas for the Nb + Nb reaction the value of θ_F is nonzero and increases with increasing multiplicity of the particles. The dependence of the flow angle on the mass number is evident from comparison of the results for Nb + Nb and Au + Au given in Figs. 27 and 28. An increase in the mean flow angle on the transition to the collision of the heavier ions is clearly seen. In these figures one can also follow the energy dependence of the flow angle, θ_F becoming smaller with increasing energy of the primary beam.

Models that take into account the compression energy in some form must reflect the effect of the finite flow angle and reproduce the experimental tendencies noted above. For the system Nb + Nb there have been recent hydrodynamical calculations[126] that confirmed theoretically the presence of a finite flow angle. The method of nuclear–molecular dynamics[87] (see the discussion of the theoretical approaches in Sec. 2) also predicts a jet of nuclear matter. This result was reverified in recent studies.[90,186–188] In this class of models, the effect of the compression energy is due to the explicit allowance for the nucleon–nucleon forces. We should mention the approach based on the Vlasov–Uehling–Uhlenbeck equation, which describes simultaneously two signals of the compression effect—the jet picture of the interaction and the energy dependence of the pion yield. This success is weighty proof for a hard ($K \simeq 380$ MeV) equation of state of nuclear matter (see Ref. 127). The experimental tendencies are also reproduced qualitatively in the model based on the Boltzmann–Enskog equation.[129] It can be seen from the results of a calculation in accordance with the cascade model of Yariv and Fraenkel,[96] which are shown in Fig. 27, that the employed variant of the model does not explain the experimental data, predicting a peak at angle $\theta_F = 0°$ irrespective of the particle multiplicity. This strong discrepancy can be interpreted as one further proof for the existence of a flow or jet of nuclear matter. However, the actual situation with regard to the possibility that the cascade model reproduces the jet picture of the nuclear interaction is contradictory, since a nonzero flow angle was also obtained in calculations using the standard cascade model (Refs. 103, 179, 189, and 190). For a more detailed analysis of the possibility of generating a jet of hadrons in the framework of the cascade approach, see Ref. 179.

Pion excitation function. The point of departure for the attempt to estimate the form of the energy-density functional $E(\rho, T)$ was the discovery of a significant discrepancy between the measured and calculated (in the cascade model) multiplicity of π^- mesons produced in central Ar + KCl collisions in the energy range $E_0 \simeq 0.35$–1.8 GeV/nucleon.[181] If it is assumed that this discrepancy is entirely due to the compression effect, which is not taken into account in the standard cascade model, then from the difference between the values of the pion excitation functions it is possible to determine the compression energy and then compare it with the nucleon density calculated in the framework of the cascade model. The results of such an analysis are shown in Fig. 29. The parabolic approximation of the resulting dependence of the compression energy on the density gives a value of the compressibility appreciably greater than the expected value $K \simeq 200$ MeV (see Sec. 1).

The model based on the Vlasov–Uehling–Uhlenbeck equation reproduces the π^- yield, but at compressibility $K = 380$ MeV. The situation here is still unclear. Recent cascade-model calculations[190] reproduce well the pion excitation function. At the same time, there are comments on the method of deducing the compression energy, but a more systematic analysis leads to a quite unrealistic value of the compressibility: $K \simeq 800$ MeV.[191]

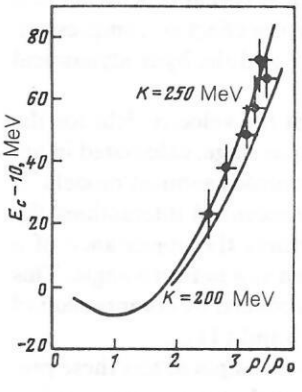

FIG. 29. Equation of state extracted from the observed difference between the experimentally measured excitation function for π^- mesons produced in Ar + KCl central interactions[181] and this function calculated in accordance with the cascade model. The curves correspond to Eq. (14) with the indicated values of the compressibility.

Strange particles and the hadron gas

Strange particles are of interest because, it is assumed, they can give us information about the reaction mechanism of the high-energy interaction and serve as a signal of the possible development of the quark–gluon phase at relativistic collision energies $E_0 \gtrsim 10$ GeV/nucleon. Since the cross section for scattering of, for example, the K^+ meson by the nucleon is approximately four times less than the NN scattering cross section and almost ten times less than the πN interaction cross section, the scattering of the produced K^+ meson by the surrounding nucleons will not be very great. Thus, a produced positive kaon can be regarded as a messenger about the stage of the interaction in which the nuclear matter was in a strongly heated and compressed state. With regard to the formation of a quark–gluon plasma in the course of a reaction with relativistic heavy ions, it is very important to have reliable experimental data on the production of strange particles in the region of energies up to several giga-electron-volts per nucleon and to know the predictive power of the theoretical methods applied to the hadron-gas phase. The importance of this circumstance is due to the fact that the theory of Refs. 192 and 193 predicts, as one of the signals of a phase transition of hadrons into quarks, a sharp increase in the yield of strange particles from the quark–gluon plasma.

To understand the mechanism of production of strange particles, and also of antibaryons and the lightest hyperfragments, we use two models that are contrary to each other in their initial assumptions and then, having demonstrated their validity, we make certain predictions for future experiments. The models that we shall use are the nuclear-firestreak model and the cascade model. The firestreak model is based on the concept of thermodynamic equilibrium and corresponds to the maximally collective interaction mechanism, whereas the intranuclear-cascade model corresponds to the two-particle interaction mechanism. We analyze the results obtained with the accelerators at Dubna and Berkeley. This will make it possible to estimate the reliability of the predictions for other combinations of nuclei in the region of energies up to 10–15 GeV/nucleon.

Details of the theoretical description of strange particles

Firestreak model. The inclusive spectrum of particles of species i in the firestreak model can be expressed by[194,197]

$$\frac{d^3\sigma}{dp^3} = \int d\eta \, \frac{d\sigma}{d\eta} L_{\mathbf{p}^* \to \mathbf{p}} f_i(\mathbf{p}, \eta), \tag{66}$$

where the distribution function with respect to "streaks" is uniquely determined by the nuclear density ρ and the "geometry" of the collision process. The factor $L_{p^* \to p}$ corresponds to a Lorentz transformation of the particles from the rest frame to the laboratory system. The complete system is regarded as a mixture of a noninteracting gas of hadrons, and the single-particle distribution function for the particles of species i is [cf. (35)]

$$f_i(\mathbf{p}^*, \eta) = \frac{V \mathscr{Z}_{\text{int}}}{(2\pi)^3} \left[\exp \frac{\sqrt{p^{*2} + m_i^2} - \mu_i}{T} \pm 1 \right]^{-1}. \tag{67}$$

Here, $\mathscr{Z}_{\text{int}} = g \exp(E_B/T)$ is the internal part of the partition function. From the conservation laws for the baryon number, charge, energy, and strangeness we find the chemical potentials $\mu_i \equiv \mu_i(\eta)$ for all particles and the local temperature $T = T(\eta)$ if the establishment of local chemical equilibrium is assumed. The only free parameter that remains is the interaction volume V per nucleon, which is fixed by introducing the streak decay density $\rho_{\text{st}} = 0.12$ F^{-3}.[194,196,197]

Since strangeness is conserved, it must be borne in mind that the production of a particle with a definite strangeness s is always accompanied by the production of a particle of opposite strangeness $\tilde{s}$, $s + \tilde{s} = 0$. The same is true for other processes like the production of antinucleons, particles with "flavor," etc. This associative nature of the production process is an essentially new element (see Refs. 194 and 197), which must be included in the thermodynamic description, this being implemented by replacing the single-particle distribution function (67) by a conditional distribution function:

$$\tilde{f}_s(\mathbf{p}^*, \eta) = f_s(\mathbf{p}^*, \eta) \sum_k \delta(s + \tilde{s}_k) \int d^3p' \, d^3r K(\mathbf{r}, \mathbf{r}') f_{\tilde{s}_k}(\mathbf{p}', \mathbf{r}'), \tag{68}$$

where we have summed over all channels k that contribute to the production of a strange particle of species s.

The correlation function $K(\mathbf{r}, \mathbf{r}')$ characterizes the size of the source that emits the strange particles. For high-energy hadron–hadron collisions, the correlation function was found to be local, $K(\mathbf{r}, \mathbf{r}') \sim \delta(\mathbf{r} - \mathbf{r}')$, a result that was established by Hagedorn and Ranft in the framework of statistical theory.[198] In the firestreak model, $K(\mathbf{r}, \mathbf{r}') \to \delta(\eta - \eta')$, and Eq. (68) reduces to

$$\tilde{f}_s(\mathbf{p}^*, \eta) = f_s(\mathbf{p}^*, \eta) V \sum_k \delta(s + \tilde{s}_k) \nu_{\tilde{s}_k}, \tag{69}$$

where the density ν_i of the particles of species i is given by

$$\nu_i(\eta) = \frac{1}{V} \int d^3p f_i(\mathbf{p}, \eta). \tag{70}$$

Comparing Eqs. (69) and (67), we see that allowance for the associative nature of the production of strange particles leads to a suppression factor $V \sum_k \delta(s + \tilde{s}_k) \nu_{\tilde{s}_k}$. Depending on the mass of the particle, the suppression may reach about 20–40, and this significantly improves the agreement between the thermodynamic models and experiment.[194,197] It should be noted that $\tilde{f}_s$ reduces to f_s in the limit of a large volume or a large number of produced particles.

The intranuclear-cascade model. The cascade model (see above) is extended to the production of strange particles by including processes involving the production of strange particles at the level of the interaction of hadrons with nucleons.[199] In the modeling of elementary-particle collisions, the strangeness conservation law and, thus, the associative nature of the production process are automatically taken into account. However, direct use of the Monte Carlo algorithm is not effective because of the smallness of the strange-particle production cross section, and therefore to increase the effectiveness of the calculation special meth-

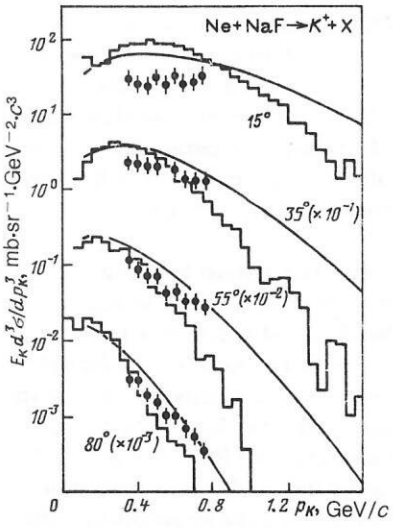

FIG. 30. Invariant spectrum of K^+ mesons from the Ne + NaF reaction (2.1 GeV/nucleon). The experimental points are taken from Ref. 202. The histogram corresponds to the results of calculation in accordance with the cascade model,[199] and the curves to calculations in accordance with the firestreak model.[196,197]

ods are developed.[199-201] It should be noted that the extension of the cascade model to strange-particle production processes does not require the introduction of any new parameters. However, the experimental cross sections for the elementary event are known with a large degree of uncertainty, and therefore calculations of the strange-particle production cross sections cannot pretend to an accuracy better than 15%. Near the production thresholds or for rare channels (for example, for the production of negative kaons) the accuracy may be even worse.

Comparison with experimental data. Region of energies of the Berkeley accelerator

Figure 30 shows the spectrum of K^+ mesons from the Ne + NaF reaction at 2.1 GeV/nucleon. Both theoretical models reproduce qualitatively the experimental results of Ref. 202. The firestreak model overestimates the experimental values by a factor 2–3, but not by 30–40 times, as in the statistical model,[203] which ignores the associative nature of the production of strange particles. The intranuclear-cascade model,[199] agreeing with the results of other cascade calculations (Refs. 200, 201, 204, and 205), predicts a softer spectrum than the firestreak model, which is a model of collective type. This difference becomes more appreciable in the region $p \gtrsim 1$ GeV/c, where at present there are no experimental data.

The spectrum of K^- mesons was measured in Ref. 206 at angle $\theta_{\text{lab}} = 0°$ in the Si + Si reaction at $E_0 = 2.1$ GeV/nucleon. As can be seen from Fig. 31, the shape of the spectrum is well reproduced by the cascade model, in which subsequent interactions of the produced K^- mesons are also taken into account. However, the calculated absolute cross section is almost four times lower than the experimental value. It should be noted that the reaction threshold is about 2.5 GeV for the channel $NN \to NNK^+K^-$, i.e., the production of K^- mesons in this reaction is an essentially below-threshold process. By virtue of the strong energy dependence of the cross section for the production of negative kaons, interactions with a correlated pair of nucleons can make an appreciable contribution. Introducing the effective energy spectrum of the two-nucleon correlation as the convolution of the Fermi distributions for the participating nucleons, we can estimate the relative efficiency of production of the K^- meson on the nucleon, W_N, and on a correlated two-nucleon pair, W_{FL}, for the given reaction as

$$\int_{S_{\text{th}}} W_N(S)\,\sigma_{NN}(S)\,dS \Big/ \int_{S_{\text{th}}} W_{FL}(S)\,\sigma_{FL}(S)\,dS \simeq \frac{1}{30},$$

where S is the accessible energy of the system. Thus, in the considered energy region interactions with correlated nucleons, called fluctons, are extremely important. These interactions were taken into account in the cascade approach by assuming that the differential distributions for the nucleon–nucleon and nucleon–flucton interactions are equal at the same accessible energy in the center-of-mass system of the colliding particles. Figure 31 shows the relative contributions from the interactions with fluctons of the projectile nucleus and the target nucleus. It is obvious that the former make the main contribution to the K^- spectrum at angle $\theta_{\text{lab}} = 0°$. For the Ne + NaF → $K^+ + X$ reaction at $E_0 = 2.1$ GeV/nucleon a 2% admixture of fluctons, which hardly changes the shape of the calculated spectrum, only slightly increases the yield of K^+ mesons in the region $p > 1$ GeV/c.

The predictions of the firestreak model for the spectrum of K^- mesons exceed the experimental values by 5–6 times. This excess is not remarkable, since the model ignores the

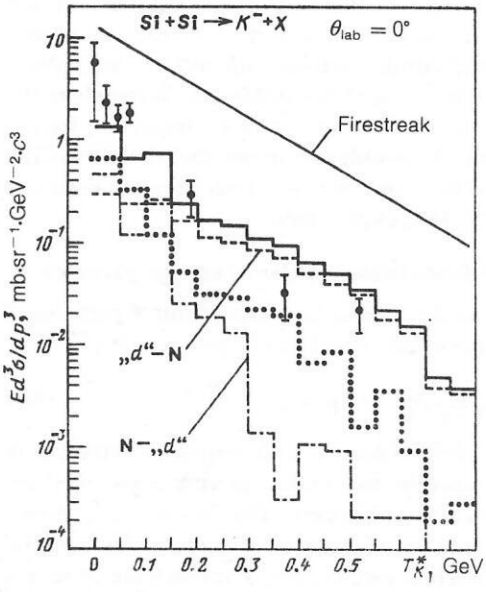

FIG. 31. Invariant spectrum (in the center-of-mass system) of negative kaons emitted at angle $\theta_{\text{lab}} = 0°$ in Si + Si collisions (2.1 GeV/nucleon). The experimental points are taken from Ref. 206. The thick continuous histogram and the dotted histogram show the results of cascade calculations,[199] respectively, with and without allowance for a 2% admixture of "fluctons"; the contributions of interactions with fluctons in the projectile nucleus and the target are shown separately; the thin line shows the predictions of the firestreak model.

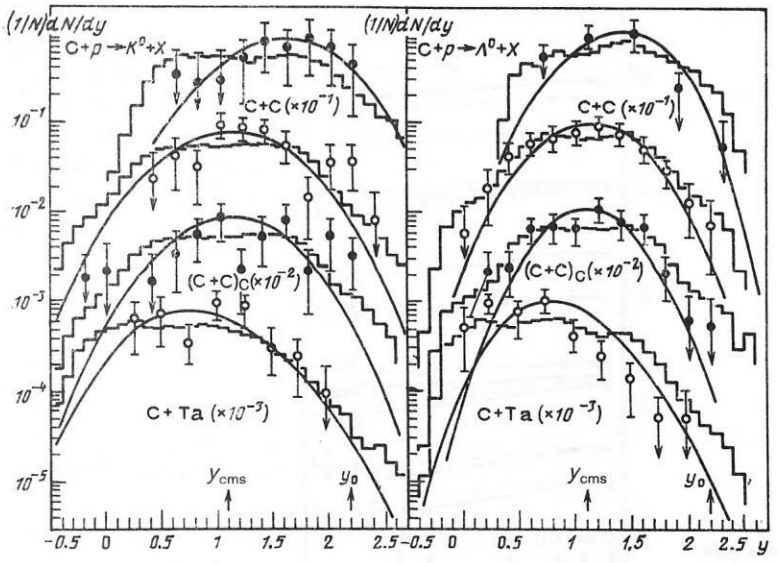

FIG. 32. Rapidity distributions of K^0 and Λ^0 particles produced in collisions of carbon ions with energy 3.4 GeV/nucleon and nuclei of hydrogen, carbon (all events and central interactions), and tantalum. The experimental points are taken from Refs. 208 and 209; the histograms and curves are the theoretical predictions made in the framework of the cascade model[199] and the nuclear-firestreak model.[196,197]

effect of the transparency of nuclear matter, and the entire energy of the relative motion of the nuclear streaks is transformed into thermal energy. The assumption of complete thermalization may be unjustified, and this leads to an excessively large yield of produced particles. Such a tendency is observed not only for the yield of strange particles but also for pions (see Refs. 195–197). Thus, more reliable predictions in the framework of the firestreak model can be made for the relative yields of the produced particles. In particular, for the ratio of the yield of Λ^0 hyperons to that of π^- mesons in Ar + KCl central collisions at 1.8 GeV/nucleon the model predicts $\Lambda^0/\pi^- = 9\cdot10^{-3}$ (including the contribution from the decay $\Sigma\to\Lambda^0$), a result that is close to the experimental value $7\cdot10^{-3}$ of Ref. 207.

Energy region of the Dubna synchrophasotron. Measurements of neutral strange particles were made by means of propane[208,209] and streamer[210] chambers. Figures 32 and 33 show the distributions with respect to the rapidity and transverse momentum for K^0 mesons and Λ^0 hyperons from reactions induced by a carbon nucleus with energy 3.4 GeV/nucleon (see Refs. 208 and 209). Both models reproduce qualitatively correctly the change in the rapidity spectrum as a function of the mass of the target nucleus, but the cascade model gives a broader distribution which is closer to the experimental points. In the case of a heavy target, the cascade model predicts the appearance of structure in the rapidity spectrum due to secondary interactions in the target. It is interesting to note that the fractions of Λ^0 and K^0 particles produced through the pion channel are 25 and 40%, respectively, in the case of a C + Ta collision.

With regard to the transverse momentum distributions, better agreement is observed in this case with the firestreak model, a result that may indicate the need to take into account interactions with fluctons in the framework of the cascade model. However, for definitive conclusions about the magnitude of the flucton admixture it will be necessary to

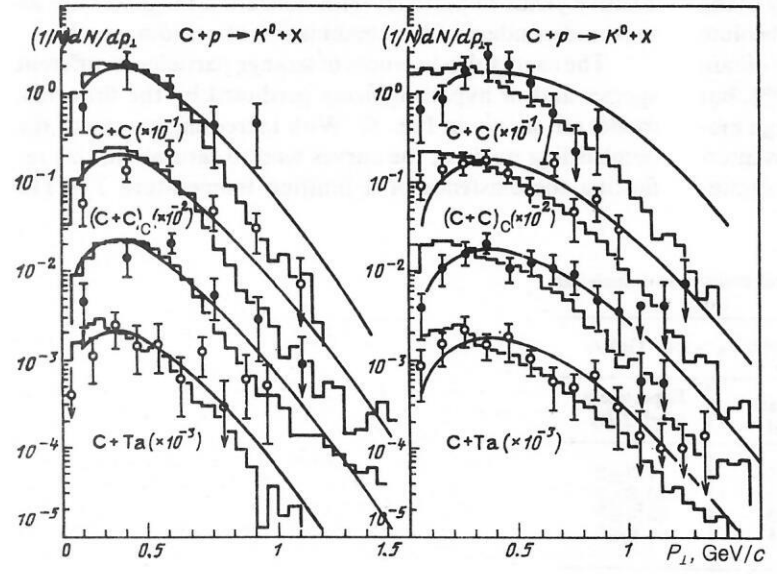

FIG. 33. Distributions with respect to the transverse momentum of the produced K^0 mesons and Λ^0 hyperons. The notation is the same as in Fig. 32.

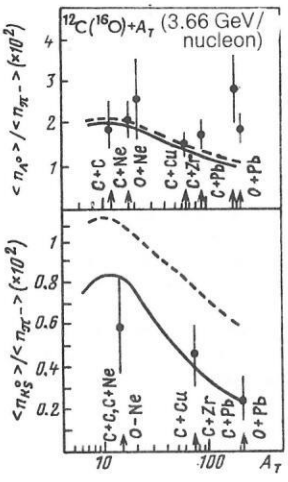

FIG. 34. The A dependence of the relative yields of K^0 mesons and Λ^0 hyperons in central collisions induced by carbon and oxygen ions with $E_0 = 3.66$ GeV/nucleon. The experimental points are taken from Ref. 210. The theoretical curves are calculated in the framework of the firestreak model[196,197] with (continuous curves) and without (broken curves) allowance for the experimental restrictions on the momentum of the observed particle: $p_K > 0.61$ GeV/c and $p_\Lambda > 0.46$ GeV/c.

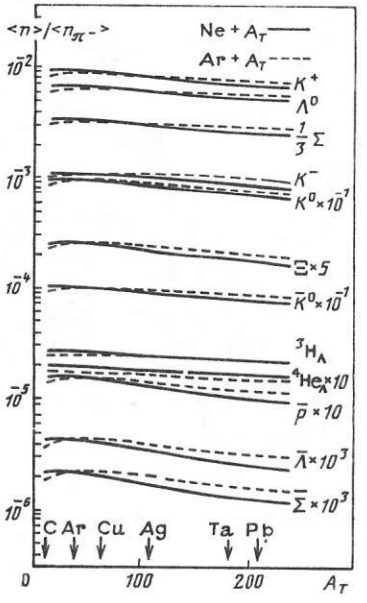

FIG. 35. Predictions of the firestreak model for the A dependence of the relative yield of secondary particles at primary energy $E_0 = 2.1$ GeV/nucleon. The continuous and broken curves correspond to the reactions induced by neon and argon ions, respectively.

improve considerably the accuracy of the measurements in the region of large momentum transfers, $p_\perp > 1$ GeV/c.

Figure 34 shows the ratio of the mean multiplicities of the K^0 and Λ^0 particles to the yield of π^- mesons in central collisions of carbon and oxygen ions with different nuclei at 3.66 GeV/nucleon. The nuclear-firestreak model reproduces well the A dependence of the relative yield if one takes into account the fact that particles with small momenta, $p_\Lambda < 0.46$ GeV/c and $p_K < 0.61$ GeV/c, are not detected under the conditions of the experiment.[210] At the same time, the cascade model predicts absolute values of the particle yield close to the experimental values. This can be seen from the results given in Table II.

The analysis shows that both models are capable of describing the basic tendencies in the production of strange particles from the hadron-gas phase. The firestreak model gives reasonable estimates for the relative multiplicity of the produced strange particles, but overestimates the absolute values by 2–3 times. The cascade model can be used to obtain the absolute cross sections to an accuracy of 20%–30%, but for below-threshold processes and reactions with large momentum transfers the results are not so reliable unless interactions of hadrons with correlated nucleon pairs are eliminated *a priori*. Thus, both models have recommended themselves fairly well for use in predicting experimental tendencies at the higher energies to be achieved in the near future.

Predictions of the models

In Figs. 35 and 36 we give the predictions of the firestreak model for the A dependence of the relative yields of strange mesons, hyperons, antiprotons, and the lightest hyperfragments for different combinations of the colliding nuclei and the two energies at which intensive experimental investigations are currently being made. It can be seen that already at the energy of the Dubna synchrophasotron the relative yields of particles with nonzero strangeness are almost independent of the combination of colliding nuclei.

The energy dependences of strange particles of different species and of hyperfragments predicted by the firestreak model are shown in Fig. 37. With increasing energy of the bombarding nucleus, the curves tend to saturation, this reflecting the existence of a limiting temperature $T_0 \simeq 115$

TABLE II. Yield of K^0 mesons and Λ^0 hyperons from central collisions of nuclei at primary energy 3.6 GeV/nucleon.

$A_P + A_T$	$n_{K^0}\cdot 10^2$, $p_K > 0.61$ GeV/c		$n_\Lambda \cdot 10^2$, $p_\Lambda > 0.46$ GeV/c	
	Cascade model	Experiment (Ref. 210)	Cascade model	Experiment (Ref. 210)
C+C	2.2	2.6±1.0	8.5	7.3±2
C+Cu	3.4	3.2±1.0	16.0	10.3±2
C+Zr	3.3		17.0	13.4±3
C+Pb	3.7	2.2±0.9	18.8	23.0±7

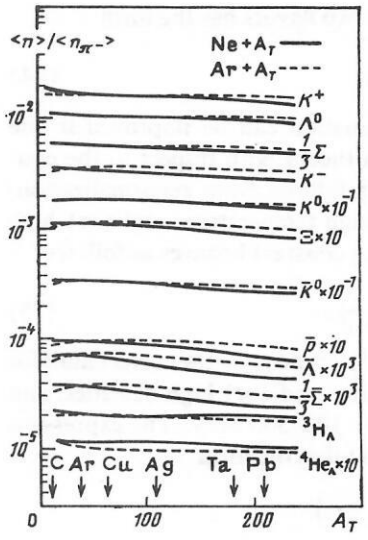

FIG. 36. The same as in Fig. 35 but for the region of energies of the Dubna synchrophasotron, $E_0 = 3.66$ GeV/nucleon.

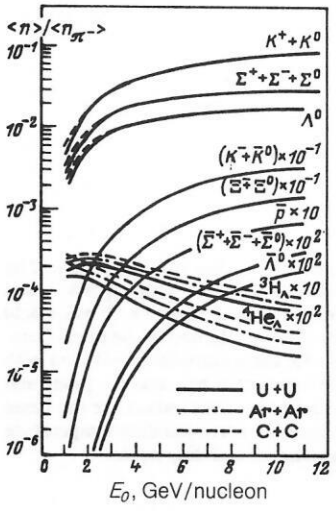

FIG. 37. Energy dependence of the relative yield of secondary particles predicted by the nuclear-firestreak model.

MeV in the statistical model of Pomeranchuk used in the nuclear-firestreak model.

The results given here were obtained under the assumption that the strangeness conservation law holds locally [see (34)]. A deviation from locality can be regarded as a signal of quark deconfinement, something that can be manifested experimentally in the shape of the spectrum of the effective masses of the produced K^+K^- or $\Lambda\Lambda^-$ pairs, as was noted in Ref. 197.

In Fig. 38, we give the predictions of the cascade model for the K^+ and Λ^0 yields. At a primary energy above 8–10 GeV/nucleon the mean multiplicities of these particles increase almost logarithmically, copying the energy dependence that the elementary *pp* interactions follow. Note that these results were obtained with neglect of the interaction with correlated nucleon pairs, and therefore the predictions of the model for a near-threshold energy are to be regarded as a minimal estimate.

Thus, extrapolation of the known hadron-gas behavior to higher energies makes it possible to obtain a picture of the main tendencies in the production of strange particles, antinucleons, and hyperfragments in heavy-ion collisions. A significant deviation from this global behavior can be used as a signal of a phase transition to a quark–gluon plasma (see Sec. 3).

3. COLLISIONS OF ULTRARELATIVISTIC HEAVY IONS

We have considered two energy regions in which the main reaction mechanism changes from an interaction described by the average field at low beam energies to the microscopic mechanism of nucleon–nucleon collisions at energies between 20 and 100–200 MeV/nucleon. At even higher energies of the bombarding ion, it is also necessary to take into account the interactions between the nucleons and other produced particles such as pions, kaons, etc., and resonances. At energies above 10–20 GeV/nucleon (see Sec. 1), the global reaction mechanism changes from the hadron type to quark–quark and quark–gluon interactions. At the present time, the transition region is being studied mainly theoretically. The existing experimental data have been obtained in experiments with cosmic rays. However, already in the immediate future heavy-ion beams of ultrarelativistic energies will be accessible. Experiments at CERN and Brookhaven in the United States are now in the preparation stage.

In what follows, we shall consider qualitatively the equation of state of the quark–gluon phase and present very briefly a two-phase model and the lattice QCD approach for the calculation of the critical temperature. At the end of the section, we shall discuss possible signals of the transition to the deconfinement phase.

Equation of state of quark matter

During the last 20 years, the concept of elementary particles has undergone fundamental changes. We now understand hadrons as composite systems consisting of quarks and gluons. Quantum chromodynamics (QCD) predicts that at large distances the quark binding energy increases (quark

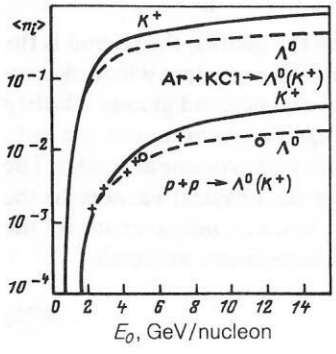

FIG. 38. Predictions of the cascade model for the energy dependence of the number of K^+ mesons and Λ^0 hyperons produced in central Ar + KCl collisions.[199] For comparison we show the yield of these particles from elementary *pp* interactions [the experimental points and the approximating curves (broken curves)].

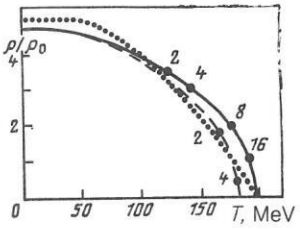

FIG. 39. Boundaries of the hadron phase of nuclear matter calculated by means of the Gibbs condition for phase equilibrium with a quark–gluon plasma. We show the results of calculation in accordance with mean-field theory with systematic allowance for the contribution of the pions (continuous curve),[216] without allowance for them (broken curve), and with simplified allowance[217] ignoring the interaction between the pions and nucleons (dotted curve). The numbers next to the curves are the beam energy (GeV/nucleon) needed to attain the corresponding temperature and density in the symmetric combination of colliding nuclei.

confinement), while at short distances the quarks behave as free particles (asymptotic freedom). The property of asymptotic freedom leads to the far-reaching consequence that at high temperatures and (or) densities a gas of quarks and gluons must behave like an ideal gas.[211] It has been estimated that the critical temperature of such a transition is about 200 MeV, and the attainment of this region of temperatures is the cherished aim of ultrarelativistic heavy-ion physics.

For a rough estimate of the critical temperature there exist several models and approaches, based mainly on a two-phase physical picture, i.e., one considers one equation of state for nuclear matter (as described in Sec. 2) and another for the quark–gluon plasma. Using the Gibbs criterion for phase equilibrium, one finds the critical temperature and density. More rigorous and reliable estimates of the critical temperature are based on Monte Carlo calculations in the framework of statistical QCD. These are the so-called QCD calculations on a lattice, which we shall briefly consider below together with the two-phase picture.

Two-phase description

We consider a free gas of massless quarks with two flavors ($N_f = 2$) and gluons. Its energy density ε can be readily calculated ($\hbar = c = 1$)[1,196]:

$$\varepsilon = \frac{6}{\pi^2}\left(\frac{7\pi^4}{60}T^4 + \frac{\pi^2}{2}T^2\mu_q^2 + \frac{1}{4}\mu_q^4\right) + \frac{8\pi^2}{15}T^4 + B. \qquad (71)$$

The first term in (71) is due to the quarks, the second is the contribution of the gluons, and B is a constant which characterizes the "bag" containing the quarks and gluons. The bag model[212] is used to describe quark–gluon matter not only within a hadron but also in some finite volume around it. The shift of the ground state from the physical vacuum to the QCD vacuum within the bag is taken into account by the addition of B. Therefore, for the pressure we obtain

$$P = \frac{1}{3}\varepsilon - \frac{4}{3}B. \qquad (72)$$

The quark-number density is

$$n_q = 2\,(\mu_q T^2 + \mu^3/\pi^2). \qquad (73)$$

Since the quark baryon number is 1/3, the baryon density in a plasma characterized by two flavors has the form

$$n_B = \frac{2}{3}\,(\mu_q T^2 + \mu_q^3/\pi^2). \qquad (74)$$

The free-gas approximation can be improved if one makes use of perturbation theory with respect to the coupling constant.[192,213,214] It follows from renormalization-group arguments that at high temperatures and (or) high densities the QCD coupling constant behaves as follows:

$$g^2 = \frac{24\pi^2}{(33 - 2N_F)\ln\,(M/\Lambda_0)^2}, \qquad (75)$$

where $M \simeq (4\mu_q^2/5 + 16T^2)^{1/2}$ and gives the correct limit for the case of high temperatures and (or) high densities, and the scale parameter is $\Lambda_0 = 100$–500 MeV. The expression for the energy density then takes the form

$$\varepsilon = \frac{2\cdot 3}{\pi^2}\left[\frac{7\pi^4}{60}T^4\left(1 - \frac{50}{84}\frac{g^2}{\pi^2}\right) + \left(\frac{\pi^2}{2}T^2\mu_q^2 + \frac{1}{4}\mu_q^4\right)\left(1 - \frac{g^2}{2\pi^2}\right)\right] + \frac{8}{15}\pi^2 T^4\left(1 - \frac{15}{16}\frac{g^2}{\pi^2}\right) - \frac{4}{3}B. \qquad (76)$$

The boundary curve of the phase transition, shown in Fig. 39, is calculated by comparing the pressure in the quark–gluon plasma with the pressure in the hadron phase at the given temperature T:

$$P_q\,(3\mu_q) = P_h\,(\mu), \qquad (77)$$

the fulfillment of the phase-equilibrium condition $3\mu_q = \mu$ being thereby ensured. For the nuclear-matter phase various descriptions (see Ref. 215) can be used. In Refs. 216–219 Walecka's equation of state was used, and pion degrees of freedom were also taken into account.[216,217] In other approaches the statistical bootstrap model[220–222] or the potential model[223] were used for the hadron phase.

Figure 39 shows a typical phase diagram (see Ref. 204) calculated by means of Walecka's equation of state for the hadron phase and Eq. (71) for the quark–gluon phase. The critical temperature varies in the range $T_c \simeq 170$–190 MeV, and the critical density is $\rho_c \simeq 5\rho_0$. Depending on the choice of the description (see the caption to the figure) of the two phases, the transition parameters change somewhat, but the general picture presented in Fig. 39 remains the same.

QCD lattice calculations

To describe the statistical properties of the QCD system, it is necessary to calculate the partition function (integral) of the state, which can be expressed in terms of a Euclidean functional integral[224]:

$$\mathfrak{Z}\left(\beta = \frac{1}{T},\ V\right) = \int [dA\,d\psi\,d\bar{\psi}]\exp\left(-\int_V d^3x \int_0^{\beta} \mathcal{L}\,(A, \psi, \bar{\psi})\right), \qquad (78)$$

where $\mathcal{L}$ is the QCD Lagrangian density, and the integrals are taken over the gluon and quark fields. The vector and spinor fields must satisfy, respectively, periodic and antiperiodic conditions. In the thermodynamic limit, the spatial integration over $\mathcal{L}$ becomes infinite, whereas the integration

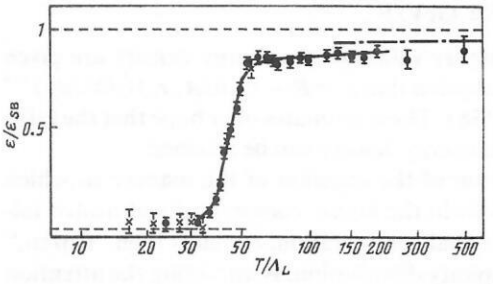

FIG. 40. Energy density ε of the system described by the $SU(2)$ gauge field theory.[227] The results are normalized to the ideal-gas limit ε_{SB}, and the number of cells is $10^3 \times 3$. The chain line shows the limiting value for an ideal gas with the requirement that the complete system be colorless.[230]

with respect to the imaginary time is over a finite interval.

For the calculation of $\mathcal{Z}(T, V)$, the space–time continuum is replaced by a discrete lattice with $V = (N_\sigma a_\sigma)^3$ and $\beta = N_\tau a_\tau = 1/T$, where a_σ and a_τ are the distances between the lattice faces (the lattice constant) in the space and time directions, and N_σ and N_τ are the numbers of the corresponding partitionings. As a result of this transformation (see Refs. 215, 225, and 226),

$$\mathcal{Z}(T, V) \to \mathcal{Z}(N_\sigma, N_\tau, g^2), \tag{79}$$

where g^2 is the coupling constant. In the calculation of thermodynamic variables like the pressure or energy density in terms of the partition function $\mathcal{Z}(N_\sigma, N_\tau, g^2)$ one sets $a_\sigma = a_\tau = a$, and then the coupling constant g^2 can be related to the lattice constant a by the asymptotic renormalization-group relation

$$a\Lambda_L = \exp\left\{-\frac{4\pi^2}{33-2N_F}\left(\frac{6}{g^2}\right)+\frac{1{,}59-57N_F}{(33-2N_F)^2}\log \times\left[\frac{8\pi^2}{33-2N_F}\left(\frac{6}{g^2}\right)\right]\right\}. \tag{80}$$

Thus, all the physical quantities that are calculated are measured in units of the lattice scale parameter Λ_L, which is arbitrary. One can fix Λ_L by calculating the dimensionless ratios of observable quantities or, for example, the proton mass.

Since the interaction responsible for the confinement is already contained in the part of the QCD Lagrangian associated with the purely gauge field, one can consider the interesting case of the transition to the state of deconfinement without quarks. Figure 40 shows the density for the $SU(2)$ system based on a calculation with partitioning into $N_\sigma^3 \times N_\tau = 10^3 \times 3$ cells.[227] The energy density is normalized to the ideal-gas value $\varepsilon_{SB} = (3\pi^2/15)T^4$. It can be clearly seen from Fig. 40 that at high temperatures the system behaves like an ideal gas of gluons. An abrupt transition to this state occurs near the temperature $T_c \simeq 40\Lambda_L$. Figure 41 shows the corresponding results for the more interesting $SU(3)$ case calculated on an $8^3 \times 3$ lattice.[228] It is evident that in this case a jump occurs at the temperature $T_c \simeq 80\Lambda_L$. Using the results for the surface tension of a string at comparatively small g, we obtain[225,226]

$$T_c \simeq 150 - 200 \text{ MeV},$$

a result in reasonable agreement with the results obtained in the two-phase treatment.

The deconfinement phase transition means that color states can be realized in regions of space whose dimensions appreciably exceed the hadron scale of about 1 F. However, the system as a whole must remain colorless. As is shown in Refs. 229 and 230, allowance for this condition has the consequence that in the high-temperature limit the energy density of the system is below the value of ε_{SB} (see Figs. 40 and 41).

The further development of the approach is associated with the inclusion in the Lagrangian of massive quarks, one of the consequences of which is the breaking of the chiral symmetry. In the confinement region there are constituent quarks with a mass of about 300 MeV (for the u and d quarks), whereas in the region of the plasma, consisting of "highly excited" quarks, the chiral symmetry is restored. Thus, QCD leads to one further transition, namely, the transition from the state with broken chiral symmetry to the state in which it is restored. The question of the connection between the restoration of the chiral symmetry and deconfinement has still not yet found a satisfactory answer.[225]

The partition function of the state (78) that includes the quarks contains anticommuting spinor fields ψ, $\bar{\psi}$, over which it is necessary to integrate. This leads to the inclusion of determinants measuring $(12N_\sigma N_\sigma)^2$, and this involves great technical difficulties. Therefore, at the present time it is necessary to rely on approximate schemes.[225] Figure 42 shows the energy density calculated in an expansion with respect to the so-called hopping parameter for an $8^3 \times 3$ lattice.[231] The case $N_f = 2$ is considered. As can be seen from Fig. 42, there is an abrupt transition near $T_c \simeq 150\Lambda_L$. Transforming this quantity into units of Λ_L for the case of zero flavor, which was considered above for the thermodynamics of the pure gauge field, we obtain $T_c/T_{\Lambda^+} \sim 100$, a result that must be compared with the value $T_c/\Lambda_L \simeq 80$ given above. Thus, the critical values of the temperature obtained from the lattice calculations at zero baryon density is

$$T_c \sim 200 - 250 \text{ MeV}.$$

For a discussion of the specific nature of the phase transitions described briefly above, the order parameters, and so forth, we refer the reader to the review of Ref. 225.

The complete phase diagram of the strongly interacting

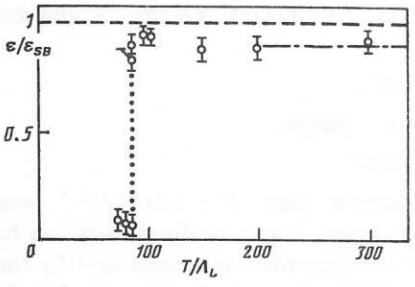

FIG. 41. Energy density ε of the system described by the $SU(3)$ gauge field theory.[228] The number of cells is $8^2 \times 3$. The chain line shows the limiting value of the energy density of an ideal gas with the requirement that the complete system be colorless.[230]

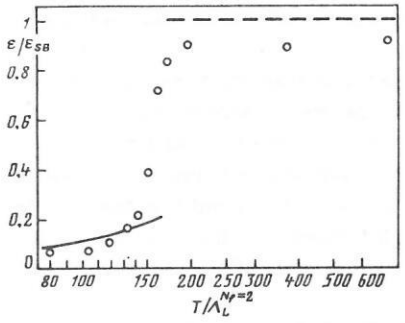

FIG. 42. Energy density calculated in the framework of QCD with dynamical quarks.[231] The number of cells is $8^3 \times 3$.

matter must describe the phase boundary as a function of the temperature T and the baryon-number density ρ_B. This complicated problem is the ultimate aim of QCD lattice calculations. The first steps in this direction have already been taken (see Refs. 215, 225, and 226).

Ultrarelativistic nucleus–nucleus collisions and signals of the deconfinement phase

The energy density of nuclear matter in the ground state is $\varepsilon_0 = m_N \rho_0 \simeq 0.15$ GeV/F^3, whereas the energy density within a proton already reaches the value $\varepsilon_p \simeq 0.45$ GeV/F^3. However, for the formation of a quark–gluon plasma an even higher density is required. It can be most readily estimated using Eq. (71), which gives ($\mu_q = 0$) $\varepsilon = (37/30)\pi^2 T^4 + B \simeq (2.5\text{–}3)$ GeV/F^3 at temperature $T \simeq 200$ MeV. For these purposes, knowledge of the exact value of B is unimportant. Low-energy hadron spectroscopy gives the value $B \simeq 40\text{–}60$ MeV/F^3, whereas the QCD sum rules give larger values $B \simeq 400$ MeV/F^3. The approximate value obtained for the energy density must be compared with the energy density that can be attained in a collision of ultrarelativistic nuclei.

Following Bjorken[232] (see also Refs. 233 and 234), we can estimate the energy density using the rapidity distribution dN/dy of the produced particles

$$\varepsilon = \frac{\langle m_\perp \rangle}{\tau_0 A_\perp} \frac{dN}{dy}, \tag{81}$$

where $\langle m_\perp \rangle$ is the averaged transverse mass (of order 0.5 GeV) and $A_\perp = \pi R^2$ is the cross section (about 40 mb for pp collisions). In (81), τ_0 characterizes the hadronization time, and as a typical value of it one usually takes $\tau_0 \simeq 1$ F/c. For pp collisions in the region 50–100 GeV, $dN/dy \simeq 4$, and this gives

$$\varepsilon_{p-p} \simeq 0.5 \text{ GeV/F}^3,$$

and for a central U + U collision

$$\varepsilon_{U-U} \simeq 2.7 \text{ GeV/F}^3,$$

where we have assumed that $R = 1.2(238)^{1/3}$ and $dN/dy = 4 \cdot 238$. Even higher values of the density can be extracted from the events recorded in cosmic rays by the JACEE collaboration.[235] For example, in the case of the Si + Ag interaction it was found that dN/dy (charged) is $\simeq 200$ at an estimated laboratory energy $E_0 = 4$ TeV/nucleon. In accordance with the estimate (81), we obtain

$$\varepsilon_{CR} \simeq 3.6 \text{ GeV/F}^3.$$

In Ref. 215, higher values of the energy density are given under the assumption that $\varepsilon = B + (1.6/A_\perp \tau_0)(dN/dy)^{4/3}$ (see also Ref. 236). These estimates offer hope that the critical value of the energy density can be attained.

Investigation of the question of the manner in which matter evolves from the highly compressed and heated initial state to the final configuration, which is then "frozen," forming the rapidity distribution, is attracting the attention of many theoreticians. So far, mainly hydrodynamical models have been used to study the expansion of the plasma bunch (see Refs. 215, 233, 234, and 236–238). We here omit the discussion of this very interesting process of evolution from the quark–gluon phase to hadron matter (see the literature quoted above) and make some comments about how the formation of a plasma could be verified experimentally.

Measurement of lepton pairs. To penetrate into the early stage of the collision process, it is necessary to measure particles with very small interaction cross sections having a large mean free path. Ideal particles for this are lepton pairs, since they interact mainly through electromagnetic processes, the cross sections for which are small (see Refs. 192 and 239–242). The recent estimates made in Ref. 243 show that the production of lepton pairs in the plasma phase is suppressed by 3–5 times compared with production in the Drell–Yan mechanism. In order to verify this effect, it is necessary to measure the production of lepton pairs for a definite nucleus–nucleus collision, and then investigate the probability of production at higher energies or for heavier systems. If the yield of lepton pairs is reduced, this will be a signal of the formation of a quark–gluon plasma.

Measurement of the transverse momentum. The transverse momentum of secondary hadrons can serve as a measure of the temperature of the system (see also Sec. 2). Investigation of its dependence on the multiplicity (primary energy) could, as is shown in Fig. 43, lead to detection of the deconfinement phase from the characteristic change in this dependence due to the release of latent heat of the transition.[244] The most recent data from the proton–antiproton collider are not sufficient for definitive conclusions to be drawn. The interpretation of the JACEE-collaboration data obtained in cosmic-ray experiments are fairly optimistic, since one can see indications that the transition region has been reached.[235]

Production of strange particles. If the quark–gluon plasma is in the state of chemical equilibrium with respect to the different quark "flavors," then the fraction of strange quarks

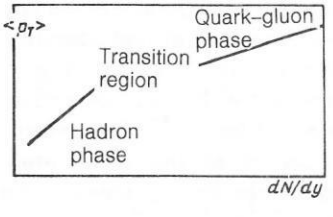

FIG. 43. Dependence of the mean transverse momentum of the secondary particles on the density of particles in the rapidity space.

in the number of all quarks and antiquarks will no longer be negligibly small (see Refs. 193, 245, and 246). This means that the probability for the production of strange particles increases when the plasma phase is attained. Valuable information about the appearance of the quark-plasma phase could be obtained by measuring the ratio of the particle and antiparticle yields, for example, K^+/K^-, $\Omega/\bar{\Omega}$, $\Xi/\bar{\Xi}$ (see also the end of Sec. 2).

Signals associated with a phase transition of the first kind. Hitherto, we have discussed experimentally measurable quantities that can give us information about the appearance of the quark–gluon plasma. From the theoretical point of view, much interest attaches to the actual dynamics of the phase transition, and in this connection additional signals can be investigated. In addition, the existence of a latent heat of the transition will lead to a large energy "wandering" in the system. For phase transitions of the first kind, such phenomena are associated with superheating and supercooling of the system. The process itself may have an explosive nature[247] of the type of deflagration or detonation processes[247,248] (see also Ref. 215).

Some of these processes are rather hypothetical, and the entire scenario described above depends critically on the validity of equilibrium thermodynamics. Only if the mean free path of the quarks and gluons is short compared with the dimension of the system will the description in terms of an expanding plasma bunch with subsequent transition into hadronic matter appear valid.

4. CONCLUSIONS

As we have seen above, the physics of heavy-ion collisions has indeed opened up rich possibilities for investigating the behavior of nuclear matter in a wide range of temperatures and densities. At the present time, the main results relate to the region of the hadron phase, this reflecting the spectrum of masses and accessible heavy-ion energies in existing accelerators. Approaches to the fundamental problem—the study of the equation of state of heated and compressed nuclear matter—have already been outlined. For all the complexity of the physical phenomena that unfold in this region, the combined efforts of the theoreticians and experimentalists have succeeded in identifying characteristics that are the most sensitive to the various canonical parameters of the equation of state. The abundance of theoretical models, sometimes based on opposite physical assumptions, is somewhat suspect, but the models nevertheless successfully describe the general experimental features of heavy-ion interactions. In this connection it is necessary to emphasize the need for correlation and 4π measurements, which could serve as a critical test of existing models.

The theory predicts that the passage from the intermediate region of the hadron phase into the region of both lower and higher energies of the colliding nuclei may lead to the discovery of new physical effects and phenomena. This is related to the fact that the nuclear-matter equation of state has the features discussed above and manifested in the form of a phase transition of gas–liquid type at moderate energies and transition of the hadrons to the quark–gluon plasma phase in the region of ultrarelativistic energies. In these directions, only the first steps are being made. To a large degree, success will depend on the rapid commissioning of the new generation of heavy-ion accelerators.

[1)]In considering evolution of the system in the region of coexistence of the two phases, we basically follow Refs. 31 and 32 (see also Refs. 12 and 16).

[2)]To reduce the influence of nonequilibrium processes, a restriction is often made to the spectrum at just the angle 90°. One sometimes uses the distribution with respect to $p_\perp$; this may even be preferable in view of the invariance of this quantity.

[3)]A method of analyzing the fluxes in the plane of the transverse momentum was proposed in Ref. 182; according to the estimate of Ref. 183, this separates more effectively the dynamical correlations on the background of the large statistical fluctuations.

[1]H. Satz, Nucl. Phys. **A400**, 541 (1983).
[2]J. Kogut, A. Matsuoka, M. Stone, *et al.*, Phys. Rev. Lett. **51**, 869 (1983).
[3]J. Polonyi, H. W. Wyld, J. B. Kogut, *et al.*, Phys. Rev. Lett. **53**, 644 (1984).
[4]G. Baym, Prog. Part. Nucl. Phys. **8**, 73 (1982).
[5]G. E. Brown and W. Weise, Phys. Rep. **C27**, 1 (1976).
[6]A. B. Migdal, Fermiony i bozony v sil'nykh polyakh (Fermions and Bosons in Strong Fields), Nauka, Moscow (1978); Rev. Mod. Phys. **50**, 107 (1978).
[7]T. D. Lee, Rev. Mod. Phys. **47**, 267 (1975).
[8]G. Sauer, H. Chandra, and U. Mosel, Nucl. Phys. **A264**, 221 (1976).
[9]P. Danielewicz, Nucl. Phys. **A314**, 465 (1979).
[10]H. Schulz, L. Münchow, G. Röpke, and M. Schmidt, Phys. Lett. **B119**, 12 (1982).
[11]M. W. Curtin, H. Toki, and D. K. Scott, Phys. Lett. **B123**, 289 (1983).
[12]G. Bertsch and P. J. Siemens, Phys. Lett. **B126**, 9 (1983).
[13]P. J. Siemens, Nature **305**, 410 (1983).
[14]J. Jaqaman, A. J. Mekjian, and L. Zamick, Phys. Rev. C **27**, 2782 (1984); *ibid.* **29**, 2067 (1984).
[15]H. Stöcker, G. Buchwald, G. Graebner, *et al.*, Nucl. Phys. **A400**, 63 (1983).
[16]L. Lopez and P. J. Siemens, Nucl. Phys. **A431**, 728 (1984).
[17]A. D. Panagiotou, M. W. Curtin, H. Toki, *et al.*, Phys. Rev. Lett. **52**, 496 (1984).
[18]J. P. Kapusta, Phys. Rev. C **29**, 1735 (1984).
[19]A. L. Goodman, J. P.Kapusta, and A. Z. Mekjian, Phys. Rev. C **30**, 851 (1984).
[20]D. G. Ravenhall, C. J. Pethick, and J. M. Lattimer, Nucl. Phys. **A407**, 571 (1983).
[21]J. Knoll and B. Strack, Phys. Lett. **B149**, 45 (1985).
[22]C. M. Kiselev, Yad. Fiz. **41**, 94 (1985) [Sov. J. Nucl. Phys. **41**, 58 (1985)].
[23]B. Friedman and V. R. Randharipande, Nucl. Phys. **A361**, 502 (1981).
[24]D. Q. Lamb, J. M. Lattimer, C. J. Pethick, and D. G. Ravenhall, Phys. Rev. Lett. **41**, 1623 (1978); Nucl. Phys. **A360**, 459 (1981).
[25]J. D. Walecka, Ann. Phys. (N.Y.) **83**, 491 (1974); Phys. Lett. **B59**, 109 (1975).
[26]G. Röpke, L. Münchow, and H. Schulz, Nucl. Phys. **A379**, 536 (1982); Phys. Lett. **B110**, 21 (1982).
[27]G. Röpke, M. Schmidt, L. Münchow, and H. Schulz, Nucl. Phys. **A399**, 587 (1983).
[28]D. Vautherin and D. M. Brink, Phys. Rev. C **5**, 626 (1972).
[29]M. Barranco and J.-R. Buchler, Phys. Rev. C **24**, 1191 (1981).
[30]W. Schied, H. Müller, and W. Greiner, Phys. Rev. Lett. **32**, 741 (1974).
[31]H. Schulz, B. Kämpfer, H. W. Barz, *et al.*, Phys. Lett. **B147**, 17 (1984).
[32]H. Reinhard and H. Schulz, Nucl. Phys. **A432**, 603 (1985).
[33]H. Reinhard and H. Schulz, in *Proceedings of the Topical Meeting on Phase-Space Approach to Nuclear Dynamics*, Trieste (Sept. 30–Oct. 9, 1985), World Scientific, Singapore (1986).
[34]J. S. Langer, in *Fluctuations, Instabilities, and Phase Transitions*, edited by T. Riste (Plenum, New York, 1975), p. 19.
[35]H. Schulz, D. N. Voskresensky, and J. Bondorf, Phys. Lett. **B110**, 141 (1983).
[36]J. Cugnon, Phys. Lett. **B135**, 374 (1984).
[37]A. M. Poskanzer, G. W. Butler, and E. K. Hyde, Phys. Rev. C **3**, 882 (1971).

[38]G. D. Westfall, R. G. Sextro, A. M. Poskanzer, *et al.*, Phys. Rev. C **17**, 1368 (1978).
[39]B. D. Wilkins, S. B. Kaufman, E. P. Steinberg, *et al.*, Phys. Rev. Lett. **43**, 1080 (1979).
[40]A. Gaidos, L. J. Gutay, A. S. Hirsch, *et al.*, Phys. Rev. Lett. **42**, 82 (1979).
[41]R. E. I. Green and R. G. Korteling, Phys. Rev. C **22**, 1594 (1980).
[42]E. Finn, S. Agarwal, A. Bujak, *et al.*, Phys. Rev. Lett. **49**, 1321 (1982).
[43]R. W. Minich, S. Agarwal, A. Bujak, *et al.*, Phys. Lett. **B118**, 458 (1982).
[44]G. Röpke, H. Schulz, L. Andronenko, *et al.*, Phys. Rev. C **31**, 1556 (1985).
[45]K. A. Frankel and J. D. Stevenson, Phys. Rev. C **23**, 1511 (1981).
[46]U. Lynen, H. Ho, W. Kühn, *et al.*, Nucl. Phys. **A387**, 129 (1982).
[47]H. Gutbrod, A. I. Warwick, and H. Wieman, Nucl. Phys. **A387**, 177 (1982).
[48]A. I. Warwick, A. Baden, H. H. Gutbrod, *et al.*, Phys. Rev. Lett. **48**, 1719 (1982).
[49]A. I. Warwick, H. H. Wieman, H. H. Gutbrod, *et al.*, Phys. Rev. C **27**, 1083 (1983).
[50]B. V. Jacak, G. D. Westfall, C. K. Gelbke, *et al.*, Phys. Rev. Lett. **51**, 1846 (1983).
[51]C. B. Chitwood, D. J. Fields, C. K. Gelbke, *et al.*, Phys. Lett. **B131**, 289 (1983).
[52]W. A. Friedman and W. G. Lynch, Phys. Rev. C **28**, 16 (1983).
[53]S. Bohrmann, J. Hufner, and M. C. Nemes, Phys. Lett. **B120**, 59 (1983).
[54]J. Hüfner and H. M. Sommermann, Phys. Rev. C **27**, 2090 (1983).
[55]J. Randrup and S. Koonin, Nucl. Phys. **A356**, 223 (1981).
[56]S. Das Gupta and A. Z. Mekjian, Phys. Rep. **72**, 131 (1981).
[57]J. P. Bondorf, Nucl. Phys. **A387**, 25 (1982).
[58]G. Fai and J. Randrup, Nucl. Phys. **A381**, 557 (1982); **A404**, 551 (1983).
[59]J. Bondorf, I. N. Mishustin, and K.-V. Pesik, in Tr. mezhdunarodnoĭ shkoly-seminara po fizike tyazhelykh ionov (Proceedings of the International Seminar School on Heavy-Ion Physics) (Alushta, 14–21 April 1983), D7-83-644, Dubna (1983), p. 354.
[60]D. H. E. Gross, Phys. Scr. **T5**, 213 (1983).
[61]J. P. Bondorf, R. Donangelo, I. N. Mishustin, *et al.*, Phys. Lett. **B150**, 57 (1985).
[62]Sa Dan-Hao and D. H. E. Gross, Nucl. Phys. **A437**, 643 (1985).
[63]J. P. Bondorf, R. Donangelo, I. N. Mishustin, *et al.*, Nucl. Phys. **A443**, 321 (1985).
[64]J. P. Bondorf, R. Donangelo, I. N. Mishustin, *et al.*, Nucl. Phys. **A444**, 460 (1985).
[65]J. Aichelin and J. Hüfner, Phys. Lett. **B136**, 15 (1984).
[66]J. Aichelin, J. Hüfner, and R. Ibarra, Phys. Rev. C **30**, 107 (1984).
[67]D. J. Fields, W. G. Lunch, C. B. Chitwood, *et al.*, Phys. Rev. C **30**, 1912 (1984).
[68]W. Bauer, D. R. Dean, V. Mosel, and V. Post, Phys. Lett. **B150**, 53 (1984).
[69]X. Campi and J. Desbois, in Proceedings of the Seventh High Energy Heavy Ion Study, GSI-Report, Darmstadt (1985), p. 707.
[70]J. P. Bondorf, R. Donangelo, H. Schulz, and K. Sneppen, Phys. Lett. **B162**, 30 (1985).
[71]S. Song, M. F. Rivet, R. Bimbot, *et al.*, Phys. Lett. **B130**, 14 (1983).
[72]M. E. Fisher, Physics **3**, 255 (1967).
[73]H. W. Barz, J. P. Bondorf, R. Donangelo, and H. Schulz, Phys. Lett. **B169**, 318 (1986).
[74]G. English, N. T. Porile, and E. P. Steinberg, Phys. Rev. C **10**, 2268 (1974).
[75]J. Boguta and A. R. Bodmer, Nucl. Phys. **A292**, 413 (1977).
[76]J. Boguta and H. Stöcker, Phys. Lett. **B120**, 289 (1983).
[77]U. Heinz, W. Greiner, and W. Scheid, J. Phys. G **5**, 1383 (1979).
[78]D. Hahn and H. Stöcker, Report MSUCL-505, Michigan (1985).
[79]R. Hagedorn, Suppl. Nuovo Cimento **3**, 147 (1965).
[80]P. Bonche, S. Koonin, and J. W. Negele, Phys. Rev. C **13**, 1226 (1976).
[81]J. R. Nix, Prog. Part. Nucl. Phys. **2**, 237 (1979).
[82]S. Nagamiya and M. Gyulassy, Adv. Nucl. Phys. **13**, 201 (1984).
[83]A. R. Bodmer and C. N. Panos, Phys. Rev. C **15**, 1342 (1977).
[84]L. Wilets, E. M. Henley, M. Kraft, and A. D. MacKeller, Nucl. Phys. **A282**, 341 (1977).
[85]L. Wilets, Y. Yariv, and R. Chestnut, Nucl. Phys. **A301**, 359 (1978).
[86]D. J. E. Callaway, L. Wilets, and Y. Yari, Nucl. Phys. **A327**, 250 (1979).
[87]A. R. Bodmer, C. N. Panos, and A. D. MacKeller, Phys. Rev. C **22**, 1025 (1980).
[88]A. R. Bodmer and C. N. Panos, Nucl. Phys. **A356**, 517 (1981).
[89]S. M. Kiselev, Yad. Fiz. **38**, 911 (1983); *ibid.* **39**, 32 (1984). [Sov. J. Nucl. Phys. **38**, 547 (1983); *ibid.* **39**, 18 (1984)].
[90]J. J. Molitoris, J. B. Hoffer, H. Krase, and H. Stöcker, Phys. Rev. Lett. **53**, 899 (1984).
[91]J. P. Bondorf, H. T. Feldmeier, G. Garpman, and E. C. Halbert, Phys. Lett. **B65**, 217 (1976); Z. Phys. A **279**, 385 (1976).
[92]J. Hüfner and J. Knoll, Nucl. Phys. **A290**, 460 (1977).
[93]K. K. Gudima and V. D. Toneev, Phys. Lett. **B73**, 292 (1978); Yad. Fiz. **27**, 658 (1978) [Sov. J. Nucl. Phys. **27**, 351 (1978)].
[94]J. D. Stevenson, Phys. Rev. Lett. **41**, 1702 (1978).
[95]K. K. Gudima, H. Iwe, and V. D. Toneev, J. Phys. G **5**, 229 (1979).
[96]Y. Yariv and Z. Fraenkel, Phys. Rev. C **20**, 2227 (1979).
[97]K. K. Gudima and V. D. Toneev, Yad. Fiz. **31**, 1455 (1980) [Sov. J. Nucl. Phys. **31**, 755 (1980)].
[98]J. Cugnon, Phys. Rev. C **22**, 1885 (1980).
[99]J. Cugnon, T. Mizutani, and J. Vandermeulen, Nucl. Phys. **A352**, 505 (1981).
[100]J. Cugnon, J. Knoll, and J. Randrup, Nucl. Phys. **A360**, 444 (1981).
[101]K. K. Gudima and V. D. Toneev, in High Energy Nuclear Physics, Sixth Balaton Conf. on Nuclear Physics, edited by J. Erö (1983), p. 409.
[102]H. Stöcker, C. Reidel, Y. Yariv, *et al.*, Phys. Rev. Lett. **47**, 1807 (1981).
[103]V. D. Toneev and K. K. Gudima, Nucl. Phys. **A400**, 73 (1983).
[104]A. A. Amsden, G. F. Bertsch, F. H. Harlow, and J. R. Nix, Phys. Rev. Lett. **35**, 905 (1975).
[105]A. A. Amsden, F. H. Harlow, and J. R. Nix, Phys. Rev. C **15**, 2059 (1975).
[106]A. A. Amsden, J. N. Ginocchio, and F. H. Harlow, Phys. Rev. Lett. **38**, 1055 (1977).
[107]J. P. Bondorf, S. I. A. Garpman, and J. Zimanyi, Nucl. Phys. **A296**, 320 (1978).
[108]A. A. Amsden, A. S. Goldhaber, F. H. Harlow, and J. R. Nix, Phys. Rev. C **17**, 2088 (1978).
[109]G. F. Bertsch and A. A. Amsden, Phys. Rev. C **18**, 1293 (1978).
[110]H. Stöcker, J. Maruhn, and W. Greiner, Z. Phys. A **293**, 173 (1979).
[111]H. Stöcker, R. Y. Cusson, J. A. Maruhn, and W. Greiner, Z. Phys. A **294**, 125 (1980).
[112]H. H. K. Tang and C. Y. Wong, Phys. Rev. C **21**, 1846 (1980).
[113]H. Stöcker, J. A. Maruhn, and W. Greiner, Phys. Rev. Lett. **44**, 725 (1980).
[114]H. Stöcker, J. Hofmann, J. H. Maruhn, and W. Greiner, Prog. Part. Nucl. Phys. **4**, 133 (1980).
[115]L. P. Csernai and H. W. Barz, Z. Phys. A **296**, 173 (1980).
[116]L. P. Csernai and W. Greiner, Phys. Lett. **B99**, 85 (1981).
[117]G. Buchwald, L. P. Csernai, J. A. Maruhn, and W. Greiner, Phys. Rev. C **24**, 135 (1981).
[118]L. S. Roshal' and V. N. Russkikh, Yad. Fiz. **33**, 1520 (1981) [Sov. J. Nucl. Phys. **33**, 817 (1981)].
[119]H. Stöcker, L. P. Csernai, G. Graebner, Phys. Rev. C **25**, 1871 (1982).
[120]L. P. Csernai, W. Greiner, H. Stöcker, *et al.*, Phys. Rev. C **25**, 2482 (1982).
[121]J. R. Nix, D. Strottman, Y. Yariv, and Z. Fraenkel, Phys. Rev. C **25**, 2491 (1982).
[122]L. P. Csernai, I. Lovas, J. A. Maruhn, *et al.*, Phys. Rev. C **26**, 149 (1982).
[123]H. W. Barz, L. P. Csernai, and W. Greiner, Phys. Rev. C **26**, 740 (1982).
[124]H. Stöcker, G. Buchwald, L. P. Csernai, *et al.*, Nucl. Phys. **A387**, 205 (1982).
[125]G. Buchwald, G. Graebner, J. Theis, *et al.*, Phys. Rev. C **28**, 2349 (1983).
[126]G. Buchwald, G. Graebner, J. Theis, *et al.*, Phys. Rev. Lett. **52**, 1594 (1984).
[127]J. J. Molitoris and H. Stöcker, in Proc. of the Seventh High Energy Heavy Ion Study, GSI-Report 85-10, Darmstadt (1985), p. 197.
[128]J. Aichelin and G. Bertsch, Phys. Rev. C **31**, 1730 (1985).
[129]R. Malfliet, Phys. Rev. Lett. **53**, 2386 (1984).
[130]J. Randrup, Nucl. Phys. **A314**, 429 (1979).
[131]J. Knoll and J. Randrup, Nucl. Phys. **A324**, 445 (1979).
[132]H. A. Gustafsson, H. H. Gutbrod, B. Kolb, *et al.*, Phys. Lett. **B142**, 141 (1984).
[133]L. A. Didenko, V. G. Grishin, M. Kowalski, *et al.*, Communication El-84-54, JINR, Dubna (1984).
[134]C. K. Gelbke, in *Local Equilibrium in Strong Interaction Physics* (*LISIP 1*), edited by D. K. Scott and P. M. Weiner (World Scientific, 1985), p. 307.

[135]H. Stöcker, M. Gyulassy, and J. Boguta, Phys. Lett. **B103**, 269 (1981).
[136]N. K. Glendenning and Y. I. Karant, Phys. Rev. C **21**, 1501 (1980).
[137]S. Nagamiya, M. C. Lemaire, E. Moeller, *et al.*, Phys. Rev. C **24**, 971 (1981).
[138]S. Nagimiya, Nucl. Phys. **A418**, 239 (1984).
[139]M. Anikina, A. Golokhvastov, K. Iovchev, in Proceedings of the Seventh High Energy Heavy Ion Study, GSI-Report 85-10, Darmstadt (1985), p. 829.
[140]J. Pochnodzalla, W. A. Friedman, C. K. Gelbke, *et al.*, Phys. Lett. **B161**, 275 (1985).
[141]B. V. Jacak, G. D. Westfall, C. K. Gelbke, *et al.*, Phys. Rev. Lett. **51**, 1846 (1983).
[142]G. I. Konylov and M. I. Podgoretskiĭ, Yad. Fiz. **15**, 392 (1972) [Sov. J. Nucl. Phys. **15**, 219 (1972)].
[143]G. I. Kopylov, Phys. Lett. **B50**, 472 (1974).
[144]R. Hanbury-Brown and K. Q. Twiss, Nature **178**, 1046 (1956).
[145]R. Lednitski and M. I. Podgoretskiĭ, Yad. Fiz. **30**, 837 (1979) [Sov. J. Nucl. Phys. **30**, 432 (1979)].
[146]K. B. Yano and S. E. Koonin, Phys. Lett. **B78**, 556 (1978).
[147]M. Biyajima, Phys. Lett. **B92**, 193 (1980).
[148]S. E. Koonin, Phys. Lett. **B70**, 43 (1977).
[149]R. Lednitski, V. L. Lyuboshits, and M. I. Podgoretskiĭ, Yad. Fiz. **38**, 251 (1983) [Sov. J. Nucl. Phys. **38**, 147 (1983)].
[150]M. Biyajima, Phys. Lett. **B132**, 299 (1983).
[151]A. Zajc, J. A. Bistirlich, R. R. Bossingham, *et al.*, Phys. Rev. C **29**, 2173 (1984).
[152]J. Bartke and M. Kowalski, Phys. Rev. C **30**, 1341 (1984).
[153]S. Y. Fung, W. Gorn, G. P. Kierman, *et al.*, Phys. Rev. Lett. **41**, 1592 (1978).
[154]D. Beavis, S. Y. Fung, W. Gorn, *et al.*, Phys. Rev. C **27**, 910 (1983).
[155]D. Beavis, S. Y. Chu, S. Y. Fung, *et al.*, Phys. Rev. C **28**, 2561 (1983).
[156]G. N. Agakishiev, D. Armutliĭski, N. Akhababyan, *et al.*, Yad. Fiz. **39**, 543 (1984) [Sov. J. Nucl. Phys. **39**, 344 (1984)].
[157]N. Akhababian, J. Bartke, V. G. Grishin, and M. Kowalski, Communication El-83-670, JINR, Dubna (1983).
[158]F. Zarbakhsh, A. L. Sagle, F. Brochard, *et al.*, Phys. Rev. Lett. **46**, 1268 (1981).
[159]H. A. Gustafsson, H. H. Gutbord, B. Kolb, *et al.*, Phys. Rev. Lett. **53**, 544 (1984).
[160]S. Nagamiya, in High Energy Nuclear Physics, Sixth Balaton Conf. on Nuclear Physics, edited by J. Erö (1983), p. 329.
[161]M. C. Lemaire, S. Nagamiya, S. Schnetzer, *et al.*, Phys. Lett. **B85**, 38 (1979).
[162]H. H. Gutbrod, A. Sandoval, P. J. Johanson, *et al.*, Phys. Rev. Lett. **37**, 667 (1976).
[163]A. Z. Mekjian, Phys. Rev. Lett. **38**, 640 (1977).
[164]V. V. Avdeĭchikov, N. L. Gorshkova, N. K. Zhidkov, *et al.*, Soobshchenie (Communication) 1-84-491, JINR, Dubna (1984).
[165]C. B. Chitwood, J. Aichelin, D. H. Boal, *et al.*, Phys. Rev. Lett. **54**, 302 (1985).
[166]B. V. Jacak, D. Fox, and G. D. Westfall, Phys. Rev. C **31**, 704 (1985).
[167]H. Stöcker, J. Phys. G **10**, L111 (1984).
[168]P. Siemens and J. Kapusta, Phys. Rev. Lett. **43**, 1486 (1979).
[169]G. Bertsch and J. Cugnon, Phys. Rev. C **24**, 1514 (1981).
[170]K. K. Gudima, V. D. Toneev, G. Röpke, and H. Schulz, Phys. Rev. C **32**, 1605 (1985).
[171]K. Kapusta and D. Strottman, Phys. Rev. C **23**, 1282 (1981).
[172]I. N. Mishustin, F. Myhrer, and P. J. Siemens, Phys. Lett. **B95**, 361 (1980).
[173]J. Knoll, L. Münchow, G. Röpke, and H. Schulz, Phys. Lett. **B112**, 13 (1982).
[174]H. H. Gutbrod, H. Löhner, A. M. Poskanzer, *et al.*, Phys. Lett. **B127**, 317 (1983).
[175]K. G. R. Doss, H. A. Gustafsson, H. H. Gutbrod, *et al.*, Phys. Rev. C **32**, 116 (1985).
[176]H. Sato and K. Yazaki, Phys. Lett. **B98**, 153 (1981).
[177]A. Z. Mekjian, Phys. Rev. C **17**, 1051 (1978).
[178]J. Kapusta, Phys. Rev. C **21**, 1301 (1980).
[179]J. Cugnon and D. L'Hôte, in Proceedings of the Seventh High Energy Heavy Ion Study, GSI-Report 85-10, Darmstadt (1985), p. 253.
[180]H. Schulz, G. Röpke, V. D. Toneev, and K. K. Gudima, Phys. Rev. C **33**, 1095 (1986).
[181]R. Stock, R. Bock, R. Brockman, *et al.*, Phys. Rev. Lett. **49**, 1236 (1982).
[182]P. Danielewicz and G. Odyniec, Phys. Lett. **B157**, 146 (1985).
[183]J. J. Molitoris and H. Stöcker, Phys. Lett. **B162**, 47 (1985).
[184]H. A. Gustafsson, H. H. Gutbrod, B. Kolb, *et al.*, Phys. Rev. Lett. **52**, 1590 (1984).
[185]H. G. Ritter, K. G. R. Doss, H. A. Gustafsson, *et al.*, in Proceedings of the Seventh High Energy Heavy Ion Study, GSI-Report 85-10, Darmstadt (1985), p. 67.
[186]S. M. Kiselev, Phys. Lett. **B154**, 247 (1985).
[187]H. Kruse, B. V. Jacak, and H. Stöcker, Phys. Rev. Lett. **54**, 289 (1985).
[188]J. J. Molitoris and H. Stöcker, in Proc. of the Seventh High Energy Heavy Ion Study, GSI-Report 85-10, Darmstadt (1985), p. 197.
[189]J. Cugnon and D. L'Hôte, Phys. Lett. **B149**, 35 (1984).
[190]Y. Kitazoe, H. Furutani, H. Toki, *et al.*, Phys. Rev. Lett. **53**, 2000 (1984).
[191]M. Sano, M. Gyulassy, M. Wakai, and Y. Kitazoe, Phys. Lett. **B156**, 27 (1985).
[192]E. V. Shuryak, Phys. Rep. **61**, 71 (1980).
[193]J. Rafelski and R. Hagedorn, in *Statistical Mechanics of Quarks and Hadrons*, edited by H. Satz (North–Holland, Amsterdam, 1981), p. 253.
[194]W. D. Myers, Nucl. Phys. **A296**, 177 (1978).
[195]J. Cosset, J. Kapusta, and G. D. Westfall, Phys. Rev. C **18**, 844 (1978).
[196]K. K. Gudima and V. D. Toneev, in High Energy Nuclear Physics, Sixth Balaton Conf. on Nuclear Physics, edited by J. Erö (1983), p. 423.
[197]K. K. Gudima and V. D. Toneev, Yad. Fiz. **42**, 645 (1985) [Sov. J. Nucl. Phys. **42**, 409 (1985)].
[198]R. Hagedorn and J. Ranft, Suppl. Nuovo Cimento **6**, 169 (1968).
[199]K. K. Gudima and V. D. Toneev, in Tr. VII mezhdunarodnogo seminara po problemam fiziki vysokikh énergiĭ (Proceedings of the Seventh International Symposium on Problems of High Energy Physics), D1,2-84-599, Dubna (1984), p. 567.
[200]J. Cugnon and R. M. Lombard, Nucl. Phys. **A422**, 635 (1984); Phys. Lett. **B134**, 392 (1984).
[201]H. W. Barz and H. Iwe, Phys. Lett. **B143**, 55 (1984).
[202]S. Schnetzer, M.-C. Lemaire, R. Lombard, *et al.*, Phys. Rev. Lett. **49**, 989 (1982).
[203]F. Asai, H. Sato, and M. Sano, Phys. Lett. **B98**, 19 (1981).
[204]J. Randrup and C. M. Ko, Nucl. Phys. **A343**, 519 (1980); Addendum, Nucl. Phys. **A411**, 537 (1983).
[205]C. M. Ko, Phys. Rev. C **23**, 2760 (1981); *ibid.* **29**, 2169 (1984).
[206]A. Shor, K. Ganczer, S. Abachi, *et al.*, Phys. Rev. Lett. **48**, 1597 (1982); *ibid.* **51**, 616(E) (1983).
[207]J. W. Harris, A. Sandoval, R. Stock, *et al.*, Phys. Rev. Lett. **47**, 229 (1981).
[208]K. Iovchev, T. Kanarek, E. N. Kladnitskaya, *et al.*, Yad. Fiz. **42**, 194 (1985) [Sov. J. Nucl. Phys. **42**, 122 (1985)].
[209]D. A. Armutliĭski, E. Bogdanovich, A. P. Gasparyan, *et al.*, Soobshchenie (Communication) Rl-85-220, JINR, Dubna (1985).
[210]M. Anikina, M. Gazdzicki, A. Golochvastov, *et al.*, in High Energy Nuclear Physics, Sixth Balaton Conf. on Nuclear Physics, edited by J. Erö (1983), p. 433.
[211]J. Collins and M. Perry, Phys. Rev. Lett. **34**, 1353 (1975).
[212]A. Chodos, R. L. Jaffe, K. Johnson, *et al.*, Phys. Rev. D **9**, 3471 (1974).
[213]J. Kapusta, Nucl. Phys. **B148**, 461 (1979).
[214]O. K. Kalashnikov and V. V. Klimov, Phys. Lett. **B88**, 328 (1979).
[215]J. Cleymans, R. V. Gavai, and E. Suhonen, Phys. Rep. **130**, 217 (1986).
[216]B. Kämpfer, H. Schulz, and C. J. Horowitz, Ann. Phys. (N.Y.) **41**, 291 (1985).
[217]S. A. Chin, Phys. Lett. **B78**, 552 (1978).
[218]J. Kuti, B. Lukacs, J. Polonyi, and K. Szlachnyi, Phys. Lett. **B95**, 75 (1980).
[219]E. Suhonen, E. Turunen, and V. V. Dixit, Z. Phys. C **22**, 179 (1984).
[220]R. Hagedorn and J. Rafelski, Phys. Lett. **B97**, 136 (1980).
[221]V. V. Dixit, H. Satz, and E. Suhonen, Z. Phys. C **14**, 275 (1982).
[222]M. I. Gorenstein, V. V. Petrov, and G. M. Zinovjew, Phys. Lett. **B106**, 327 (1981).
[223]K. A. Olive, Nucl. Phys. **B198**, 461 (1982).
[224]C. Bernard, Phys. Rev. D **9**, 3312 (1974).
[225]E. V. Shuryak, Phys. Rep. **115**, 151 (1984).
[226]Yu. M. Makeenko, Usp. Fiz. Nauk. **143**, 161 (1984) [Sov. Phys. Usp. **27**, 401 (1984)].
[227]J. Engels, F. Karsch, I. Montvay, and H. Satz, Phys. Lett. **B101**, 89 (1981); Nucl. Phys. **B205**, 545 (1982).
[228]T. Celik, J. Engels, and H. Satz, Phys. Lett. **B129**, 323 (1983).
[229]M. I. Gorenstein, O. A. Mogilevski, V. K. Petrov, and G. M. Zinoviev, Z. Phys. C **18**, 13 (1983).
[230]M. I. Gorenshteĭn and G. M. Zinov'ev, in Tr. VII mezhdunarodnogo seminara po problemam fiziki vysokikh énergiĭ (Proceedings of the Seventh International Symposium on Problems of High Energy Physics), D1,2-84-599, Dubna (1984), p. 521.
[231]T. Celik, J. Engels, and H. Satz, Report BI-TP 84/09, Bielefeld (1984).

[232]J. D. Bjorken, Phys. Rev. D **27**, 140 (1983).
[233] K. Kajantie and L. McLerran, Nucl. Phys. **B124**, 261 (1984).
[234]M. Gyulassy and T. Matsui, Phys. Rev. D **29**, 419 (1984).
[235]T. H. Burnett, S. Dake, M. Fuki, *et al.*, Phys. Rev. Lett. **50**, 2062 (1983); in Proceedings of the Seventh High Energy Heavy Ion Study, GSI-Report 85-10, Darmstadt (1985), p. 317.
[236]L. McLerran, in *Local Equilibrium in Strong Interaction Physics* (LESIP 1), edited by D. K. Scott and R. M. Weiner (World Scientific, 1985), p. 70.
[237]G. Baym, B. L. Friman, J. P. Blaizot, *et al.*, Nucl. Phys. **A407**, 541 (1983).
[238]K. Kajantie, P. Raitio, and P. V. Ruuskanen, Nucl. Phys. **B222**, 152 (1983).
[239]E. V. Shuryak, Phys. Lett. **B78**, 150 (1978).
[240]K. Kajantie and H. Miettinen, Z. Phys. C **9**, 341 (1981); *ibid.* **14**, 357 (1982).
[241]G. Domokos and J. I. Goldman, Phys. Rev. D **23**, 203 (1981).
[242]G. Domokos, Phys. Rev. D **28**, 123 (1983).
[243]L. D. McLerran and T. Toimela, Phys. Rev. D **31**, 545 (1985).
[244]L. Van Hove, Phys. Lett. **B118**, 138 (1983).
[245]T. W. Biro and J. Zimanyi, Nucl. Phys. **A395**, 525 (1983).
[246]J. Rafelski and B. Müller, Phys. Rev. Lett. **48**, 1066 (1982).
[247]L. Van Hove, Z. Phys. C **21**, 93 (1983).
[248]M. Gyulassy, K. Kajantie, H. Kuski-Suonio, and L. D. McLerran, Nucl. Phys. **B237**, 477 (1984).

Translated by Julian B. Barbour